OBSERVATIONAL STUDY OF GALAXIES IN CLUSTERS

Harvey Thomas MacGillivray

B.Sc. (Edinburgh)

Presented for the Degree of Doctor of Philosophy

at the University of Edinburgh

1975 October

ABSTRACT OF THESIS

A method has been developed which allows the computer to distinguish automatically between the images of galaxies and those of stars from measurements made with the COSMOS fast, automatic, plate-measuring machine at the Royal Observatory Edinburgh. Using this technique, measurements carried out on 6 rich clusters of galaxies on plates taken with the UK 48-inch Schmidt Telescope in Australia are analysed with a view to examining the cluster properties.

The results indicate that all 6 clusters are elongated. There is no general evidence for large scale luminosity segregation, although significant segregation (i.e. $>$ 50% difference in core radii between the distribution of bright and faint members, accompanied by a higher degree of flattening) has been detected in one cluster. The degree of segregation is found to increase with increasing elongation, indicating that more flattened systems are more relaxed. The degree of segregation is also found to increase with increasing concentration, indicating that clusters with high concentrations are more relaxed, their extensive halos being lost in the general background of galaxies.

Comparison of the measurements for one cluster on a red and on a blue plate reveals that the galaxies are more centrally concentrated and form a more flattened configuration on the blue plate than on the red. The results are consistent with a picture for the structure of the cluster in which the bluer galaxies form a flattened core while the redder galaxies form a more spherical halo.

Measurements have also been made by eye, with the aid of a binocular microscope, of the properties of distant groups and clusters on a plate out to a redshift $z \sim 0.5$. These groups and clusters are significantly clustered, existing in systems of pairs up to large cloud complexes. They are also predominantly highly flattened The presence of the cosmological distortion effect is not detected, nor is there found to be any appreciable effect of evolution on the cluster properties.

To Chris, my wife.

CONTENTS

I. CLUSTERS OF GALAXIES

I. 1. Introduction

This thesis is concerned with the study of galaxies in clusters. The underlying aim of the investigation has been to collect and to assess new observational data on the properties of clusters. The results presented herein are as yet preliminary but serve, at least, to indicate promising lines for future research.

But first, why should one be interested in studying clusters of galaxies? The answer is significant: with clusters we have a means for investigating directly problems of immediate cosmological importance, such as the large scale structure, mass distribution and dynamical properties of the Universe. In order to do this, we must first understand the nature of these entities.

Observational studies of clusters of galaxies are still in their infancy (Noonan 1961, 1971, 1972, 1974a, 1974b; Kwast 1966; Rudnicki & Baranowska 1966; Rudnicki 1967; Rood & Baum 1967; Clark 1968; Sastry 1968; Bahcall 1971, 1972, 1973a, 1973b, 1973c, 1974; Rood, Page, Kintner & King 1972; Rood & Sastry 1972; Oemler 1974; Austin & Peach 1974a, 1974b; Austin, Godwin & Peach 1975; Gregory 1975). Results from these are usually conflicting and very often directly opposed. The situation is such that definitive conclusions concerning the structure and state of clusters of galaxies are premature at this time.

In this thesis, new measurements of the properties of galaxies in rich clusters obtained with the COSMOS automatic plate-measuring machine at the Royal Observatory Edinburgh are presented. The purpose of these measurements is to obtain information of importance in an understanding of the structure, present state and formation of clusters of galaxies.

Visual measurements of the properties of extremely distant clusters are also presented. The purpose of these is to examine observable properties of matter, on the large scale, within the Universe. Observations of this type have direct cosmological significance.

In this first chapter, the importance of clusters of galaxies in present-day observational extra-galactic astronomy is discussed and a review of the results of investigations by other authors is presented. The present state of our knowledge regarding clusters is examined and incompleteness in our understanding pointed out. Finally, the aim of this thesis and the particular type of investigation to be carried out are discussed in more detail.

In the following chapters, details of the tools, materials and experimental techniques used in this investigation and the analysis of the data are described. The results are synthesised and final conclusions drawn in the last chapter.

I. 2. The distribution of galaxies and of clusters of galaxies

The nature of the large scale distribution of matter in the Universe is important for cosmology and especially for any theory of the origin of galaxies and of clusters of galaxies. The usual

assumption made is that although irregularities exist on small scales, the distribution of the matter is uniform on a large enough scale. The small scale irregularities represent the "graininess" of the overall structure. The state of our knowledge regarding the nature of the distribution of galaxies and of clusters of galaxies is examined here and it will be seen that clustering exists over a wide spectrum of scales.

The tendency for galaxies to clump together has been known for some time. De Vaucouleurs (1971) has reviewed the large body of evidence for clumping. Most bright galaxies exist in systems of pairs, triplets or multiplets which are themselves usually subsystems of larger groups or clouds of galaxies (de Vaucouleurs 1971). Harrison (1968) argues there are several reasons for thinking that inhomogeneities are imprinted in the early history of the Universe. The very real effect of gravitational clustering (Saslaw 1972), however, must not be neglected in this respect.

The distribution of galaxies has been statistically characterised by Neyman & Scott (1952), Neyman, Scott & Shane (1953) and Limber (1953, 1954). Neyman & Scott (1952) presented a model on the assumption that all galaxies existed in clusters. In the model the distribution of cluster centres was taken to be completely random, the numbers of galaxies in a cluster was governed by a probabilistic law, and the distribution of galaxies in each cluster and their luminosity function followed a Gaussian function. The model was used by Scott, Shane & Swanson (1954) to construct a statistically synthetic plate. Comparison of the observed distribution of galaxies on the

synthetic plate with that for a real plate revealed a few surprises. There was, of course, the chance superposition of bright galaxies in different clusters producing lines and whirls of galaxies but, most surprising of all, the real plate showed clustering to a greater degree than was evidenced on the synthetic plate. The conclusion deduced from this experiment was that the tendency for galaxies to cluster is greater than at first thought. Galaxies are intensively clustered.

Peebles (1974a) has found that the large-scale clustering of matter shows continuity to a first approximation. Clusters of galaxies range on all scales, from rich aggregates of thousands of members like the Coma cluster down to relatively poor groups like the Local Group consisting of about 20-30 members.

A recent analysis of the distribution of galaxies on a deep IIIaJ Schmidt Telescope plate (Dodd et al. 1975) has shown that the results are consistent with the hypothesis that all galaxies are contained in clusters containing from 2-6 members. The concept of 'field galaxy' takes on a new meaning in the light of these results. The uniform background galaxy distribution is none other than the superposition of galaxies in many different clusters (Abell 1962).

The question of the distribution of clusters of galaxies and the possible existence of superclustering (i.e. clustering of clusters of galaxies) is one of the most disputed in astronomy today. Zwicky and his colleagues have shown, in a series of papers (Zwicky & Rudnicki 1963; Zwicky & Berger 1965; Zwicky & Karpowicz 1965,

1966), that the distribution of clusters in the Zwicky catalogue is completely random. On the other hand, from an analysis of the distribution of rich clusters on the plane of the sky, Abell (1958, 1961) has shown that there is a marked non-random clustering of the rich clusters. Abell's claim is further substantiated by the results of Kiang (1967) and Kiang & Saslaw (1969) from the same data.

Criticism has, however, been levelled at Abell's results due to the presence of selection effects (e.g. galactic absorption) which unavoidably introduced bias into Abell's catalogue. A discussion of these effects has been presented by Yu & Peebles (1969). From a re-analysis of Abell's data using the technique of power spectra analysis, Yu and Peebles find no significant tendency for superclustering above that expected for a completely random distribution. They place an upper limit of 10% on the possible fraction of clusters of galaxies that might be found in superclusters.

Further tests, of a different nature, by Fullerton & Hoover (1972) confirmed the conclusions of Yu and Peebles, that systematic errors in Abell's catalogue were responsible for the observed non-random behaviour in the distribution of rich clusters. However, Bogart & Wagoner (1973) have extended the method of nearest-neighbour statistical tests developed by Wagoner (1967) and applied it to test for angular correlations among various sets of extragalactic objects. They found that within their respective distance groups Abell's distant rich clusters of galaxies are significantly clustered.

The method of power spectra analysis was re-applied to

the Abell catalogue by Hauser & Peebles (1973). Their conclusions were completely opposite to those of Yu & Peebles (1969). They found clear and direct evidence for superclustering with small angular scale in agreement with the results of Bogart & Wagoner (1973). The structure corresponds to 2 to 3 clusters per supercluster.

The figure of 2 to 3 clusters per supercluster is significant. The scale of galaxy clustering in the measurements of Dodd et al. (1975) was found to be 2-6 galaxies per cluster with linear cluster sizes ranging from 3.5 to 7 Mpc. De Vaucouleurs (1971) estimates that the average size of a group or cluster of galaxies is about 2 Mpc with centres separated by about 7 Mpc. In this light, the scale of clustering detected by Dodd et al. (1975) is more characteristic of superclustering than of clustering of galaxies. The galaxies may be brightest members of separate clusters rather than individual members of the same cluster.

Another important observation from the measurements of Dodd et al. (1975) is that the density of galaxies within about 150 Mpc of the Galaxy was found to be higher than the corresponding density beyond 150 Mpc, i.e. there is a local excess of galaxies out to about 150 Mpc. Comparison with galaxy counts made by Hubble, covering much of the sky, reveals that this excess is more or less isotropic over the whole sky. The Galaxy may, therefore, be near the centre of a local supercluster.

There are many theories for the formation of large scale inhomogeneities in the Universe. Most notable amongst these are the

heirarchical models of Wertz (1971) and Haggerty (1971). Giovanelli (1964) proposed a cosmological model in which he envisaged fluctuations occurring on all observable scales. More recently, Peebles (1974b) has suggested a model for the continuous heirarchy of clustering.

The observable evidence for a successive heirarchy of clustering of galaxies cannot be reconciled, however, with the results of Sandage, Tammann & Hardy (1972) who set limits on the local deviation of the Universe from a homogeneous model. This was accomplished in two different ways. Firstly, the redshift-magnitude diagram shows no deviation from that which is expected in the homogeneous case. This result is puzzling in the light of large local clouds of inhomogeneous matter such as the Coma-Virgo Cloud and the Ursa Major Cloud. Secondly, the method of galaxy counts has also shown no deviation outside that expected in the homogeneous case. Sandage, Tammann and Hardy conclude that there is no significant departure from homogeneity in effects on dynamics or the average distribution of matter in the observable universe.

Perhaps the matter will only finally be settled by detecting the observational consequences of anisotropies or large-scale inhomogeneities in the Universe of the type discussed by Kristian & Sachs (1966), Refsdal (1970) and Dyer & Roeder (1974).

I. 3. Classifications of clusters of galaxies

Clusters of galaxies, then, are most likely the fundamental concentrations of matter in space and, as such, enable astronomers to

investigate the large-scale mass distribution and dynamical properties of the Universe. A step towards understanding the nature of clusters of galaxies is to classify them according to some optical property of their member galaxies. Several classification schemes have been developed in the literature, and it is worthwhile at this point to describe the more useful of these.

Zwicky et al. (1961-68) characterized clusters of galaxies by three groups according to the concentration of their bright members:-

compact clusters show a single outstanding concentration among the bright members. Within this concentration ten or more galaxies appear in actual contact. Many of these clusters display a high degree of spherical symmetry.

medium-compact clusters are characterized by either a single concentration where, however, the ten brightest galaxies are not in contact but are separated by several of their own diameters, or by several distinct condensations, some of which may be quite compact.

open clusters contain no obvious condensations, but in various locations the numbers of galaxies per square degree is at least five times as great as in the surrounding field such that the cluster appears as a cloud superimposed on the background.

Abell (1965) has proposed a two-part classification of clusters according to their degree of circular symmetry:-

regular clusters show a high degree of spherical symmetry and strong central concentration. They are rich clusters, most probably containing about a thousand members brighter than Mpg = -15. Their

bright members are all or nearly all elliptical and SO galaxies; giant spirals are either completely lacking or are exceedingly rare. Examples of regular clusters are the Coma cluster (Abell 1656) and the Corona Borealis cluster (Abell 2065).

irregular clusters do not show marked spherical symmetry or strong (if any) central concentration. They are more or less amorphous in appearance. Their bright members consist of all types of galaxies - spirals as well as ellipticals and SO's. In richness irregular clusters range from populous aggregates of more than a thousand members down to small groups of a few members. Often they have small sub-condensations, and are generally far more numerous than the regular clusters. Examples are the Hercules cluster (Abell 2151), the well-known Virgo cloud and the Local Group.

Rood & Sastry (1971) introduced the "tuning fork" classification scheme for rich clusters on the basis of the distribution of the ten brightest member galaxies. The cluster types fall naturally into an ordered sequence with criteria varying systematically from one end to the other. The sequence can be represented by a tuning fork diagram:-

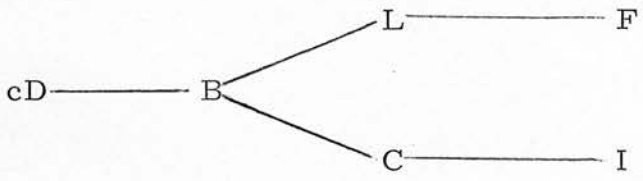

where the classification criteria are:-

cD (supergiant) A cluster containing an outstandingly bright member, a cD galaxy (originally defined by Morgan & Lesh 1965).

The usual definition is that the size (semi-major axis plus semi-minor axis) is $\geqslant 3$ times that of any other galaxy in the cluster. If the main body is multiple or shows any other peculiarity, a subscript p is added to the type designation.

B (binary) — Two supergiant galaxies separated by $\leqslant 10$ diameters of the larger galaxy, and with combined sizes $\geqslant 3$ times that of any other cluster member. A subscript b indicates a connecting bridge between the supergiant binary, or the components of one or both of its members.

L (line) — Three or more brightest galaxies among the top ten members arranged with comparable separations in a line, and numerous fainter members distributed around them.

C (core-halo) — Four or more of the top ten brightest members with comparable separations located near the centre, and numerous fainter ones distributed around them.

F (flat) — Several of the top ten brightest members and a large fraction of fainter galaxies distributed in a flattened configuration.

I (irregular) — The galaxies are distributed irregularly, or without a well-defined centre.

The "brightest galaxy" morphology was devised by Bautz & Morgan (1970) and applied to seventysix rich clusters. A further one hundred and eleven were subsequently classified by Bautz (1972). This is a five-part classification depending on the relative optical

contrast of the brightest galaxy to others in each cluster. The notation is:-

I — Clusters containing a centrally located cD galaxy.

I-II — Intermediate.

II — Clusters whose brightest galaxy or galaxies are intermediate in appearance between the class cD and the Virgo-type giant ellipticals.

II-III — Intermediate.

III — Clusters containing no dominant galaxy.

I. 4. The Virial Theorem and clusters of galaxies

On the assumption that a cluster of galaxies is gravitationally isolated and in dynamical equilibrium (stable), the mass of the system may be estimated by application of the virial theorem.

Assuming that the galaxies move like point masses, interacting by gravitation alone, the acceleration of the i^{th} galaxy is:-

$$\frac{d^2\underline{r}_i}{dt^2} = \sum_{j\neq i} \frac{Gm_j(\underline{r}_j - \underline{r}_i)}{|\underline{r}_j - \underline{r}_i|^3} \qquad (1)$$

where m_j is the mass of the j^{th} galaxy and the coordinates $\underline{r}_i$ are with respect to the centre of mass. On taking the scalar product of this equation with $m_i\underline{r}_i$ and summing over i, one finds:-

$$\frac{d^2}{dt^2}\sum_i \frac{m_i r_i^2}{2} - \sum_i m_i v_i^2 = \sum_i \sum_{j\neq i} Gm_i m_j \underline{r}_i \cdot \frac{(\underline{r}_j - \underline{r}_i)}{|\underline{r}_j - \underline{r}_i|^3}$$

$$= \tfrac{1}{2}\sum_i \sum_{j\neq i} Gm_i m_j \frac{(\underline{r}_i - \underline{r}_j)\cdot(\underline{r}_j - \underline{r}_i)}{|\underline{r}_j - \underline{r}_i|^3}$$

$$= -\tfrac{1}{2}\sum_i \sum_{j\neq i} \frac{Gm_i m_j}{|\underline{r}_j - \underline{r}_i|} \qquad (2)$$

which can be identified as the virial theorem. It is more commonly expressed as:-

$$\frac{1}{2}\frac{d^2 I}{dt^2} = 2T + U \qquad (3)$$

where I is the moment of inertia, T the kinetic energy, and U is the gravitational energy. If the system is in equilibrium, i.e. stable against contraction or expansion, then the left hand side of equation (3) disappears and it follows, in the time average, that the kinetic energy is one half the magnitude of the gravitational energy:-

$$T = -\frac{1}{2} U \qquad (4)$$

For a cluster of total mass M, effective radius R, and velocity dispersion V we have from the virial theorem:-

$$MV^2 = \frac{qGM^2}{R} \quad \text{or} \quad M_{V.T.} = RV^2/qG \qquad (5)$$

where q depends on the mass distribution (e.g. q = 3/5 for a sphere).

A long-standing problem in the dynamics of groups and clusters of galaxies is that the mass of a cluster estimated from the virial theorem is generally larger, often by an order of magnitude or more, than the mass obtained from summing the masses of the individual galaxies (Limber 1962; Rood, Rothman & Turnrose 1970). This has given rise to the so-called "mass discrepancy" in groups and clusters. The observational basis and hypothesised solutions for this effect have been widely discussed in the literature (Zwicky 1957; Limber 1962; Neyman, Page & Scott 1961; Karachentsev 1966;

Noerdlinger 1970; Burbidge & Sargent 1971; Field & Saslaw 1971; Aarseth & Saslaw 1972; Dearborn 1973; Gott, Wrixon & Wannier 1973; Geller & Peebles 1973; Rood 1974a, 1974b).

Two main hypotheses have been proposed to account for the missing mass. Ambartsumian (1961) suggested that the total energy of clusters of galaxies is positive, that the clusters are flying apart and the virial mass discrepancy is due to their expansion. However, the crossing times for galaxies in typical clusters ($t = 2R/V$) are very much smaller than the age of the Universe and one should expect that clusters would have disrupted long ago. On the contrary, the galaxies in clusters are mainly E's and SO's which, on the basis of our present understanding, are thought to be very old ($\sim 10^{10}$ years), and hence clusters must be stable systems.

The other hypothesis is that there is a vast amount of "hidden mass" (i.e. matter in the form of ionised hydrogen, neutral hydrogen, stars, faint galaxies) lying between the galaxies (e.g. Oort 1958) and stabilising the clusters. Many attempts have been made to try to detect the presence of non-luminous matter in clusters, in particular in the Coma cluster since it is one of the nearest rich clusters (for a review see Tarter & Silk 1974).

Doubts have been cast regarding the reliability of mass determinations. Wolf & Bahcall (1972) have shown that the mass-luminosity ratios for some galaxies can be several times larger. Dynamical evidence has been obtained (Einasto, Kaasik & Saar 1974), supported by morphological evidence (Einasto, Kaasik, Saar & Chernin

1974), indicating that galaxies have extremely massive coronas, thus increasing their mass by a factor of 10 or more. Napier & Guthrie (1975) suggest that the hidden mass is in the form of black dwarf stars with masses down to $\sim 10^{-2} M_{\odot}$ which formed massive halos around the galaxies.

There are increasing reasons, thus, to believe, that the masses of ordinary galaxies have been underestimated by a factor of 10 or more. An interesting consequence of this observation is the effect of the mean mass density of the Universe (Ostriker, Peebles & Yahil 1974). The current estimate (Shapiro 1971) for the ratio of gravitational energy to kinetic energy in the Universe is about $\Omega = 0.01$. If the estimated mass of each galaxy were increased by a factor in excess of 10, then this ratio is increased by the same amount and it is concluded that the observations may be consistent with a Universe which is "just closed" ($\Omega = 1$).

I. 5. Formation and evolution of clusters

Our understanding of the formation and subsequent evolution of clusters of galaxies is at an early and uncertain stage. It is pertinent, however, in this study to describe briefly current theories for the formation of clusters and outline certain predictions of theory which may be useful for observational tests.

An exotic origin for clusters of galaxies as due to the decay and subsequent fragmentation of quasars has been proposed by Vorontsov-Vel'yaminov (1970).

This hypothesis is based on the empirical observation that quasars are not, as a rule, found associated with clusters of galaxies (Burbidge & O'Dell 1973). The evidence for this is not, however, compelling, and this matter is not pursued further here. Until such time as our knowledge of the nature of quasars is increased, the theory cannot usefully be commented upon.

It is thought by many authors that spherical clusters of galaxies were formed in the early, homogeneous, expanding Universe after the decoupling of matter and radiation by a "gravitational instability" (Lemaître 1958; Schücking & Heckmann 1958; van Albada 1960, 1961; Lifschitz & Khalatnikov 1963). According to this instability picture the galaxies (or protogalaxies) making up the protocluster were initially moving apart in agreement with the general law of recession, but these galaxies had negative total energy and after a time the system stopped expanding and fell back in on itself. The subsequent evolution of the system follows that of a system of self-gravitating particles, with no forces present apart from their mutual gravitational attraction.

A straightforward test of the instability theory is to integrate numerically the equations of motion for a number of gravitationally interacting galaxies, starting from appropriate initial conditions, and to compare the predictions of the model with the results of observations. A number of numerical experiments have been carried out on the N-body problem (Aarseth 1963, 1966, 1971). The system undergoes relaxation by two-body close encounters leading to complete dynamical

equilibrium with equipartition of energy. The gross features of the evolution of the system are represented by the growth of a massive core and the formation of an extensive halo consisting mainly of low mass objects.

Peebles (1970) has constructed a numerical model for the Coma cluster. In the model it is assumed that the matter has already fragmented into concentrated objects (galaxies, protogalaxies) before the protocluster reaches the point of maximum expansion and that the objects interact only via gravitation. The collapse of the system after maximum expansion is in effect inelastic, the central density remaining nearly constant after the time of maximum contraction. The distribution in the envelope settles down to a nearly time-independent state after two characteristic collapse times. The results of the model are found to be consistent with observations for the Coma cluster.

The formation of condensations in the early Universe due to turbulence generated by chaotic velocities was proposed by von Weizsäcker (1951). Recently these ideas have been extensively developed by Ozirnoi & Chibisov (1970), Ozernoi (1971), Silk & Ames (1972) and Stein (1974). A model for the formation of galaxies within clusters due to velocity perturbations has been presented by Icke (1973). In the model, predominantly elongated clusters are formed by galaxy formation due to turbulence within collapsing prolate spheroidal regions of space. Certain wave numbers of the perturbations are more strongly amplified than others in the protocluster leading to

peaks in the mass spectrum. The first galaxies to separate out reheat the surrounding gas, effectively increasing the Jean's mass and shifting the mass spectrum towards higher masses.

Certain predictions of the model may be tested directly:-

1) The approximate form of the mass spectrum, and hence the luminosity function, is determined.

2) The mass of the heaviest perturbation that separates out is determined by the final temperature of the gas in the collapsing protocluster. Since this temperature is nearly equal for all clusters one may expect that the most massive galaxies inside a cluster have rather uniform properties.

3) The shear is larger near the boundary of the contracting protocluster and hence the specific angular momentum of galaxies is higher. One would expect, therefore, to find more spiral galaxies in the outer regions and more ellipticals in the centre.

4) Low mass galaxies separate out before the high mass galaxies. Therefore one would expect smaller galaxies to have a more spherical distribution than the larger ones.

5) The asymmetry due to the initial shape of the parent protocluster causes an asymmetry in the appearance of the perturbations. The result is that the galaxies show a preference to align with the major axis of the cluster.

I. 6. Observations

The Coma cluster is one of the nearest rich, regular clusters of galaxies and is thus an excellent object for study. It is

unfortunate that the existing observations lead to uncertain and even conflicting results.

The size of the Coma cluster has been the centre of a great deal of disagreement (Zwicky 1957; Noonan 1961; Abell 1962; Omer, Page & Wilson 1965; Rood, Page, Kintner & King - hereafter referred to as RPKK - 1972). Conclusions range from under 2 degrees to over 6 degrees for the radius of the cluster. The difficulty lies in the uncertain correction that must be applied for the background field count. The problem may only be satisfactorily resolved with more radial velocity measurements.

The presence of mass segregation in the Coma cluster, in the form of a concentration of the brighter members toward the centre, has not been decisively settled one way or the other. Zwicky (1957) has found evidence for pronounced mass segregation. No such effect was, however, detected by Noonan (1961) in a re-analysis of Zwicky's counts, nor by RPKK (1972) using radial velocity data. Of great weight in this matter are the measurements of Bahcall (1973b). Counts of galaxies were made to three limiting magnitudes and the projected Emden isothermal gas sphere distribution was fitted to each of the spatial densities. The results revealed the same core radius for the three sets of counts. The bright and faint galaxies in the Coma cluster are thus distributed evenly. There is evidence, however, to suggest some degree of mass segregation in the Coma core (Rood & Turnrose 1968; Rood 1969). This may be a consequence of partial dynamical relaxation within the core.

Colour segregation has been detected in the Coma cluster by Philip & Sanduleak (1970). The bluest galaxies show a tendency to be more concentrated to the cluster centre than do the reddest galaxies. Red galaxies may be the result of internal reddening in edge-on galaxies, as well as indicative of a strong M-star population. Some spirals are members of the cluster (RPKK 1972; Rood 1974c).

The cluster is stabilised by a missing mass some 7-8 times the total mass of the galaxies and distributed in the same way as the galaxies (RPKK 1972). Tarter & Silk (1974) have reviewed the various possible means of accounting for the dynamical mass. The recently obtained evidence, however, for the underestimation of the masses of galaxies (Einasto, Saar & Kaasik 1974; Einasto, Saar, Kaasik & Chernin 1974) is consistent with this value.

The situation concerning observations of other clusters of galaxies is equally confused. There is evidence for definite luminosity segregation in some clusters - in the Corona Borealis cluster (Noonan 1971), in Abell 234 and in cluster 0024 + 1654B (Noonan 1974a) - although luminosity segregation is not present as a rule. Likewise, colour segregation has been found in a few clusters - in the Hercules cluster (Philip 1970) and in Abell 194 (Philip & Sulentic 1973) bluer galaxies are more centrally concentrated than redder galaxies, while in others the redder galaxies are the more centrally concentrated (Kwast 1966).

Austin & Peach (1974b), from photometry of the galaxies in the cluster Abell 1413, have found that the luminosity function for the cluster is in good agreement with the form for the mass spectrum

predicted by Icke's (1973) model. They also found, however, a discordance between the model and observations for the distribution of bright and faint members. The elongated shape of the cluster is reflected in the distribution of the faint galaxies. The bright galaxies have, on the other hand, a more spheroidal distribution.

In a search for systematic properties, Oemler (1974) found that clusters of galaxies may be divided into three groups - spiral rich, spiral poor and cD clusters. Clusters with cD galaxies are rich in ellipticals, have smooth, spherical mass distributions of high density and central concentration, have a deficiency of spirals in the core and show a considerable tendency towards energy equipartition. Spiral poor clusters are dominated by SO galaxies, show segregation by mass and morphological type, but are not as smooth, dense or centrally condensed as cD clusters. Spiral rich clusters have irregular mass distributions of low density and no central concentration, and show no signs of segregation of members according to mass or morphological type. Oemler concludes that spiral poor clusters represent a later evolutionary state of spiral rich clusters but that cD clusters, while the most evolved, are intrinsically different.

An analysis of the distribution of galaxies in the cluster Abell 2199, one of the cD clusters represented in Oemler's (1974) sample, has been carried out by Bahcall (1973c). Counts of galaxies were made to four different limiting magnitudes. The results indicated that the bright and faint galaxies in the cluster are distributed in the same way, a completely opposite conclusion to that of Oemler (1974).

Detailed observational studies of the geometrical properties of galaxies in rich clusters have only recently begun (Rood & Baum 1967; Sastry 1968; Bahcall 1971, 1972; Rood & Sastry 1972). Rood & Baum (1967) carried out a survey of the core of the Coma cluster. They presented a catalogue of the 315 brightest galaxies and analysed the position angles of the major axes, ellipticities and morphological types of the individual galaxies. The position angles of the major axes of the galaxies were randomly orientated and SO and SBO galaxies were well represented among the cluster galaxies.

For several cD clusters, Sastry (1968) has analysed position angle, ellipticity, compactness and centre of distribution of the galaxies. There was a strong tendency for the major axis of the distribution of galaxies to be orientated along the major axis of the cD galaxy. There was also a correlation between the relative compactness of brighter and fainter members and the presence of radio emission from the cD galaxy, indicating that the radio cD clusters are dynamically younger than the nonradio cD clusters.

Rood & Sastry (1972) have analysed static properties for 170 galaxies in a 2 square-degree region centred on the Abell 2199 cluster. They found a strong tendency for the galaxies to lie along the major axis of the cD galaxy, and a tendency for the position angles of the galaxies to lie approximately along the major axis of the cD galaxy or perpendicular to it. Galaxies with small ellipticity, major axis perpendicular to that of the cD galaxy, red colour, elliptical and SO type are concentrated towards the cluster centre. Ellipticals and blue galaxies lie along the major axis of the cD galaxy.

The anisotropy in the distribution of galaxies in the Perseus cluster (classified as type 'L' in the tuning-fork classification of Rood & Sastry 1971) has been studied in detail by Bahcall (1974). The results indicate that the distribution of galaxies in the cluster is elongated in the direction of the line of bright galaxies. A possible explanation for this effect other than chance projection is that we are observing a disk-like cluster edge-on. No apparent rotation is observed, however, in the measured velocities of the galaxies (Chincarini & Rood 1971).

I. 7. Cosmology and clusters of galaxies

Cosmology is the study of the history and structure of the Universe. A central goal in observational cosmology is to test cosmological models by looking for relativistic effects in the appearance of distant objects. Clusters of galaxies play an important part in present-day observational cosmology as principal cosmological test objects.

In Appendix I the mathematical basis for the cosmological world models is outlined, tests for distinguishing between the various world models are described and the role of clusters of galaxies in cosmology is examined. It is seen that in two of the tests (redshift-magnitude and angular diameter-redshift) clusters of galaxies are suitable test objects. Statistical fluctuations in any sample area due to the intense clustering of galaxies precludes the use of the third test (number-magnitude count) as a means for determining the world model.

The uncertainties in the results obtained so far from the cosmological tests are due mainly to a lack of knowledge of the intrinsic properties of clusters. An understanding of the nature of clusters of galaxies would help to reduce the inherent uncertainties.

I. 8. Aim of the thesis

In this first chapter, the importance of clusters of galaxies has been discussed, first of all as fundamental building blocks with which we may investigate the large-scale distribution and dynamical properties of the matter in the Universe, and secondly as principal cosmological test objects for deciding between the various world models. It has become apparent, however, that the observations of clusters have produced a diversity of conclusions. Our knowledge of the nature of clusters is confused, our understanding of their formation uncertain.

In this thesis there are two aims. Firstly to investigate those properties of rich clusters of use in a study of their structure, present state and formation, and secondly to use observations of the appearance of distant clusters on photographic plates to examine the properties of matter, on the large scale, within the Universe. Investigations of the first type involve measurements made with the COSMOS (Coordinate, Size, Magnitude, Orientation and Shape) fast, automatic, plate-measuring machine at the Royal Observatory Edinburgh of galaxies in rich clusters on plates taken with the UK 48-inch Schmidt Telescope in Australia. Those of the latter involve visual measurements of the static properties (positions, sizes, orientations and shapes) of distant clusters on the same plates.

Although the characteristics may vary from one cluster to another, a search is made for systematic effects in their gross features. In particular, the detection of non-random effects will be important. For the rich nearby clusters, the presence of segregation effects (i.e. the concentration of the brighter members toward the centre, etc.) will be noted and relationship with other properties examined. Comparison of plates in different colours may reveal dependence of these properties on waveband. For the distant clusters, a search is made for systematic effects in the distribution of their geometrical parameters and the relationships between them.

Details of the equipment, materials and techniques used in this investigation are now described in the following chapters.

II. TOOLS AND MATERIALS

II. 1. The UK 48-inch Schmidt Telescope

The UK 48-inch Schmidt Telescope, a classical wide-angle Schmidt, was designed and constructed by Grubb Parsons of Newcastle upon Tyne in just under two years, and has its site at the Australian National University's Siding Spring Observatory. Plate I is a photograph (reproduced here by courtesy of the Science Research Council) of the telescope, one of the largest of its kind in the world. Details of the telescope are given in Table 1; this information was communicated by the UK Schmidt Telescope Unit of the Science Research Council based at the Royal Observatory Edinburgh.

The telescope normally takes two sizes of photographic plate, 356mm square and 160mm square. The larger ($\approx$14in. square) is the more frequently used; this corresponds to a field of 6 arcdegrees on the sky (12 times the diameter of the moon) with a plate scale of 67.1 arcsec/mm. The unique design of the Schmidt camera allows several hundreds of thousands of images to be recorded on a single photograph. For example, the whole of the Small Magellanic Cloud ($\approx 4^{o} \times 3^{o}$), our nearest neighbouring galaxy, may be photographed on one plate, allowing study along lines which are otherwise extremely difficult if not impossible.

Large paraboloid telescopes are, of course, important astronomical tools in their own right. They are, however, designed

Plate I: The UK 48-inch Schmidt Telescope

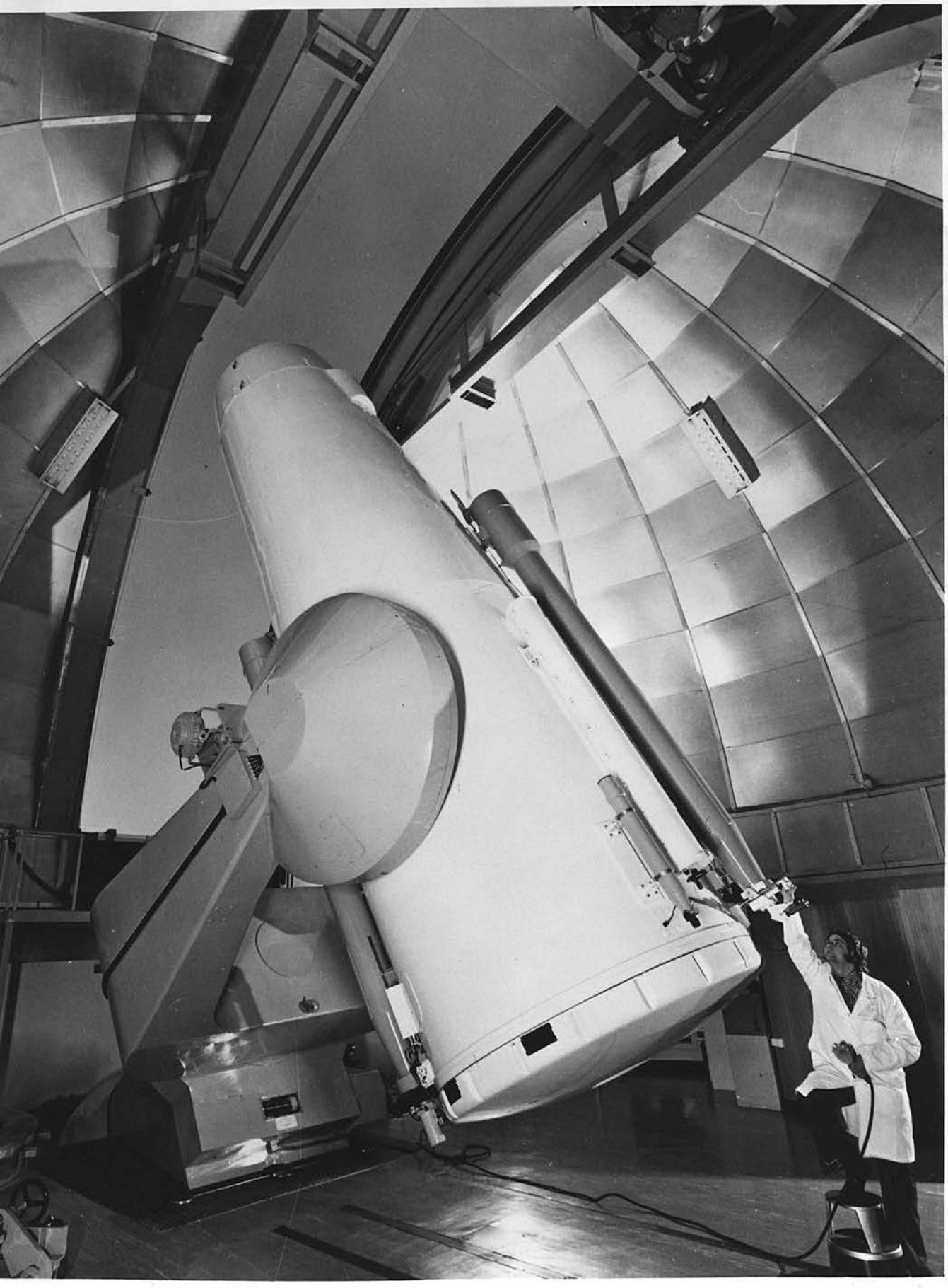

for a specific purpose; using the 200-inch telescope is like looking at the Universe through a keyhole - what one gains in depth in space along the line of sight, one loses in width of field. It is difficult to determine, for example, whether a particular distant galaxy is an individual object in space or is a member of a much larger group or cluster of galaxies.

The Schmidt telescope, on the other hand, has a wide field of view, enabling the study of large numbers of objects and their environment simultaneously. The presence of many galaxies on one plate means that important and far-reaching problems, such as the structure of the visible Universe, may be studied directly. Indeed, a new and exciting era of astronomical research is already beginning thanks to this recent acquisition by British and Australian astronomers.

The tremendous impact of the Schmidt telescope in astronomy may best be judged from the literature. Prior to the Palomar survey only about 25 clusters of galaxies were known (Shapley 1933). Since the survey Abell (1958) recorded 2712 rich clusters in the northern sky alone, and Zwicky recorded 3523 clusters in the first two volumes of the Zwicky et al. (1961-68) catalogue, covering only about 1/10th of the total area of the sky.

The UK 48-inch Schmidt Telescope was built in order to carry out a systematic survey of the southern sky from declinations -20° to -90°, paralleling that of the Palomar survey of the northern sky. Since the telescope became operational in July 1973, over a thousand plates have been taken. The combination of high-quality optics, new emulsions and improved sensitising techniques has enabled

Table 1

Parameters for the UK 48-inch Schmidt Telescope:-

mirror diameter:	1.83 metres
aperture diameter:	1.24 metres
focal length:	3.07 metres
photographic plate sizes:	356mm square, 160mm square
thickness:	1mm
radius of curvature of focal plane:	3.07 metres
unvignetted field radius:	147mm = 2.73 arc degree
plate scale:	67.1 arc sec/mm = 14.9 μm/arc sec
corrector plates:	i) Schott BK7 glass, corrected wavelength 4200Å; gives image diameter of about 2 arc sec with bandwidth of 1000Å centred about the corrected wavelength.
	ii) achromat (ready 1975); gives image diameters $\leq$ 1 arc sec in any bandwidth from 3500Å to 9000Å.

the telescope to photograph objects down to magnitude B = 23 (Corben, Reddish & Sim 1974), fainter than any previous survey. Hundreds of thousands of faint galaxies, with distances out to several thousand million light years (Dodd et al. 1975), $z \approx 0.3\text{-}0.7$, are recorded on a single plate. The huge quantities of data involved make manual measurements out of the question from a practical view, not to mention bias through severe physiological, subjective and selective effects (Holmberg 1946; Öpik 1969, and references therein). It was necessary, therefore, to develop a high-speed machine capable of performing, objectively and accurately, the measurements of the properties (positions, sizes, etc.) of the very large numbers of faint images (stars and galaxies) recorded on the photographs. Such a machine, COSMOS, has been built and is currently in operation at the Royal Observatory Edinburgh.

II. 2. COSMOS

The COSMOS high-speed, automatic, plate-measuring machine was developed jointly by Computer Applications Service of the Heriot-Watt University and scientists of the Royal Observatory Edinburgh. A photograph of the machine appears in this thesis (plate II) by courtesy of the Science Research Council. The first measurements were made with the machine early in November 1974, and these indicated that the performance specification (Table 2) was being met.

COSMOS finds and measures the Co-Ordinates, Sizes, Magnitudes, Orientations and Shapes of images of stars and galaxies

Plate II: The COSMOS automatic, plate-measuring machine


COSMOS

on the photographs at rates of up to a thousand per second. The measurements are recorded on magnetic tape and subsequently analysed in the Science Research Council's Atlas Computer Laboratory at Chilton, Didcot, Oxon.

The plate to be measured is carried in a horizontal X-Y carriage, motion being provided by hydraulic rams and positioning measured by moiré gratings, giving control to $\pm\frac{1}{2}\mu$m over the entire area of the plate. Machine operation is under the control of a dedicated multi-purpose mini-computer which institutes all the commands.

Image detection and measurement are provided via two independent densitometer systems, one of which provides a linear scan of variable length, the other a generalised elliptical scan of variable diameter, axial ratio and orientation. The light sources are microfocus cathode ray tubes positioned above the plate, together with the optics necessary to focus an image of the source in the plane of the emulsion and also the components needed to monitor continuously the light from the C.R.T. phosphor. In the case of the linear scan system, the spot position is continuously measured and related to the main carriage position. The transmitted light is measured by photomultipliers and associated electronics.

There are three modes of machine operation (Table 3):-

Coarse Measurement - provides output for a rapid analysis of images on the whole or part of a plate. The linear C.R.T. scan and the Y-axis motion of the compound carriage generate a television type raster scan. The measured output on magnetic tape allows the calculation of position, area, shape and minimum transmission for each image. Images can

Table 2

COSMOS

photographic plate size:	up to 356mm x 356mm
plate carriage:	moved hydraulically and positioned by a transmission grating system to $\pm 0.5\,\mu$m.
scanning systems:	two independent microspot cathode ray tubes, one giving a raster scan the other a spiral scan.
machine control:	general purpose mini-computer with 8192 words of 16 bit storage.
machine output:	machine tape deck of 1600 bits per inch, 75 inches per second.
raster scan systems:	spot sizes of 8, 16 or 32 μm with corresponding lane widths of 1, 2 or 4mm respectively; for the 8 μm spot the scanning rate is 2 square mm per second, or one full-sized plate per day; transmission digitised to 127 levels.
spiral scan system:	three magnifications give field scanning diameters on the plate of 256, 820 and 2048 μm respectively; generates family of 1024 general ellipses, centres on image and determines best fitting ellipse.

be handled at up to 4000/sec. The time to measure the whole of a plate depends on the resolution (8, 16 and 32 μm) with corresponding measuring times of 18, 5 and $1\frac{1}{2}$ hours.

Mapping - the same type of scan as that in coarse measurement but the output consists of a measure of the transmission to an accuracy of 1% at every 8 μm increment. Since only a single character is recorded in this way for each increment, the scanning speed is the same as that for the 8 μm resolution of coarse measurement.

Fine Measurement - image position information (either from coarse measurement, mapping, or an external source of acceptable accuracy) is used to compile an input tape containing the coordinates of images for which more precise data are required. The tape is read and the carriage is positioned to bring the images in turn onto the axis of the elliptical scanning system. The control then performs a series of iterations which centres the image with precision, measures the ellipticity and orientation and determines the magnitude by comparison with stored data. The accuracy attained is $\pm\frac{1}{2}$ μm for position, $\pm$0.01 in magnitude and 2% for ellipticity and orientation. The speed of measurement is limited since it involves motion of the carriage under control of the centring servos, 900 images/hour for circular images and 300 images/hour for elliptical images. In this mode it is also possible to measure objective prism spectra.

The combination of good quality plates from the UK Schmidt Telescope and accurate, objective, high-speed measures from COSMOS provides a powerful system for astronomers to investigate questions

Table 3

COSMOS measurement modes:-

Mapping:	transmission value output for each scan element; 1200 square mm per magnetic tape; measuring rate - $2mm^2s^{-1}$.
Coarse Measurement:	hardware pattern analyser gives X, Y coordinates to $\pm 3\mu m$, area, X extent, Y extent, minimum transmission and orientation for each image detected above threshold; 1 million images per magnetic tape.
Fine Measurement:	X and Y coordinates to $0.5\mu m$, magnitudes to $0^m.01$, ellipticity and orientation to 2%; measuring rate - 300 elliptical images or 900 circular images per hour.
Spectrum Scanning:	measures of transmission or line positions in objective prism spectra.

of major cosmological importance, indeed to study the very structure and evolution of the Universe.

In order to carry out investigations of this type, methods must first be sought by which the computer may use the output from the machine to distinguish automatically between the images of stars and those of galaxies; only then may the required analysis (in this investigation, that of the properties of galaxies) proceed. Fine measurement produces the type of information useful in the study of the properties of faint galaxy images (positions, sizes, shapes and orientations); it has been seen, however, that this mode of measurement is rather slow, a good deal slower than coarse measurement. It is more efficient, therefore, to use the data from coarse measurement to pick out the galaxies, thus providing a finding list for fine measurement.

Methods have been developed which do allow the computer to distinguish automatically between the images of stars and galaxies from coarse measurement data and these are described in the next chapter. At the time of writing this thesis, the fine measurement mode of COSMOS is not yet in full operation. Analyses of the distributions of orientations and shapes for galaxies in clusters would have provided much insight for this investigation. Use can still be made, however, of the coarse measurement parameters, position and area, for galaxies.

In the remaining sections of this chapter, the means of data reduction and analysis are described.

II. 3. The 1906A computer and SD 4020 graph plotter

Because of the large quantities of information obtained from COSMOS, computer analysis of the data is essential. The raw data on magnetic tape are processed on the 1906A multi-access computer at the Atlas Computer Laboratory and transferred onto other magnetic tapes in user-compatible format ready for access by programs written in a high-level computer language (Algol or Fortran).

The 1906A is one of the larger members of the ICL 1900 range of computer. It has a core store of 256K words, with a word of 24 bits plus a parity bit to detect machine malfunction. Program scheduling and organising is controlled by the GEORGE operating system.

The Observatory has a 2050 remote job-entry terminal linked directly to the peripheral processing unit (PPU) of the Atlas 1906A. A remote job-entry terminal consists of a "cluster" of input/output devices sited remote from the machine itself, for user convenience, by means of which jobs may be submitted to the machine and output redirected back to the terminal. The ROE terminal has a card reader, tape reader, tape punch and line printer. Data transfer down the line is too slow for a magnetic tape deck to be a practical part of the terminal. Magnetic tapes from COSMOS are sent directly to the Atlas Laboratory where they may be readily on-lined by any job submitted through the terminal.

The SD 4020 "Microfilm Recorder" is a sophisticated microfilm and hard copy plotter which can be used as either on-line or off-line peripheral equipment for the computer. The most obvious use is for rapid production of graphical output.

The basic components of the SD 4020 at the Atlas Laboratory are:-

a magnetic tape deck;

a tape adapter which accepts data from the magnetic tape and assembles the information into plotting instructions;

the charactron shaped beam tube, a special cathode ray tube upon which are displayed vectors, axes and characters;

microfilm camera; there are two cameras available, 16mm and 35mm. Both are sprocket controlled and the operator can load one or other of the cameras. The film advance and shutter control are controlled by SD 4020 instructions.

hard copy camera - similar in operation to the microfilm camera. The photo-recording paper must be developed before viewing.

The operation of an SD 4020 camera is basically different from that of a standard camera in that an SD 4020 camera tends to have its shutter open most of the time. A complete scene is built up by a large number of lines and characters appearing on the charactron tube face for short periods of time.

II. 4. Software

A number of computer programs have been written, both in Algol and in Fortran, to analyse measurements of the type made by COSMOS. Most of these are rather long with several internal diagnostic checks. For this reason, listings of all the programs are not included in this thesis. A brief description of the purpose of each program is, however, presented in Appendix II. Most of the

programs were intended to deal with the fine measurement data from COSMOS, when available, but were found to be useful also for the analysis of the coarse measurement data and the visual data on the geometric parameters for the distant clusters in this investigation and hence are included here.

The programs were designed to be as general as possible in order to have a fairly wide application. Although they were written with the purpose of the analysis of the properties of galaxies and of clusters in mind, the same programs may be used to investigate the properties of any object appearing on the plates (dwarf galaxies, star clusters, etc.).

For practical purposes, the programs were required to cope equally efficiently with any size of measured region, from a small area on a plate (having at most a few hundred images) up to the whole of a plate (with hundreds of thousands of images).

Altogether some thirty-five computer programs have been written. Their overall aim was directed towards detecting the presence of deviations in the data from a statistically random distribution. Output is obtained in both of two forms - numerical (frequency distributions, contingency tables, etc.) and graphical on the SD 4020 plotter.

III. DISTINGUISHING BETWEEN GALAXIES AND STARS

III. 1. Method

In order to use COSMOS effectively as a tool for exploring the Universe from analyses of the images of distant galaxies on photographic plates, satisfactory methods must be developed to enable the computer to distinguish automatically between the images of galaxies and those of stars.

The development of such methods from Coarse Measurement data is the subject of study in this chapter. The approach adopted is of a chronological description of the steps leading to the final adoption of a suitable working procedure. In this way the reason for the particular choice of method and experimental technique will become clear.

Galaxies are identifiable visually from stars on photographic plates by their generally tenuous appearance (odd shape and/or low surface brightness). These qualities distinguishing galaxy images may similarly be used by the computer for separating the two types.

It will be seen that the separation of galaxies and stars by shape is not a powerful means, at least from these measurements. At the faint end of the scale, non-circularity is blurred by the effects of seeing. At the bright end, the resolution is "burned out" since there are many star images with diffraction spikes which are obviously selected by shape criteria. In between, the extended nature of

galaxies is not general enough to have practical usage. On the other hand, the lower surface brightness (in general) of galaxy images is a more sensitive means for their separation.

Practical criteria have been developed allowing the computer to fit, completely automatically, a discrimination setting between galaxies and stars. The way in which this is carried out is described in this chapter along with tests on some preliminary data. Also described is the procedure adopted for allowing this setting to vary with variations in plate background. A computer program for carrying out all these operations on Coarse Measurement data has been written and its salient features are outlined. Finally, checks are made for systematic effects in the procedure with variations in threshold.

III. 2. Preliminary measurements from COSMOS

Early in November 1974, some Coarse Measurement measures in two areas, each about 7.5cm square, near the centre of the UK Schmidt Telescope plate number 149 were carried out by COSMOS. Details of plate 149 are given in Table 4; the limiting magnitude of the plate is estimated to be about $B \geqslant 23$ (Dodd et al. 1975).

A small region, about 1.5cm square, in one of the areas was chosen for detailed study and the Coarse Measurement data for the images detected by COSMOS, with area greater than 10 units above the threshold, was output to the line-printer for the purpose of optical identification. In retrospect, this artificial "cut" ($A > 10$)

on the images was too high. About 30% of images are below this point. It was satisfactorily established, however, that at present these smaller images cannot be unambiguously separated into galaxies and stars. Indeed some ambiguity persists for larger images. More work was required in optimising the choice of threshold before matters could be improved.

In all, 220 images, with area greater than 10 units above threshold, were detected by COSMOS in this region. These images were identified on the original plate and their type (star, galaxy, etc.) noted. Details of the optical identifications are given in Table 5. Wherever possible images were categorised; a few, however, eluded definite classification and are classified as "uncertain". From Table 5 it is seen that nearly 50% of these images are galaxies, the remainder comprising a number of categories - stars, double images of one sort or another, uncertain identifications and two data-processing faults. Real images were present on the plate at the positions of the faults; they had occurred in the data processing stage rather than in the measuring stage. Data processing faults in this sample account for 1% of the data and are unbiased with respect to image type (one image was a star, the other a galaxy). Modifications have since been made to eliminate as far as possible faults of this nature; it is safe to say, however, that at most only 1% of the galaxies are lost in this way.

The frequency of double images in this region is only about 1.5% of the total number of images. If double star images cannot be separated from galaxies, then the effect in this case is only about 2% on the galaxy statistics.

Table 4

Parameters for plate 149:-

Date taken:	2-3 September 1973
Emulsion:	Eastman Kodak IIIaJ, nitrogen sensitised
Filter:	Schott GG395
Exposure:	120 minutes
Plate centre:	R.A. (1973.5) $02^{h}42^{m}.0$
	Dec (1973.5) $-29^{o}54'$
Sky brightness:	B = 22.1
Limiting magnitude:	B $\geqslant$ 23

Table 5

Optical identifications:-

Type	Number	%
Galaxy	107	48.5
Star	89	40.5
Uncertain	19	8.5
Double star	2	1.0
Compound image (S + G)	1	0.5
Data processing fault	2	1.0
TOTAL	220	100.0

In Table 6 the Coarse Measurement parameters for each image are tabulated; column 1 contains a running count, column 2 the optical identifications (S for star, G for galaxy, PF for processing fault, SS for double star and SG for the superimposed star + galaxy), columns 3, 4 and 5 contain the parameters for minimum transmission (Tmin), area of image (in 8 μm x 8 μm squares) detected above threshold and the logarithm of the area respectively and column 6 contains the extents (in 8 μm increments) of the image in the X and Y directions respectively.

These parameters are sufficient for a crude examination of the shape and surface brightness properties of stars and galaxies. In this respect, examination of the distribution of the quantities area/extension area (i.e. area/(X-extent * Y-extent)) and diameter/greatest extent (i.e. (2 * $\sqrt{}$(area/π))/(greater of X-extent and Y-extent)) and the distribution of minimum transmission with size may prove of particular value.

In figure 1 the ratio of the area to the extension area is plotted against the ratio of diameter (defined as 2 * $\sqrt{}$(area/π)) to the greatest extent; plus-signs represent the optically identified galaxies, filled circles the optically identified stars, open circles the uncertain identifications, diagonal crosses the processing faults, 'S'-signs the double star images and the triangle represents the superimposed star + galaxy. The two arrows point to the position expected for a perfectly circular image measured with an infinitely small spot (area/extension area = π * $r^2/4r^2$, diameter/greatest extent = 2r/2r). Although there is a correlation between the two

Table 6

Parameters for the images detected by COSMOS

(1)	(2)	(3)	(4)	(5)	(6)	(7)	(8)	(9)
No.	Type	Tmin	Area	Log (area)	Extents	Tmin	Area	Log (area)
1	G	44	38	1.58	11 x 7			
2	G	39	39	1.59	7 x 8			
3	S	16	506	2.70	35 x 32	17	679	2.83
4	S	16	579	2.76	40 x 32	17	688	2.84
5	S	17	855	2.93	48 x 48	16	1046	3.02
6	G	43	45	1.65	8 x 7	41	60	1.78
7	S	47	21	1.32	5 x 5	48	31	1.49
8	S	36	35	1.54	7 x 7	39	44	1.64
9	S	23	72	1.86	9 x 11	24	85	1.93
10	S	45	23	1.36	6 x 5	47	30	1.48
11	S	17	994	3.00	48 x 47			
12	G	55	12	1.08	3 x 4	55	22	1.34
13	S	43	25	1.40	6 x 5	42	34	1.53
14	U	54	11	1.04	4 x 3	52	21	1.32
15	S	21	106	2.03	12 x 11	20	126	2.10
16	G	52	13	1.11	5 x 4	52	23	1.36
17	S	40	30	1.48	7 x 6	39	36	1.56
18	G	51	16	1.20	4 x 5			
19	PF	31	23	1.36	4 x 8			
20	PF	34	23	1.36	4 x 8			
21	G	55	12	1.08	5 x 4	55	25	1.40
22	S	23	87	1.94	11 x 10			
23	S	18	404	2.61	31 x 23	18	470	2.67
24	S	18	284	2.45	22 x 20	19	322	2.51
25	S	44	23	1.36	6 x 5	46	29	1.46
26	G	53	13	1.11	4 x 4	54	22	1.34
27	G	51	15	1.18	5 x 4	51	28	1.45
28	S	45	18	1.26	4 x 5	46	25	1.40
29	S	33	44	1.64	7 x 8	34	52	1.72
30	G	51	15	1.18	4 x 5	52	32	1.51
31	G	38	64	1.81	9 x 9	38	74	1.87
32	U	43	24	1.38	6 x 5	46	32	1.51
33	S	52	13	1.11	4 x 5	50	17	1.23
34	S	28	61	1.79	9 x 9	27	77	1.89
35	G	34	64	1.81	8 x 11	35	77	1.89
36	S	27	61	1.79	9 x 8	28	72	1.86
37	S	18	210	2.32	18 x 17	19	242	2.38
38	G	33	54	1.73	8 x 9	34	67	1.83
39	S	26	61	1.79	9 x 9	28	71	1.85
40	S	16	944	2.97	53 x 56	17	1107	3.04

Table 6 continued

(1) No.	(2) Type	(3) Tmin	(4) Area	(5) Log (area)	(6) Extents	(7) Tmin	(8) Area	(9) Log (area)
41	S	22	100	2.00	12 x 11	23	109	2.04
42	S	33	39	1.59	7 x 7	33	52	1.72
43	S	36	39	1.59	8 x 7	35	46	1.66
44	S	41	23	1.36	6 x 5	42	32	1.51
45	S	18	357	2.55	27 x 22	18	407	2.61
46	G	43	62	1.79	11 x 8	46	78	1.89
47	G	51	19	1.28	5 x 6			
48	S	36	34	1.53	6 x 7	35	44	1.64
49	G	50	24	1.38	7 x 6	52	39	1.59
50	G	50	20	1.30	5 x 5	51	28	1.45
51	S	17	540	2.73	37 x 33	18	612	2.79
52	S	27	60	1.78	9 x 8	28	71	1.85
53	G	49	16	1.20	4 x 5			
54	G	50	31	1.49	6 x 7	50	51	1.71
55	G	45	17	1.23	5 x 5	47	29	1.46
56	G	48	19	1.28	5 x 5	49	30	1.48
57	S	19	148	2.17	14 x 14	19	174	2.41
58	S	35	35	1.54	7 x 6	36	45	1.65
59	S	24	68	1.83	10 x 9			
60	S	40	21	1.32	5 x 6			
61	G	39	50	1.70	10 x 7			
62	S	40	26	1.41	6 x 5			
63	S	27	58	1.76	9 x 9	28	73	1.86
64	G	37	57	1.76	9 x 9	35	82	1.91
65	S	18	254	2.40	19 x 20	18	301	2.48
66	G	37	55	1.74	9 x 8	38	69	1.84
67	G	38	49	1.69	8 x 8			
68	S	51	13	1.11	4 x 4	50	20	1.30
69	G	43	35	1.54	7 x 6			
70	S	35	35	1.54	7 x 7	37	43	1.63
71	S	30	54	1.73	8 x 9	29	67	1.83
72	G	26	93	1.97	12 x 11	26	116	2.06
73	S	22	100	2.00	12 x 12	23	117	2.07
74	G	46	24	1.38	5 x 6	47	34	1.53
75	G	55	21	1.32	7 x 5	55	44	1.64
76	G	42	33	1.52	7 x 5	44	43	1.63
77	G	53	12	1.08	4 x 3	52	32	1.51
78	G	48	31	1.49	6 x 7	47	48	1.68
79	G	46	198	2.30	24 x 16	44	395	2.60
80	G	53	12	1.08	4 x 4	50	28	1.48
81	G	30	62	1.79	9 x 9	32	81	1.91
82	G	52	11	1.04	5 x 4			
83	G	54	13	1.11	4 x 4	57	23	1.36
84	G	44	34	1.53	6 x 8	46	49	1.69
85	S	18	310	2.49	22 x 21	18	372	2.57

Table 6 continued

(1) No.	(2) Type	(3) Tmin	(4) Area	(5) Log (area)	(6) Extents	(7) Tmin	(8) Area	(9) Log (area)
86	S	20	154	2.19	14 x 14	21	171	2.23
87	S	38	31	1.49	7 x 6	36	41	1.61
88	G	50	19	1.28	5 x 5	50	28	1.45
89	G	42	34	1.53	7 x 7	45	49	1.69
90	S	17	425	2.63	27 x 26			
91	G	50	19	1.28	5 x 5	51	36	1.56
92	G	46	51	1.71	9 x 9	47	74	1.87
93	G	55	12	1.08	5 x 4	56	35	1.54
94	S	18	808	2.91	48 x 46	17	1001	3.00
95	U	46	28	1.45	6 x 6	46	48	1.68
96	SS	20	176	2.25	15 x 17	20	202	2.31
97	G	25	111	2.05	13 x 11	25	121	2.08
98	G	20	216	2.33	15 x 20	20	260	2.41
99	G	34	70	1.85	9 x 9	31	104	2.02
100	S	47	17	1.23	5 x 4	47	23	1.36
101	G	44	26	1.41	5 x 7	44	37	1.57
102	G	33	65	1.81	9 x 10	33	76	1.88
103	G	53	14	1.15	5 x 4	52	30	1.48
104	S	49	16	1.20	4 x 4	48	29	1.46
105	G	28	75	1.88	10 x 10	28	98	1.99
106	G	46	33	1.52	8 x 7			
107	S	18	539	2.73	31 x 33	18	697	2.84
108	S	18	313	2.50	23 x 21	19	526	2.72
109	S	18	216	2.33	18 x 18	19	235	2.37
110	S	21	135	2.13	14 x 14			
111	G	42	64	1.81	8 x 12	42	91	1.96
112	S	18	463	2.67	32 x 26			
113	U	25	78	1.89	10 x 10	24	93	1.97
114	G	51	13	1.11	4 x 4	53	23	1.36
115	G	49	22	1.34	5 x 6	49	35	1.54
116	U	54	12	1.08	4 x 4	53	18	1.26
117	G	50	14	1.15	4 x 4	50	31	1.49
118	G	27	90	1.95	10 x 13	28	112	2.05
119	G	29	67	1.83	10 x 19	30	85	1.93
120	G	49	16	1.20	5 x 4	50	30	1.48
121	G	47	20	1.30	5 x 6	51	29	1.46
122	G	41	37	1.57	8 x 6	40	57	1.76
123	S	22	101	2.00	12 x 12	22	121	2.08
124	G	34	99	2.00	9 x 15	32	119	2.08
125	G	44	22	1.34	5 x 6	42	39	1.59
126	G	28	258	2.41	19 x 20	28	323	2.51
127	SS	18	467	2.67	26 x 29	18	518	2.71
128	S	40	29	1.46	6 x 7	39	35	1.54
129	U	31	43	1.63	7 x 7	33	55	1.74
130	G	55	11	1.04	4 x 4	52	17	1.23

Table 6 continued

(1) No.	(2) Type	(3) Tmin	(4) Area	(5) Log (area)	(6) Extents	(7) Tmin	(8) Area	(9) Log (area)
131	S	23	90	1.95	11 x 11	23	108	2.03
132	S	38	30	1.48	6 x 6			
133	G	42	33	1.52	6 x 8	43	51	1.71
134	S	30	50	1.70	8 x 8	30	56	1.75
135	G	52	12	1.08	3 x 4	54	22	1.34
136	G	33	97	1.99	10 x 11	32	133	2.12
137	S	40	24	1.38	5 x 5	40	36	1.56
138	S	34	37	1.57	6 x 7	36	47	1.67
139	U	38	31	1.49	6 x 6	39	40	1.60
140	U	42	30	1.48	7 x 6	42	41	1.61
141	S	24	79	1.90	10 x 10	23	88	1.94
142	U	47	18	1.26	5 x 5	46	26	1.41
143	S	21	110	2.04	11 x 13	21	131	2.12
144	S	32	47	1.67	8 x 9			
145	G	23	118	2.07	13 x 12	23	144	2.16
146	S	44	20	1.30	6 x 5			
147	G	54	12	1.08	4 x 4	52	34	1.53
148	U	49	15	1.18	4 x 4	48	24	1.38
149	G	33	74	1.87	11 x 9	34	101	2.00
150	G	48	34	1.53	7 x 6	47	46	1.66
151	G	49	17	1.23	5 x 5			
152	S	25	71	1.85	10 x 10	25	88	1.94
153	G	38	40	1.60	7 x 6	38	65	1.81
154	G	31	82	1.91	10 x 11	30	111	2.05
155	S	19	231	2.36	20 x 12	17	275	2.44
156	G	47	24	1.38	5 x 6	46	40	1.60
157	G	28	152	2.18	14 x 15	25	222	2.35
158	S	22	94	1.97	11 x 11	22	117	2.07
159	G	35	61	1.79	11 x 8	32	82	1.91
160	G	42	37	1.57	7 x 8	42	59	1.77
161	G	36	47	1.67	8 x 8	34	71	1.85
162	G	46	29	1.46	7 x 6	47	57	1.76
163	S	26	66	1.82	9 x 9	25	84	1.92
164	S	37	29	1.46	7 x 6	39	39	1.59
165	G	37	50	1.70	8 x 8	37	71	1.85
166	G	42	37	1.57	7 x 8	43	54	1.73
167	U	35	38	1.58	7 x 7	38	53	1.72
168	U	38	26	1.41	5 x 6	41	39	1.59
169	U	48	13	1.11	4 x 4	47	23	1.36
170	U	40	28	1.45	5 x 9	40	75	1.88
171	G	43	28	1.45	6 x 6	44	43	1.63
172	G	27	106	2.03	15 x 9	26	135	2.13
173	U	36	38	1.58	7 x 7	36	54	1.73
174	G	50	16	1.20	4 x 5			
175	U	36	40	1.60	7 x 7	35	51	1.71

Table 6 continued

(1) No.	(2) Type	(3) Tmin	(4) Area	(5) Log (area)	(6) Extents	(7) Tmin	(8) Area	(9) Log (area)
176	S	40	31	1.49	6 x 6	40	37	1.57
177	G	51	19	1.28	5 x 5	52	39	1.59
178	S	32	49	1.69	8 x 8	30	61	1.79
179	S	20	141	2.15	14 x 14			
180	G	38	40	1.60	7 x 8	38	59	1.77
181	S	39	31	1.49	6 x 7	36	43	1.63
182	U	42	23	1.36	6 x 5	40	36	1.56
183	S	45	17	1.23	5 x 5	42	28	1.48
184	S	20	199	2.30	17 x 16	18	238	2.38
185	G	46	34	1.53	7 x 6	46	59	1.77
186	S	18	303	2.48	22 x 21	18	360	2.56
187	G	47	18	1.26	5 x 5	47	31	1.49
188	G	48	19	1.28	5 x 5			
189	S	42	25	1.40	7 x 5	42	32	1.51
190	S	26	62	1.79	9 x 8	26	75	1.88
191	S	18	210	2.32	17 x 18			
192	G	33	55	1.74	9 x 8			
193	G	51	15	1.18	4 x 4	49	24	1.38
194	G	31	63	1.80	11 x 9			
195	G	49	24	1.38	6 x 6	46	42	1.62
196	G	51	14	1.15	4 x 4	52	30	1.48
197	G	43	30	1.48	6 x 7	43	42	1.62
198	G	54	12	1.08	5 x 4	52	23	1.36
199	G	46	34	1.53	7 x 7	45	53	1.72
200	S	24	82	1.91	10 x 10	23	102	2.01
201	G	52	13	1.11	4 x 5			
202	G	54	17	1.23	6 x 4	54	47	1.67
203	S	18	478	2.68	32 x 28	18	568	2.75
204	S	33	42	1.62	8 x 8	30	55	1.74
205	S	38	34	1.53	7 x 7	38	44	1.64
206	G	53	11	1.04	4 x 4	53	23	1.36
207	G	48	20	1.30	5 x 6	48	32	1.51
208	G	27	79	1.90	9 x 11			
209	G	28	85	1.93	9 x 12	28	111	2.05
210	S	33	43	1.63	8 x 8	31	53	1.72
211	G	52	13	1.11	4 x 4	49	21	1.32
212	U	26	73	1.86	10 x 9	26	90	1.95
213	S	18	550	2.74	36 x 33	18	657	2.82
214	G	42	34	1.53	6 x 8			
215	S	44	18	1.26	5 x 5	43	26	1.41
216	SG	31	56	1.75	11 x 8			
217	S	19	552	2.74	37 x 29			
218	S	23	97	1.99	11 x 11	22	111	2.05
219	G	52	13	1.11	4 x 4			
220	U	23	109	2.04	12 x 12			

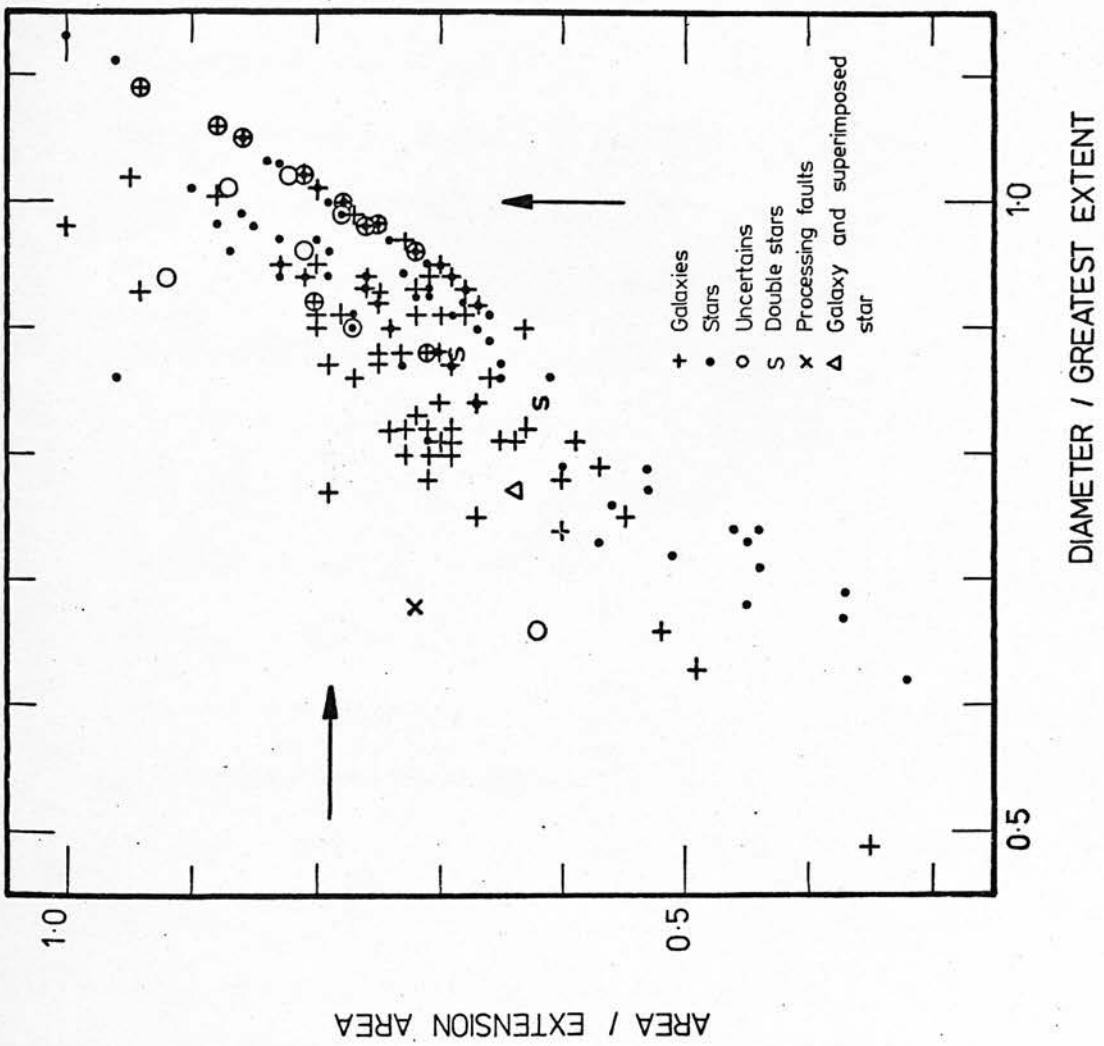

Figure 1. Plot for area/extension area versus diameter/greatest extent from the Coarse Measurement data for the images detected by COSMOS with area greater than 10 units above the threshold.

ratios, the diagram is a confused mass of points with no clear distinction between stars and galaxies.

The plots for area/extension area versus logarithm of the area, and diameter/greatest extent versus logarithm of the area, are shown in figures 2 and 3 respectively. The same convention is used with respect to symbols. The lines parallel to the log area axes represent the distributions for perfectly circular images. The points are seen to fluctuate quite wildly about the lines, but again there is no definite separation between the galaxies and stars.

Figures 1, 2 and 3 demonstrate quite markedly that it is impractical to use shape criteria from these measurements to distinguish between the images of galaxies and those of stars.

In figure 4 the minimum transmission within each image is plotted against the logarithm of image area. In this case, there does exist a clear separation between stars and galaxies, at least for much of the diagram, indicating that a surface brightness test is a much more powerful means for the separation of stars and galaxies.

It is worthwhile to point out the salient features of this diagram:-

1) The relationship between minimum transmission and log area for stars is quite linear over much of the diagram and only deviates from linearity at the faint end and where stars begin to saturate. Unfortunately, calibration of the minimum transmission parameter was not obtained with these measurements and so it is not known what this means in terms of transmission.

2) The points for galaxies tend to lie above the curve for stars due to their generally lower surface brightness. Some ambiguity does exist, however, and is most persistent at the faint and bright ends. Over the rest of the diagram a fairly good separation exists between the galaxies and stars.

3) The data processing faults produce points to the left of the star curve in this figure. Such faults are therefore automatically eliminated from the data along with the stars when only the galaxies are to be selected.

4) The double star images produce points on the star curve. This is extremely important since it means that many of these double star images will be thrown out with the stars. The advantages of such a capability are far-reaching especially for projects where the numbers of double images may be quite high, e.g. when investigating the distribution of the obscuration in our own Galaxy (near the Galactic plane) from counts of stars and faint galaxies, and in other nearby galaxies (e.g. the Magellanic Clouds), where the star densities are high.

5) Some galaxies are quite compact (i.e. have exceptionally high surface brightness for their size) and are thus not easily separable from the star images.

6) An envelope may be drawn around the star distribution thus allowing a practical means for the separation of galaxy images from the stars.

Such an envelope was drawn by hand, and from this, points were obtained which were used in a computer polyfitting procedure. The curve in figure 4 is the resulting computer-fitted envelope (with polynomial of order 3) to the star distribution. The galaxy points,

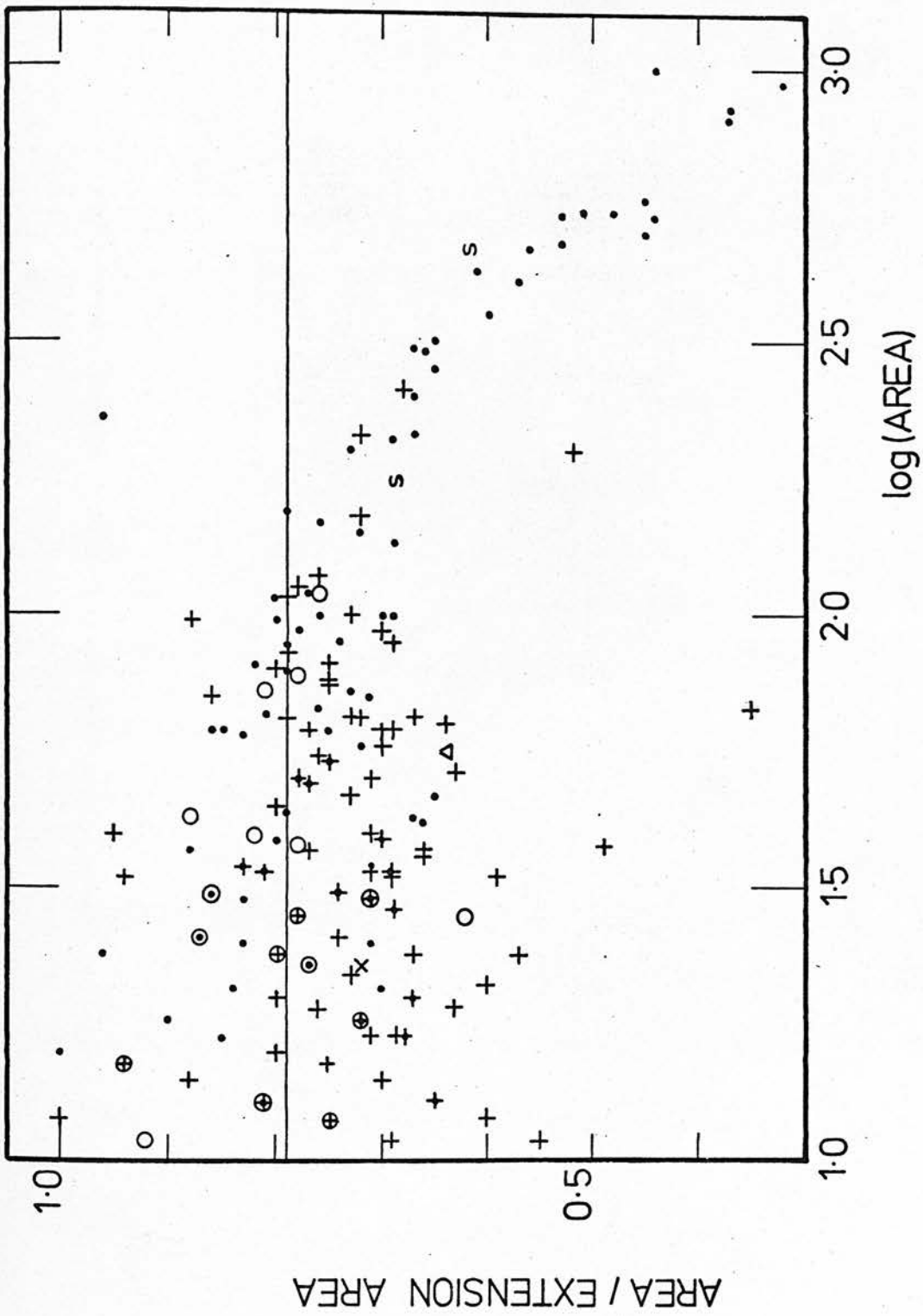

Figure 2. Plot for area/extension area versus the logarithm of area from the data showing no clear segregation of the images of galaxies from those of stars. The symbols are the same as for figure 1.

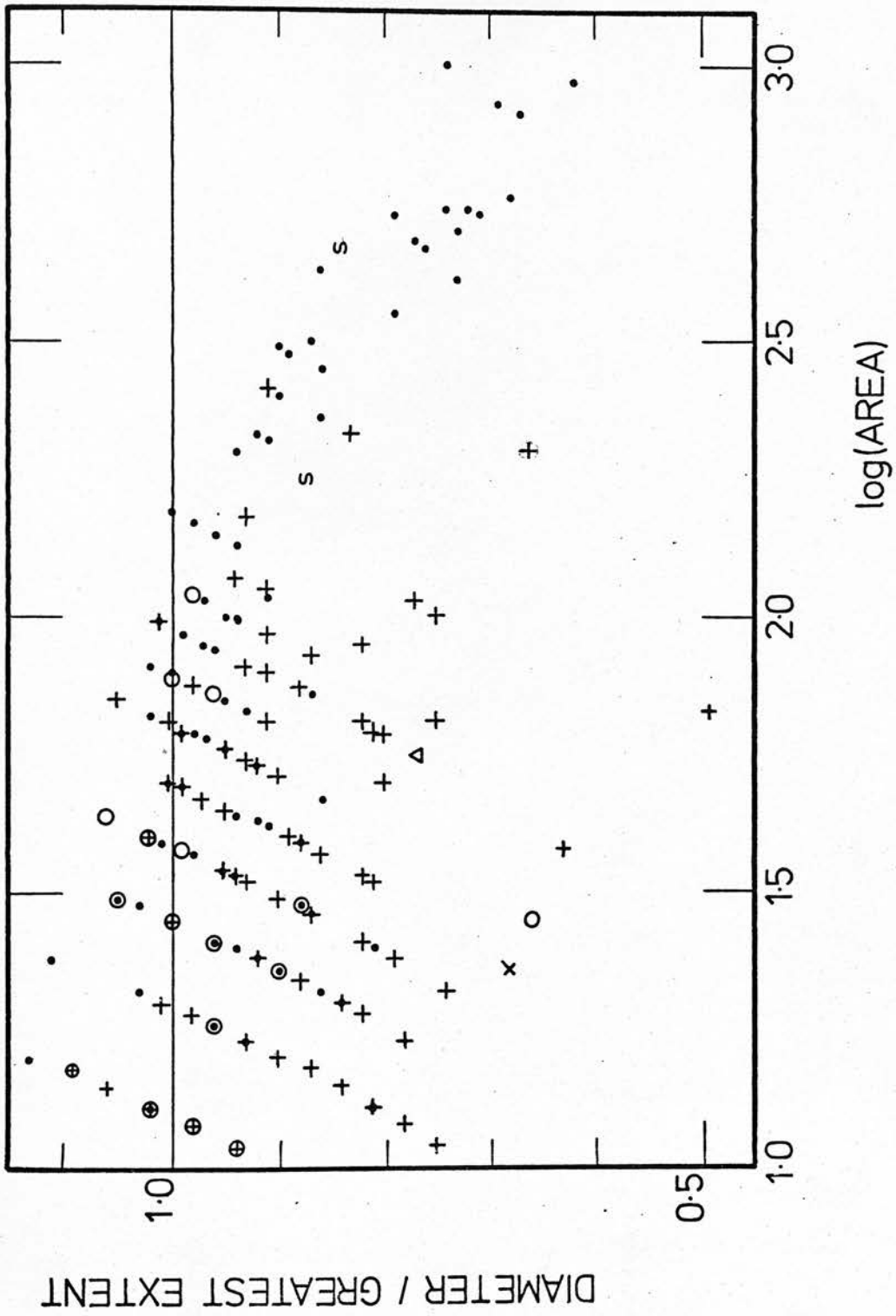

Figure 3. Plot for diameter/greatest extent versus the logarithm of area from the data showing again no clear segregation of the images of galaxies from those of stars. The symbols are the same as in figure 1.

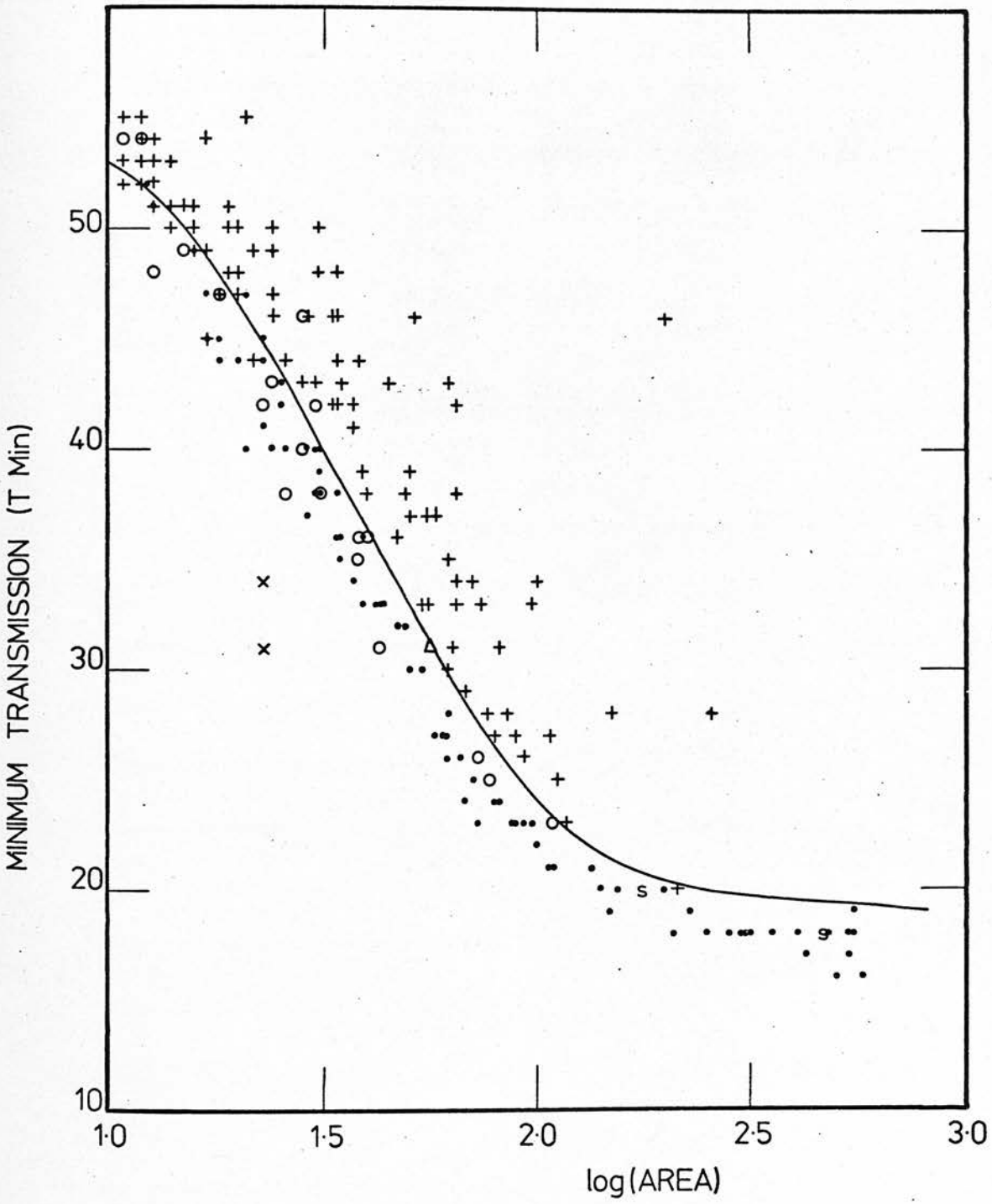

Figure 4. Plot for minimum transmission (T_{min}) versus the logarithm of area from the data showing, in this case, a clear separation between the images of galaxies and stars over much of the diagram. The symbols are the same as in figure 1.

in general, lie above the curve, the star points lie below the curve. The distribution of images above and below the curve is as follows:

above the curve:- 97 galaxies 3 stars 4 uncertains

below the curve:- 10 galaxies 86 stars 15 uncertains 2 double stars

2 processing faults superimposed star + galaxy

Thus in this preliminary attempt by the computer to fit an envelope around the star distribution the results are:- 9% of the galaxies are lost to the stars, but of the images in the galaxy category 93% are definitely galaxies, 3% are stars and 4% are uncertains.

III. 3. Comparison with measurements at a different threshold

The logical next step in the investigation is to compare the results of the last section with measurements made at a different threshold setting - if possible at a higher transmission. Several effects are to be expected from increasing the threshold transmission setting to nearer the transmission of the plate background. Imagine, for the sake of argument, a star image and a galaxy image on the plate with the same central density. Both have the same value for minimum transmission when measured by the machine (assuming no fluctuations such as variation in the light intensity from the C.R.T.). Suppose, also, that when measured at the first (lower transmission) threshold the machine skips over most of the outer faint envelope of the galaxy, detecting mainly its bright central core. Both images have more or less the same size above threshold and are indistinguishable on the plot of minimum transmission against log area. When the threshold

transmission setting is increased, the star and galaxy are now measured with different sizes since the galaxy profile falls of less steeply, due to the faint envelope, than does the star profile. The images which were inseparable when measured at the lower transmission threshold are now more easily separated on the Tmin versus log area plot.

Thus by increasing the threshold transmission setting several things are observed:-

1) More images are detected.

2) The detected size of an image is increased.

3) There is a better separation between galaxies and stars on the Tmin versus log area plot due to the more diffuse nature of the galaxy images.

4) The ambiguity between galaxy and star images is diminished.

The second set of measurements on plate 149 was made at a higher transmission threshold setting. There was considerable overlap with the first area and the small region used in the analysis of the last section was included in the overlap. Comparison of the two sets of measurements on the same images is therefore possible and the effect of increasing the threshold transmission setting investigated.

Unfortunately there was a fault in the processing of this second set of data and as a result some images were lost. This loss was, however, unbiased with respect to image type (star, galaxy, etc.) and it was still possible to use the remaining data. There were 184 images left in common with the first set.

In columns 7, 8 and 9 of Table 6 the values for minimum transmission, area and the logarithm of area respectively for the images present in the second set are tabulated. The plot of minimum transmission versus log area for these measurements is represented in figure 5. The usual convention is maintained for symbols. The differences between this figure and figure 4 are immediately apparent. The points show a better separation between galaxies and stars. The curve in the figure again represents a computer-fitted envelope to the star distribution, obtained from first drawing an envelope by hand. The distribution of images in the diagram is as follows:-

above the curve:- 82 galaxies 3 stars 7 uncertains

below the curve:- 6 galaxies 75 stars 18 uncertains 2 double stars

Thus, in this case, 7% of the galaxies are lost to the stars. Of the images falling into the galaxy category, 89% are definitely galaxies, 3% are stars and 7% are uncertains.

The results of increasing the threshold transmission to nearer the plate background are indicated in figures 4 and 5 and in the above numbers. The separation between galaxies and stars is increased with the result that the detection of galaxies is improved. The contamination by stars in the galaxy category remains the same but more objects of uncertain identification are thrown over into the galaxy side of the discrimination curve.

III. 4. Summary and discussion

It is worthwhile at this point to summarise the main conclusions which have been reached so far:-

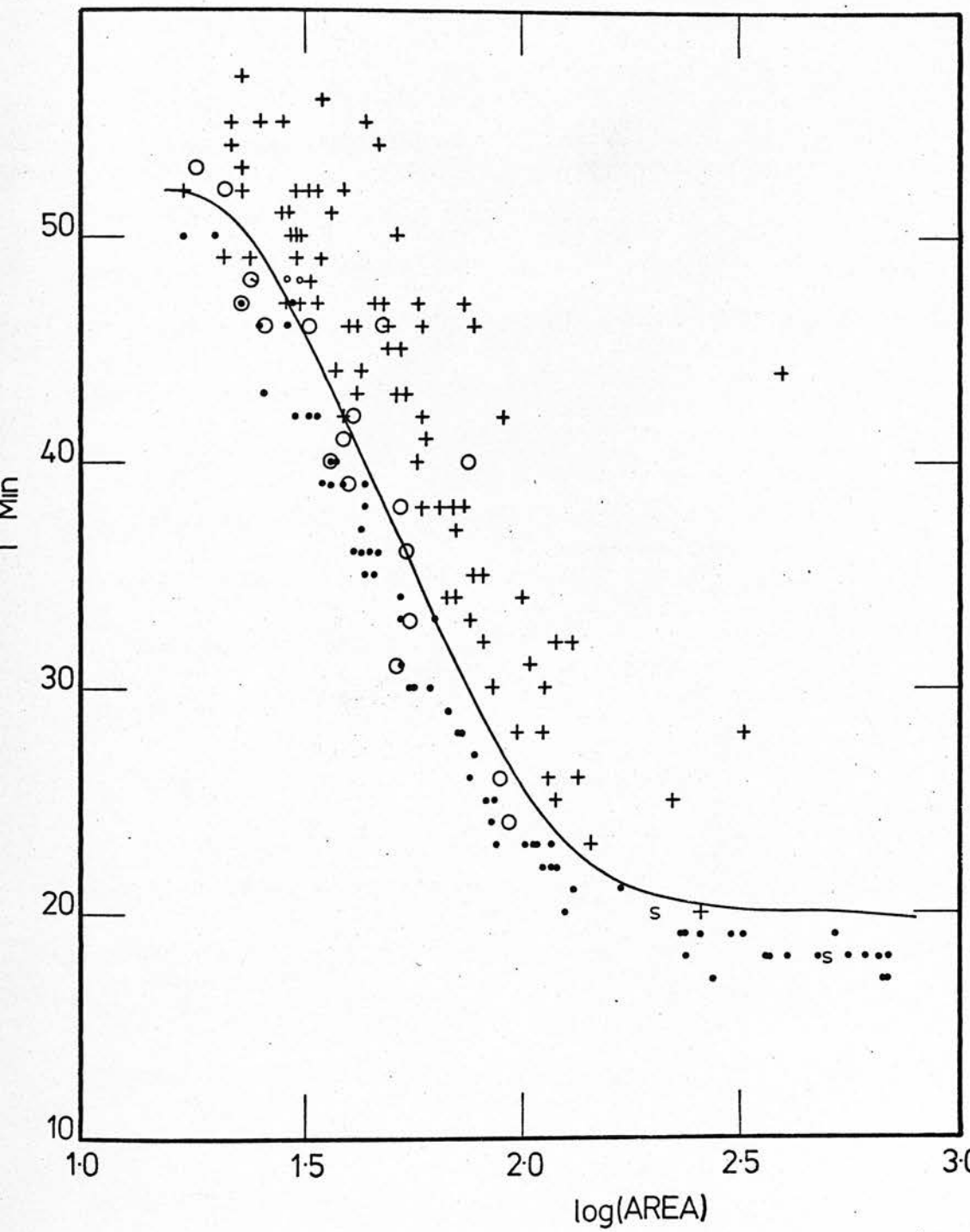

Figure 5. Plot for T_{min} versus the logarithm of area for the same images but measured at a different threshold transmission setting indicating that as the threshold transmission setting is increased, the separation between stars and galaxies is improved. The symbols are the same as in figure 1.

1) Galaxies are distinguishable from stars on photographic plates and it is possible to separate them using Coarse Measurement data from the COSMOS machine.

2) The surface brightness test is a much more powerful means for distinguishing galaxies from stars than the shape test.

3) On a plot of minimum transmission versus the logarithm of the area, the galaxies tend to lie away from the distribution for stars.

4) A discrimination envelope may be fitted around the star distribution. The results show that less than 10% of the galaxies are lost in this way. Of the images falling into the galaxy category, we can be 90% confident that these are indeed the images of galaxies.

5) By increasing the threshold transmission setting, the separation between galaxies and stars is increased, more galaxies are separated out and more objects of uncertain identification fall into the galaxy component.

More work will have to be done in finding the optimum threshold setting for future measurements. This would involve several measurements of the same region at different thresholds. Since the time-scale for this investigation, however, does not permit a digression of this nature, use is made of the material available.

One major problem which had to be tackled is that the plate background is significantly non-uniform over the plate. There are essentially two types of background variation:-

a) A constant decrease in density from the plate centre out to the edge. This is a serious problem resulting in a drop in the limiting magnitude over the plate from the centre outwards. The consequences for the

interpretation of galaxy counts over widely separated parts of the plate are important.

b) Small scale variability due to a number of causes - variation in emulsion sensitivity, non-uniform developing, static effects, nebulosity, image ghosts, bright star halos, variations around bright galaxies due to extensive faint envelopes, etc.

In order to combat these varying background effects, the COSMOS machine software was arranged to produce a varying threshold, based on an extrapolation from previous scans. The varying threshold follows as closely as possible changes in plate transmission across the region being measured. The parameters for each image are measured relative to the background local to that image. There are, of course, problems with the technique and these are brought to light in the next section.

III. 5. Measurements with the varying threshold technique

Measurements were carried out with COSMOS on a 7.5cm square region on plate 149 using the varying threshold technique. The galaxy/star separation criteria must obviously vary with the variation in threshold. There are several questions to be answered. How frequently does the threshold change? How critically does the change in galaxy/star separation criteria depend on the change in threshold (i.e. could the same criteria be used on adjacent thresholds)? Can a procedure be found by which the computer may automatically determine a set of parameters for the separation of stars and galaxies for any threshold and hence obtain a set of similar criteria with

variable parameters related to the different thresholds (i.e. can we obtain a family of discrimination curves, each one for a different threshold)? An achievement of this nature would be important and would bring the completely automatic separation of stars and galaxies into reality.

There were, again, some problems with the machine control software in these measurements. Modifications have since been made by the COSMOS group to overcome the difficulties. The first of these was that the threshold was allowed to fluctuate quite sharply over very short distances. A modification has since been introduced to dampen such sharp fluctuations.

Another problem, yet to be satisfactorily investigated, is that the threshold is very often quite different at the same scan but in adjacent lanes. This is quite serious for images split between lanes where the detected area may consequently be quite extensive in one lane but truncated in the other. A measure of the effect on the Coarse Measurement parameters for images may be obtained on comparing scans of the same region 90^{o} out of phase.

Finally, a problem is encountered on scanning through large images, such as bright stars with diffraction spikes and halos or bright galaxies with extensive envelopes. The threshold is extrapolated through such an image, giving quite nonsensical threshold values and also outputting hundreds of little "images" (due to noise) around the image. A modification has since been made to introduce a cut-off in the threshold extrapolation when a sufficiently dark threshold is encountered. As for the production of hundreds of single

increment area images, this still remains a problem. These problems are, of course, the responsibility of the COSMOS group but they affect the work being described in this thesis.

The fact that the threshold fluctuated quite sharply over short distances in these measurements meant that it was rather difficult to select only those images which had been measured at the same threshold. This in fact provided the opportunity for investigating the effect of compounding images over two or three different threshold levels. In selecting suitable regions for study, however, care had to be taken to ensure that the threshold levels were not varying too quickly to result in the inclusion of images over widely separated thresholds.

The procedure was the same as before, e.g. the images were identified on the original plate, etc. This time, however, no artificial cut in the image sizes was introduced; everything detected by COSMOS was included. In all 5 areas, each 1cm square, at different points in the 7.5cm square region, were examined in detail.

For the purpose of illustrating the results at different thresholds, the data for only two of these areas are presented here. Inclusion of the data for all the regions would serve no useful purpose and would be, in the main, repetitive. The results for all regions are summarised, however, in a later section.

In Table 7 the optical identifications for the images in the first area are presented. These represent a detection rate of 100% for the COSMOS machine; every object on the plate (apart from individual grains) was detected, although many of the galaxies were

detected with an area of only 1 unit above the threshold. Clumps of grains were also detected, and so these introduce "noise" into the statistics. Image identifications were repeated at a later date on the same objects in order to place confidence limits. It was found that 9 objects were given a different classification in the second set. The optical identifications are therefore good to the 94% confidence level.

In the sample, the galaxies account for nearly 60% of the images and there are about 2.5 times as many galaxies as stars. An important contribution to the data comes from plate flaws and noise (8%). The noise is mainly due to background variations around bright stars, diffraction spikes, and bright galaxies. It is interesting to note that the numbers of images due to noise and plate flaws is not far from what we might expect from a statistical ($\sqrt{N}$) fluctuation ($\sqrt{162} = 12.7$).

In Table 8 the parameters for each of the images are tabulated. The usual convention is maintained for the type-abbreviations but PF is now used to represent plate flaws and N is used to represent images due to noise. The plot of minimum transmission versus log area for these images is shown in figure 6; the same convention is also maintained for symbols except for the diagonal crosses which now represent points due to plate flaws and noise.

No separation between stars and galaxies is possible below log area = 0.9 and so the lower bound for figure 6 is taken at the point log area = 0.8. One point, representing a plate flaw, clearly falls well below the star curve and thus some of these flaws may easily be eliminated when selecting galaxies. On the whole, this

diagram representing the compound of images distributed over two or three threshold levels is not very much different from figures 4 and 5. This observation will prove useful if different threshold levels have to be taken together to produce separation criteria.

The optical identifications and Coarse Measurement data for the images in the second area are tabulated in Tables 9 and 10. The corresponding plot for minimum transmission versus log area is shown in figure 7. The characteristics of this diagram are the same as in the others, viz. the galaxies tend to lie above the curve for the stars and some points for plate flaws and noise fall below the star curve.

The variations due to threshold changes from one region to another are obvious from figures 6 and 7. A crude attempt to establish related separation criteria by scaling the star envelope of figure 6 up to that of figure 7 was tried but failed. The galaxy/star separation envelope displays not only a difference in scaling from one region to another but also a rotation effect.

The method for establishing separation criteria which has been developed is to calculate a whole family of separation curves, each one for a particular threshold value. The separation criteria are exactly the same in each case, only the parameters determining the actual properties of the curve are different. The method by which the curves are determined is now described.

Table 7

Identifications for images in the first region:-

Type	Number	%
Galaxies	94	58
Stars	38	23.5
Uncertains	15	9.5
Noise	10	6
Plate flaws	3	2
Double stars	2	1
TOTAL	162	100

Table 8

Coarse Measurement parameters for the images in the first region.

No.	Type	Tmin	Area	Log(A)	No.	Type	Tmin	Area	Log(A)
1	G	45	2	0.30	41	G	42	15	1.18
2	G	47	1	0.00	42	G	42	15	1.18
3	G	48	1	0.00	43	G	44	4	0.60
4	S	48	1	0.00	44	G	46	6	0.78
5	G	43	15	1.18	45	G	47	1	0.00
6	U	38	17	1.23	46	G	44	9	0.95
7	S	15	102	2.01	47	G	42	16	1.20
8	G	39	17	1.23	48	G	32	94	1.97
9	G	40	16	1.20	49	G	36	32	1.51
10	G	38	23	1.36	50	G	44	14	1.15
11	G	43	12	1.08	51	G	39	24	1.38
12	G	46	8	0.90	52	U	33	30	1.48
13	G	39	23	1.36	53	U	34	27	1.43
14	S	19	75	1.88	54	G	42	13	1.11
15	S	20	78	1.89	55	G	27	83	1.92
16	G	47	1	0.00	56	PF	41	11	1.04
17	S	26	42	1.62	57	G	45	1	0.00
18	G	46	2	0.30	58	U	45	1	0.00
19	S	32	31	1.49	59	U	41	10	1.00
20	G	46	1	0.00	60	N	46	1	0.00
21	S	12	412	2.61	61	N	45	1	0.00
22	G	38	38	1.58	62	N	46	2	0.30
23	G	35	53	1.72	63	G	36	27	1.43
24	S	20	77	1.89	64	G	36	60	1.78
25	G	48	1	0.00	65	S	13	337	2.53
26	G	42	12	1.08	66	S	38	20	1.30
27	S	43	10	1.00	67	G	24	77	1.89
28	S	25	56	1.75	68	S	42	9	0.95
29	S	31	34	1.53	69	U	16	119	2.08
30	G	44	7	0.85	70	S	25	52	1.72
31	G	46	1	0.00	71	U	45	2	0.30
32	U	23	42	1.62	72	S	26	53	1.72
33	PF	19	15	1.18	73	G	42	16	1.20
34	S	12	179	2.25	74	S	23	56	1.75
35	S	41	12	1.08	75	G	42	13	1.11
36	U	46	7	0.85	76	G	18	130	2.11
37	N	45	2	0.30	77	G	39	36	1.56
38	N	41	6	0.78	78	G	19	99	2.00
39	N	46	1	0.00	79	S	13	239	2.38
40	G	44	5	0.70	80	U	44	6	0.78

Table 8 continued

No.	Type	Tmin	Area	Log(A)	No.	Type	Tmin	Area	Log(A)
81	U	46	2	0.30	122	G	14	243	2.39
82	G	43	9	0.95	123	S	35	23	1.36
83	S	26	52	1.72	124	G	44	1	0.00
84	S	47	1	0.00	125	S	12	631	2.80
85	G	38	30	1.48	126	N	44	1	0.00
86	G	31	48	1.68	127	S	12	532	2.73
87	G	46	1	0.00	128	N	45	2	0.30
88	S	35	25	1.40	129	G	36	27	1.43
89	G	32	39	1.59	130	G	43	9	0.95
90	G	24	81	1.91	131	G	29	49	1.69
91	G	38	25	1.40	132	S	16	117	2.07
92	G	47	1	0.00	133	G	22	124	2.09
93	SS	13	519	2.72	134	G	46	1	0.00
94	N	40	4	0.60	135	G	42	21	1.32
95	S	16	106	2.03	136	G	45	8	0.90
96	S	22	69	1.84	137	G	13	323	2.51
97	S	31	41	1.61	138	U	37	16	1.20
98	G	28	49	1.69	139	G	44	2	0.30
99	G	31	52	1.72	140	G	23	82	1.91
100	S	17	102	2.01	141	G	38	20	1.30
101	G	42	12	1.08	142	G	45	5	0.70
102	S	28	45	1.65	143	G	30	79	1.90
103	SS	13	201	2.30	144	PF	46	1	0.00
104	U	46	1	0.00	145	G	34	38	1.58
105	N	44	3	0.48	146	G	20	119	2.08
106	S	17	100	2.00	147	G	38	29	1.46
107	G	46	2	0.30	148	G	45	2	0.30
108	G	38	20	1.30	149	G	45	3	0.48
109	G	43	12	1.08	150	G	32	32	1.51
110	G	41	17	1.23	151	U	39	16	1.20
111	G	41	16	1.20	152	S	29	43	1.63
112	G	40	19	1.28	153	G	31	55	1.74
113	S	30	41	1.61	154	G	41	24	1.38
114	G	44	5	0.70	155	S	38	17	1.23
115	S	23	58	1.76	156	G	35	34	1.53
116	G	39	26	1.41	157	U	40	11	1.04
117	G	38	22	1.34	158	U	40	11	1.04
118	G	39	21	1.32	159	G	37	28	1.45
119	G	45	8	0.90	160	G	38	56	1.75
120	G	31	42	1.62	161	S	39	13	1.11
121	G	33	38	1.58	162	G	48	3	0.48

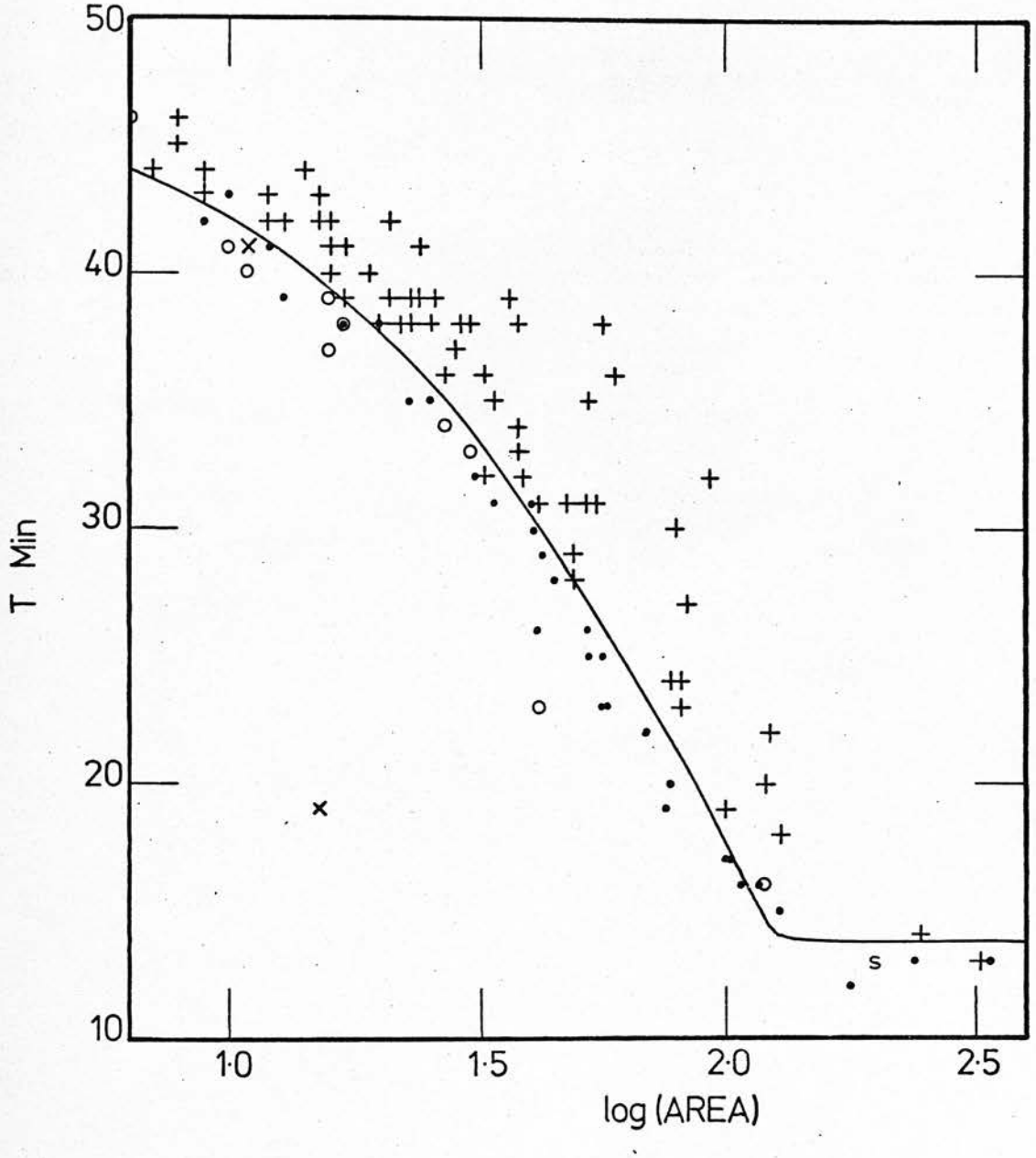

Figure 6. Plot for T_{min} versus logarithm of area for the images in the first region. The symbols are the same as in figure 1 apart from the diagonal crosses which are now used to represent images due to noise and plate flaws.

Table 9

Identifications for images in the second region:-

Type	Number	%
Galaxies	103	60
Stars	42	24.5
Uncertains	13	7.5
Noise	11	6.5
Plate flaws	3	1.5
Double stars	0	0
TOTAL	172	100

Table 10

Coarse Measurement parameters for the images in the second region

No.	Type	Tmin	Area	Log(A)	No.	Type	Tmin	Area	Log(A)
1	S	30	48	1.68	44	G	48	11	1.04
2	S	16	166	2.22	45	G	35	45	1.65
3	G	46	22	1.34	46	G	38	40	1.60
4	S	20	86	1.93	47	G	26	182	2.26
5	G	45	13	1.11	48	G	42	18	1.26
6	G	40	31	1.49	49	G	34	48	1.68
7	S	18	97	1.99	50	G	49	5	0.70
8	S	41	24	1.38	51	G	33	45	1.65
9	G	43	23	1.36	52	N	41	7	0.85
10	G	41	37	1.57	53	S	48	3	0.48
11	U	32	44	1.64	54	G	28	85	1.93
12	G	44	26	1.41	55	G	43	15	1.18
13	G	42	22	1.34	56	G	16	456	2.66
14	G	44	16	1.20	57	S	18	109	2.04
15	G	50	3	0.48	58	S	31	42	1.62
16	G	47	18	1.26	59	G	40	64	1.81
17	N	52	3	0.48	60	S	29	42	1.62
18	G	52	3	0.48	61	G	26	96	1.98
19	G	50	3	0.48	62	S	23	69	1.84
20	G	35	147	2.17	63	G	29	103	2.01
21	G	45	11	1.04	64	G	40	43	1.63
22	S	28	43	1.63	65	S	25	72	1.86
23	G	39	47	1.67	66	G	47	14	1.15
24	S	17	113	2.05	67	G	47	11	1.04
25	S	48	5	0.70	68	G	48	5	0.70
26	G	45	13	1.11	69	G	39	33	1.52
27	S	21	84	1.92	70	G	49	1	0.00
28	G	50	1	0.00	71	S	45	11	1.04
29	G	24	201	2.30	72	G	47	12	1.08
30	G	33	54	1.73	73	G	48	5	0.70
31	G	46	19	1.28	74	G	45	11	1.04
32	S	39	29	1.46	75	G	43	21	1.32
33	N	49	1	0.00	76	G	43	15	1.18
34	N	51	1	0.00	77	G	45	19	1.28
35	N	51	1	0.00	78	S	40	23	1.36
36	N	49	4	0.60	79	S	27	55	1.74
37	G	47	15	1.18	80	G	49	4	0.60
38	G	48	11	1.04	81	G	51	1	0.00
39	U	35	32	1.51	82	G	50	6	0.78
40	S	18	113	2.05	83	S	16	153	2.18
41	N	37	9	0.95	84	S	28	50	1.70
42	G	46	16	1.20	85	G	27	118	2.07
43	S	22	83	1.92	86	S	30	46	1.66

Table 10 continued

No.	Type	Tmin	Area	Log(A)	No.	Type	Tmin	Area	Log(A)
87	G	51	1	0.00	130	U	45	14	1.15
88	S	20	85	1.93	131	S	19	84	1.92
89	G	46	11	1.04	132	G	49	9	0.95
90	G	40	35	1.54	133	G	44	19	1.28
91	S	15	222	2.35	134	G	50	1	0.00
92	G	49	2	0.30	135	G	40	28	1.45
93	G	25	130	2.11	136	S	26	54	1.73
94	G	41	24	1.38	137	S	22	72	1.86
95	G	45	16	1.20	138	S	12	656	2.82
96	G	20	221	2.34	139	G	50	3	0.48
97	S	14	293	2.47	140	U	32	46	1.66
98	G	43	48	1.68	141	G	48	10	1.00
99	PF	39	15	1.18	142	U	39	27	1.43
100	G	21	124	2.09	143	G	49	7	0.85
101	G	19	110	2.04	144	U	42	24	1.38
102	G	44	19	1.28	145	G	52	1	0.00
103	G	44	15	1.18	146	S	16	153	2.18
104	G	47	14	1.15	147	S	16	127	2.10
105	G	46	10	1.00	148	G	44	24	1.38
106	U	37	32	1.51	149	G	49	1	0.00
107	N	51	1	0.00	150	G	50	1	0.00
108	G	51	1	0.00	151	N	50	1	0.00
109	S	18	118	2.07	152	U	49	10	1.00
110	S	21	66	1.82	153	G	44	14	1.15
111	G	48	6	0.78	154	G	44	12	1.08
112	U	42	12	1.08	155	U	32	40	1.60
113	PF	39	15	1.18	156	G	49	7	0.85
114	PF	43	5	0.70	157	G	48	7	0.85
115	S	38	25	1.40	158	G	45	19	1.28
116	G	23	84	1.92	159	S	14	314	2.50
117	N	41	7	0.85	160	S	16	117	2.07
118	G	42	47	1.67	161	G	49	3	0.48
119	G	28	56	1.75	162	U	46	14	1.15
120	G	31	52	1.72	163	G	45	24	1.38
121	S	17	108	2.03	164	G	46	10	1.00
122	N	48	6	0.78	165	S	34	37	1.57
123	S	14	222	2.35	166	G	40	31	1.49
124	U	39	28	1.45	167	G	36	56	1.75
125	G	45	18	1.26	168	G	40	62	1.79
126	G	45	5	0.70	169	G	14	467	2.67
127	G	44	20	1.30	170	U	19	123	2.09
128	G	51	1	0.00	171	S	15	230	2.36
129	G	32	40	1.60	172	G	49	13	1.11

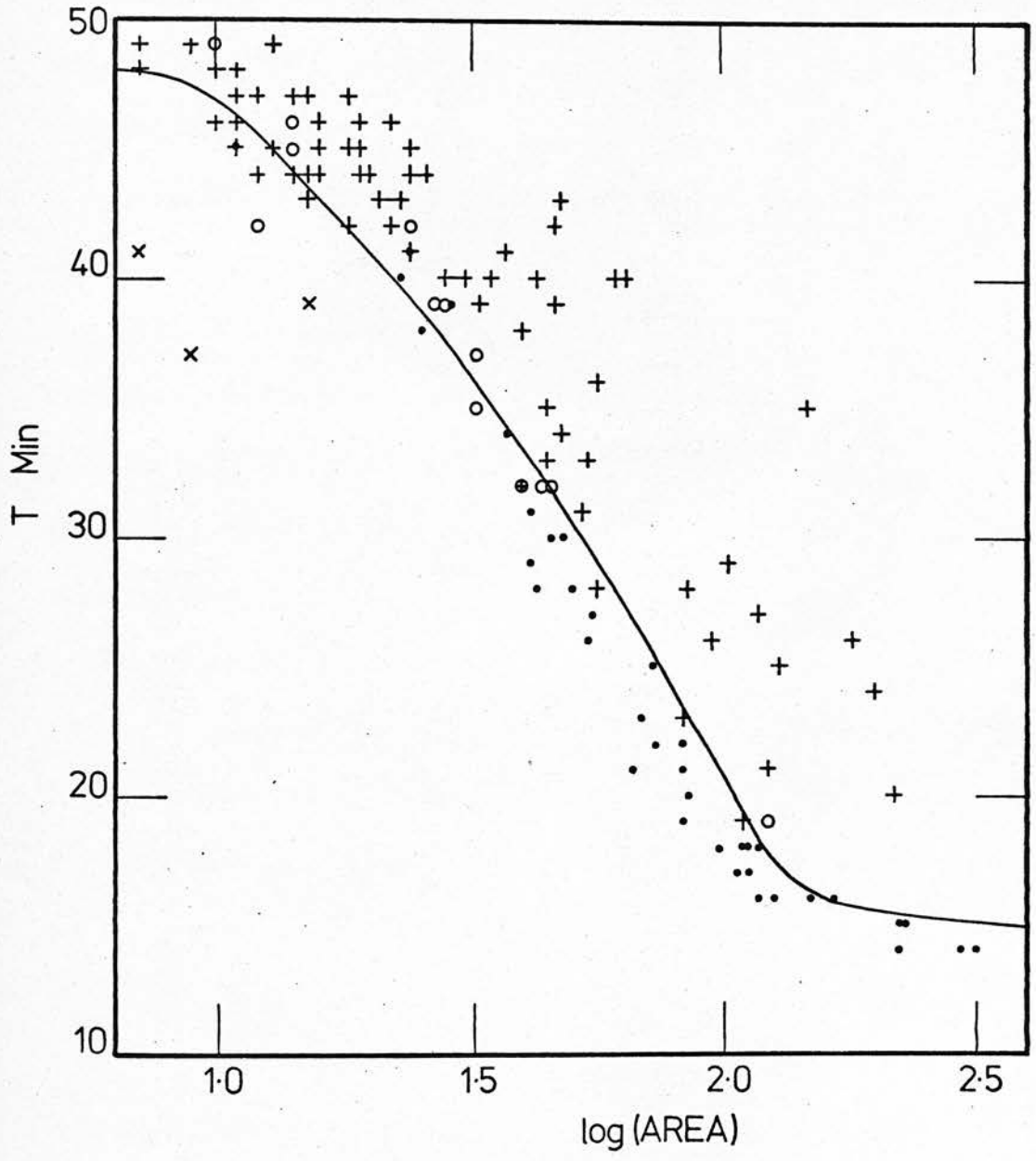

Figure 7. Plot for T_{min} versus logarithm of area for the images in the second region. The symbols are the same as in figure 1 apart from the diagonal crosses which are used to represent images due to noise and plate flaws.

III. 6. An automatic method for establishing the separation envelope

The smoothness of the lower boundary to the star curve and its constant dispersion over much of the minimum transmission versus log area plot gives a guideline for developing a method for automatically fixing by the computer a discrimination setting between the galaxies and stars.

A suitable working procedure is as follows. The lower bound to the star curve is found (neglecting odd points lying below the star curve such as those due to plate flaws and noise). Then, using a constant width for the envelope, points are calculated a constant distance away from the lower bound along the normal to the local gradient. These points are used to give the final discrimination envelope on application of a polynomial fitting technique (using a polynomial of order three).

A computer program which satisfactorily accomplishes this has been written. The results of applying the method to the data of tables 8 and 10 are described in the next section.

III. 7. Results of the computational method

The curves in figures 6 and 7 were obtained by using the method described in the previous section for determining the galaxy/star discrimination envelope. The width of the envelope used in both cases was 1.5 in transmission level (0.075 in log area). The fact that the same width of envelope may be used is another factor in our favour. At the faint end the curve is extended to log area = 0 by

a line parallel to the horizontal axis. Since no separation is possible below log area = 0.9 everything is output into the galaxy category. The contamination by faint stars in this region is noted.

The distribution of images in figure 6 is as follows:-

above the curve:- 90 galaxies 6 stars 5 uncertains 8 due to noise
1 plate flaw

below the curve:- 4 galaxies 32 stars 10 uncertains 2 due to noise
2 plate flaws 2 double stars

This is an exceptionally good result in that only 4% of the galaxies are lost. Of the images in the galaxy category, 82% are definitely galaxies and 5% are uncertain. There is a 5% contamination by stars (including the faint stars which could not be unambiguously separated from the galaxies), 7% contamination by noise and 1% contamination by plate flaws.

The contamination of images in the galaxy category due to noise and plate flaws is not insignificant (8%). There is no way round this contamination apart from comparing the measurements with those from another plate of the same region. Only then may the images of this nature be eliminated.

The distribution of images in figure 7 is as follows:-

above the curve:- 88 galaxies 8 stars 9 uncertains 8 due to noise

below the curve:- 15 galaxies 36 stars 4 uncertains 3 due to noise
3 plate flaws

The number of galaxies lost to the stars in this case is greater, 15%, being mainly faint ones. The reason for this is seen

from figure 7. There is a paucity of faint stars with which to determine the star envelope, resulting in the galaxies themselves being used. The paucity of faint stars in this region has most likely occurred by chance. This case is the worst encountered with respect to numbers of galaxies lost to the stars. Of the images falling into the galaxy category, 78% are definitely galaxies, 7% are stars, 8% uncertains and 7% are due to noise.

For the other three regions the results are very similar. The numbers of galaxies lost to the stars were static (9, 10 and 11% respectively) as were the numbers of uncertains in the galaxy category (7, 10 and 10% respectively). The contamination by stars varied from 5 to 10% and the contamination by noise and plate flaws was in the main steady (9 to 10%) but was as high as 15% in one region dominated by several bright stars and galaxies. The frequency of galaxies falling in the galaxy category was less than 70% in only the latter case, averaging overall 75% of the images in this category.

The performance of the technique in distinguishing between galaxies and stars from Coarse Measurement data from the COSMOS machine (10% of the galaxies lost on the average, and 3 out of 4 images in the galaxy category being definitely galaxies), although not perfect, is adequate for the purposes of this thesis. Using this method, then, it is safe to say that on average (for plate 149) 90% of the galaxies are selected and there is a confidence level of 75% that the images selected as galaxies are indeed the images of galaxies.

Comparing this figure of 75% with the figure of 94% confidence in visual classification indicates that the computer technique

is at present inferior in quality to the eye. However, the great advantage of the technique lies in its ability to retain a memory of the distinction between galaxies and stars and in its ability to handle very large numbers of images.

III. 8. A computer program for the automatic separation of galaxies and stars

On the basis of the results obtained in the previous sections, a computer program has been written which calculates a family of separation curves for the different threshold levels and uses these curves to separate the galaxies from the stars.

Ideally the parameters for the separation curves are to be calculated for every threshold value. In practice, however, this may not be possible for two reasons. The main limitation is set by the amount of computer store available. Prime shift program runs on the 1906A are limited to a maximum of 120K of core store. This sets a limit of, at most, about 20 sets of parameters to be determined. In a region in which the background is more or less uniform there is no difficulty and parameters may be determined for each threshold level individually. In regions where the threshold is varying quite quickly, this may not be possible and levels have to be compounded to give at most 20 different sets of parameters.

The other limitation is set by the fact that in order to calculate a reasonable separation envelope there must be sufficient numbers of "good" images (i.e. images of area > 1 unit) in the minimum transmission/log area array. A practical working figure of between

50 and 300 images is required in the array for any one threshold before meaningful criteria may be established. Where the threshold is varying rapidly this stipulation may not be met, in which case levels must be compounded to give criteria.

A block diagram illustrating all the actions demanded by a program to carry out the galaxy/star separation from Coarse Measurement data stored on magnetic tape is shown in figure 8. The complete process of calculation and manipulation is designed to be completely automatic, human intervention is kept to a strict minimum. The X and Y coordinates of those images selected as galaxies are stored on an output magnetic tape.

Such a program has been successfully developed and, since it is foreseen that it will be of considerable value particularly for projects of cosmological significance, the Algol version of the program is listed in Appendix III. A Fortran version of this program, written to follow the lines of the Algol version as closely as possible in order to produce equivalent results, is also available.

The speed with which the program determines separation criteria and carries out the separation of images into galaxies and stars depends on the rate of variation in threshold. Preliminary runs have indicated that speeds in excess of 300 images/second are normally attained. However, speeds of up to 1000 images/second have been achieved from regions in which the plate background is very nearly uniform.

A mark II version of the program is currently under consideration. The early version is practical when dealing with small

localised areas on the plate, e.g. for clusters of galaxies. For the study of much larger areas, such as the whole of a plate, we might expect other effects, e.g. image elongation due to field rotation, to be important in which case the parameters for the galaxy/star separation may also depend on the actual position of the image on the plate. In such a case, as well as a family of parameters related to threshold, an orthogonal family is required for position.

III. 9. Check for systematic effects

Figure 9 is a plot of contours representing the variation in machine threshold over the 7.5cm square area on plate 149. The contours were obtained on averaging the threshold over grids 2.048mm square (COSMOS scans in lanes 1024 μm wide with the 8 μm spot and so 1.024mm is a convenient unit) and joining up points having the same value. A suitable interval of 3 levels between contours was used. The actual variation in threshold had a range of 51 levels, from a minimum at 28 to a maximum at 78.

The overall appearance of the contour diagram is of a smoothly varying threshold from the top right to the bottom left, consistent with the radial variation in plate background from the plate centre (top right) to the plate edge (bottom left).

The contours at the bottom left of the diagram are distorted due to the presence of an image "ghost" (i.e. the ghost of a bright star image). The four dips in the otherwise smoothly varying threshold are identified with the images of bright stars on the original plate. The "lane" in the contours above the dip at the top

FIGURE 8 - Block diagram for the computer program which separates the galaxies from the stars.

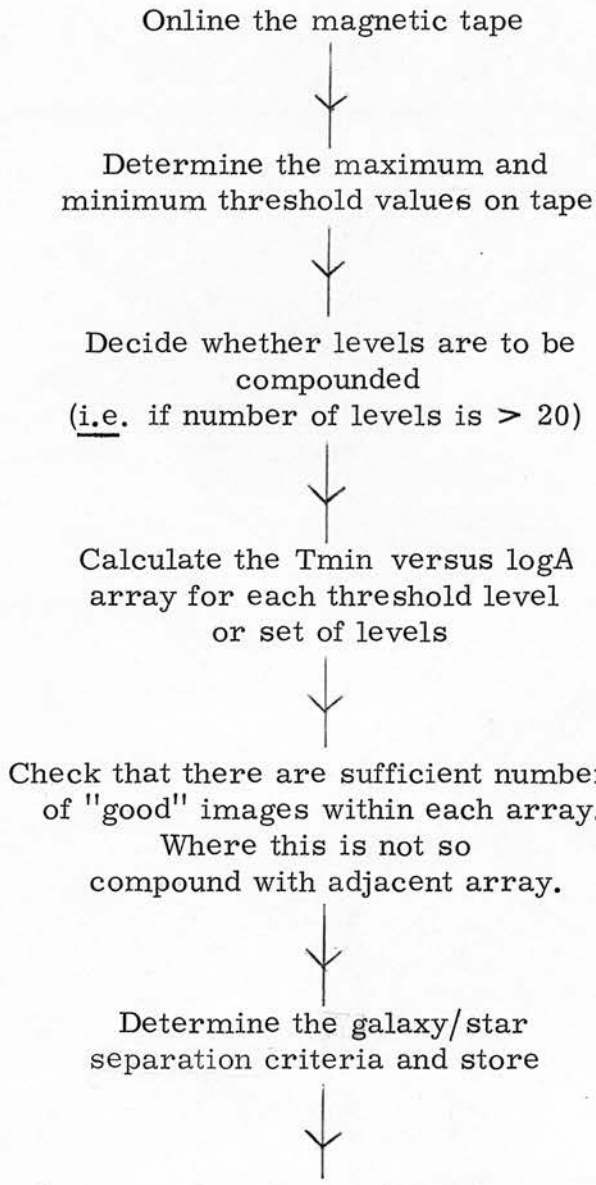

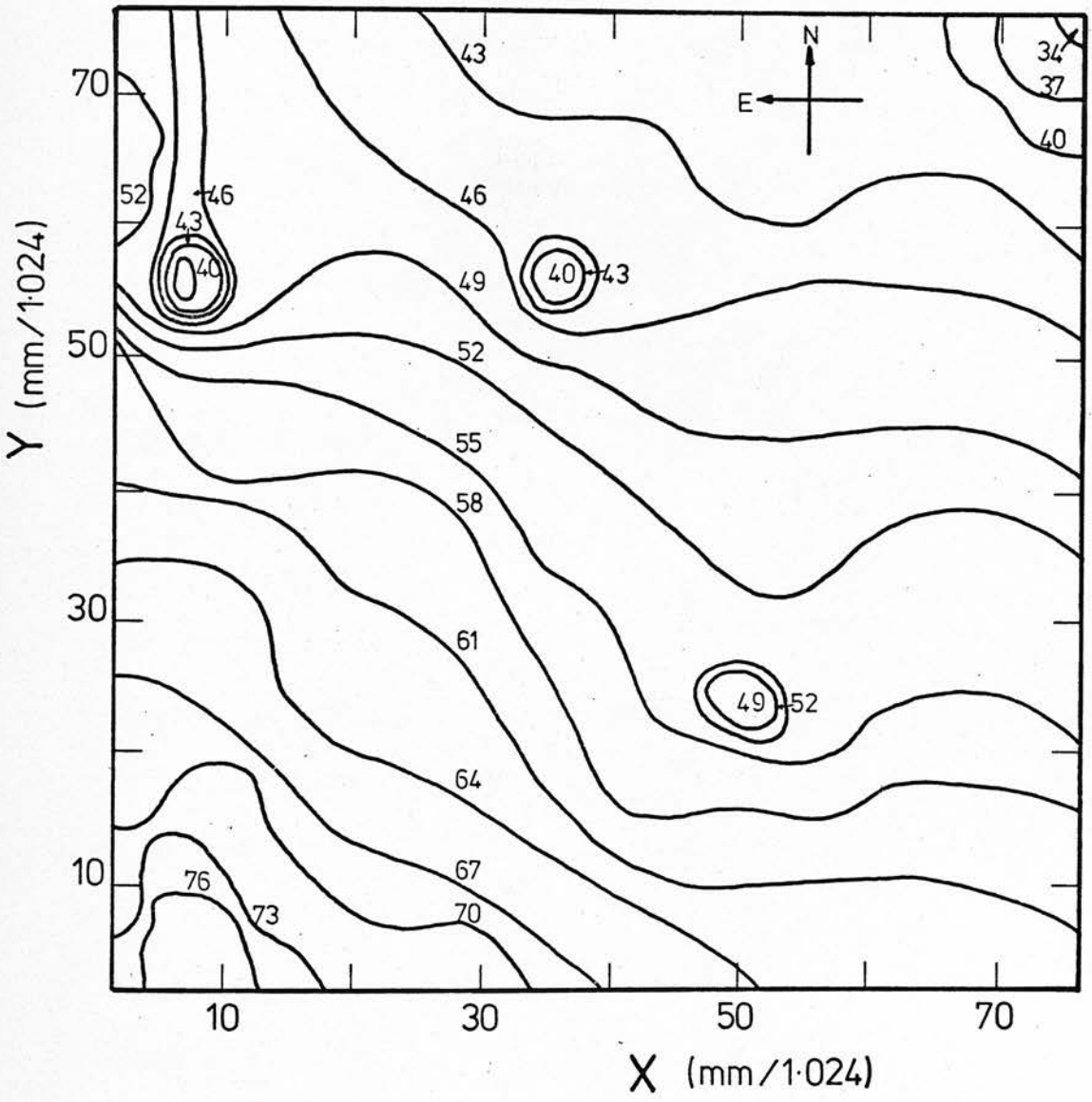

Figure 9. Contours showing the variation in machine threshold over the 7.5cm square area measured on plate 149.

left of the diagram illustrates the result when the machine loses the threshold on exit from a particularly bright star image with several superimposed fainter stars.

The levels in the contour plot were determined in exactly the same way as the galaxy/star separation program determines which thresholds are to be compounded to produce separation criteria. Thus, these contours represent contours of equal criteria for the separation of galaxies and stars. Or, another way of putting it, as one crosses a contour, the criteria for separating galaxies and stars change.

It should be expected, then, that any systematic effect in the method for separating galaxies from stars may reveal itself as a systematic trend in the numbers of either stars or galaxies from the top right of the region to the bottom left. Since plate 149 is a photograph of a region at a high galactic latitude, the distribution of stars on the plate may be expected to be uniform (apart from effects of variation in limiting magnitude over the plate which for simplicity are assumed to be negligible in this region). This provides a test for the reliability of the technique over a region of the plate.

Counts of objects which were selected as stars by the program in 2 regions, each 2cm square (one at the top right, the other at the bottom left of the larger area), indicated a difference of less than 4% in their numbers. It is concluded from this that any systematic effect due to variations in threshold in the program for distinguishing between galaxies and stars is not greater than 4%.

This technique for the automatic separation of galaxies and stars from measurements made with the COSMOS machine is now used to study the properties of rich clusters of galaxies from measurements on different plates.

IV. PROPERTIES OF RICH CLUSTERS

The distribution of galaxies in 6 rich clusters is examined in this chapter, first of all with regard to the overall structure of the cluster (i.e. its shape) and secondly with regard to the properties of the cluster core. Differences in core radii between the bright and faint members are taken to indicate the presence of luminosity segregation, i.e. the concentration of brighter members toward the cluster centre. The degree of segregation is compared with other features of the cluster in a search for systematic trends.

IV. 1. The clusters and plate material

Reject survey and non-survey 48-inch Schmidt Telescope plates were systematically scrutinised in a search for satisfactory plates on which were rich, fairly nearby clusters of galaxies. Plate and cluster selection criteria were stringent. The plates had to be of reasonable quality (i.e. such that the images were in focus and not trailed) at least in the vicinity of the cluster, and of regions at high galactic latitudes in order to reduce as much as possible the stellar component of the images. The clusters had to be sufficiently rich in order to give reasonable statistics and sufficiently nearby to have adequate apparent angular sizes on the plates.

Four plates on which were 6 rich clusters satisfying the requirements were finally selected. A fifth plate of one of the same

regions but in red light was also included due to the added interest in comparing cluster properties in different wavebands.

Details of the clusters and the corresponding plate material are presented in Table 11. Column 1 of Table 11 contains a running number, columns 2 and 3 contain the right ascension and declination respectively referred to the opoch 1950, column 4 contains the ESO/SRC field number, column 5 the plate number, column 6 the emulsion/filter combination, column 7 the exposure time (minutes), and columns 8 and 9 contain the X and Y coordinates (in mm) respectively from the lower left hand corner of the plate. The right ascension and declination were measured to the nearest tenth of a minute in time and minute of arc respectively using transparent grid overlays centred on the plate centre. The confidence limits in column 10 of Table 11 are explained in the next section.

Henceforth in this thesis, the clusters are referred to by their equatorial coordinates, e.g. the first cluster in Table 11 will be identified as the cluster 22129 -3558.

IV. 2. The measurements

During March and April of 1975, Coarse Measurement measures were carried out on a region on each plate containing the clusters. The size of region measured was in general about 5cm square apart from the measurements on plate 766. The 3 clusters on plate 766 were all quite close together and so a 12. 5cm square area containing all 3 was measured. The cluster 22315 -3800 is also present on this plate but in a vignetted region. For this reason,

Table 11

Details of the clusters and plates.

(1) No.	(2) R. A. (1950)	(3) Dec. (1950)	(4) ESO/SRC Field No.	(5) Plate No.	(6) Emulsion and Filter	(7) Exposure (minutes)	(8) X (mm)	(9) Y (mm)	(10) Confidence levels
1	$22^h12^m.9$	$-35^o58'$	405	766	IIIaJ + GG395	50	277	123	83%
2	$22^h15^m.6$	$-35^o25'$	405	766	IIIaJ + GG395	50	248	154	83%
3	$22^h14^m.6$	$-34^o57'$	405	766	IIIaJ + GG395	50	260	177	83%
4	$22^h31^m.5$	$-38^o00'$	345	844	IIIaJ + GG395	60	185	286	77%
5	$01^h45^m.4$	$-32^o16'$	414	847	IIIaJ + GG395	45	282	60	65%
6	$02^h39^m.2$	$-28^o52'$	416	149	IIIaJ + GG395	120	202	242	75%
6	$02^h39^m.2$	$-28^o52'$	416	1049	098 + RG630	60	200	238	71%

measurements on plate 844 were preferred.

The average density of images detected by COSMOS on the plates was quite uniform, from about 5×10^3 to 10^4 images per square degree. The values in column 10 of Table 11 represent confidence limits on the data that the objects selected as galaxies by the galaxy/star separation program are indeed the images of galaxies. The non-galaxy component contributes in general a uniform background distribution of objects (apart from the noise around the images of bright galaxies and stars which is "blanked off" in the computation) and thus in principle has no effect on the results presented in the rest of this chapter. Statistical fluctuations in this 'uniform' background distribution of non-galaxy objects do, however, contribute to the statistical errors of the galaxy distribution data.

IV. 3. The general distribution of cluster galaxies

The overall distributions of galaxies in and around the 4 clusters 22129 -3558, 22156 -3525, 22146 -3457 and 22315 -3800 are represented as contour maps in figures 10, 11, 12 and 13 respectively. Contour levels are drawn in terms of the number of galaxies present per square mm. The scales along the left and bottom edges of the diagram are in mm on the original plate, with zero point at the start of the COSMOS scans, while those along the top and right hand edges are in terms of right ascension and declination respectively referred to the epoch 1950.

The field around the cluster 22146 -3457 is noticeably rich in distant clusters of galaxies. The fields of all the other clusters

are generally free from such contamination apart from the cluster 22129 -3558 which has a large cloud of galaxies to the north-west. In all cases, however, the contours show that the clusters are unambiguously elongated. Although meaningful contours could not be drawn for the remaining two clusters (due to their smaller apparent angular size), plots of the output from the machine (i.e. dots at the respective positions of the galaxies) revealed that elongation was evident in their structure also.

IV. 4. Determination of cluster centres and core and halo radii

Centres for the 6 clusters were determined from the symmetrical peaks in the counts of galaxies in strips of 1mm width (0.5mm for the clusters 01454 -3216 and 02392 -2852) in both the X and Y directions across the clusters. In this way, cluster centres are accurate to 1mm (0.5mm for the clusters of smaller apparent angular size). Similarly, centres for the cluster 02392 -2852 on the blue and red plate are compatible to 0.5mm.

The radial density distributions of galaxies in the clusters from the centre outwards were found from counts of galaxies in rings of width 1mm (or 0.5mm for the smaller clusters). In Tables 12-17 the quantities tabulated for each cluster are the numbers of galaxies counted (N) within each ring, the corresponding density (ρ) of galaxies, the numbers of bright and faint (N_b and N_f) galaxies per ring (where the bright galaxies are taken to be those whose measured mean diameter above threshold - $2*\sqrt{(A/\pi)}$ - is greater than 30μm) and their corresponding densities. Also tabulated are the cumulative

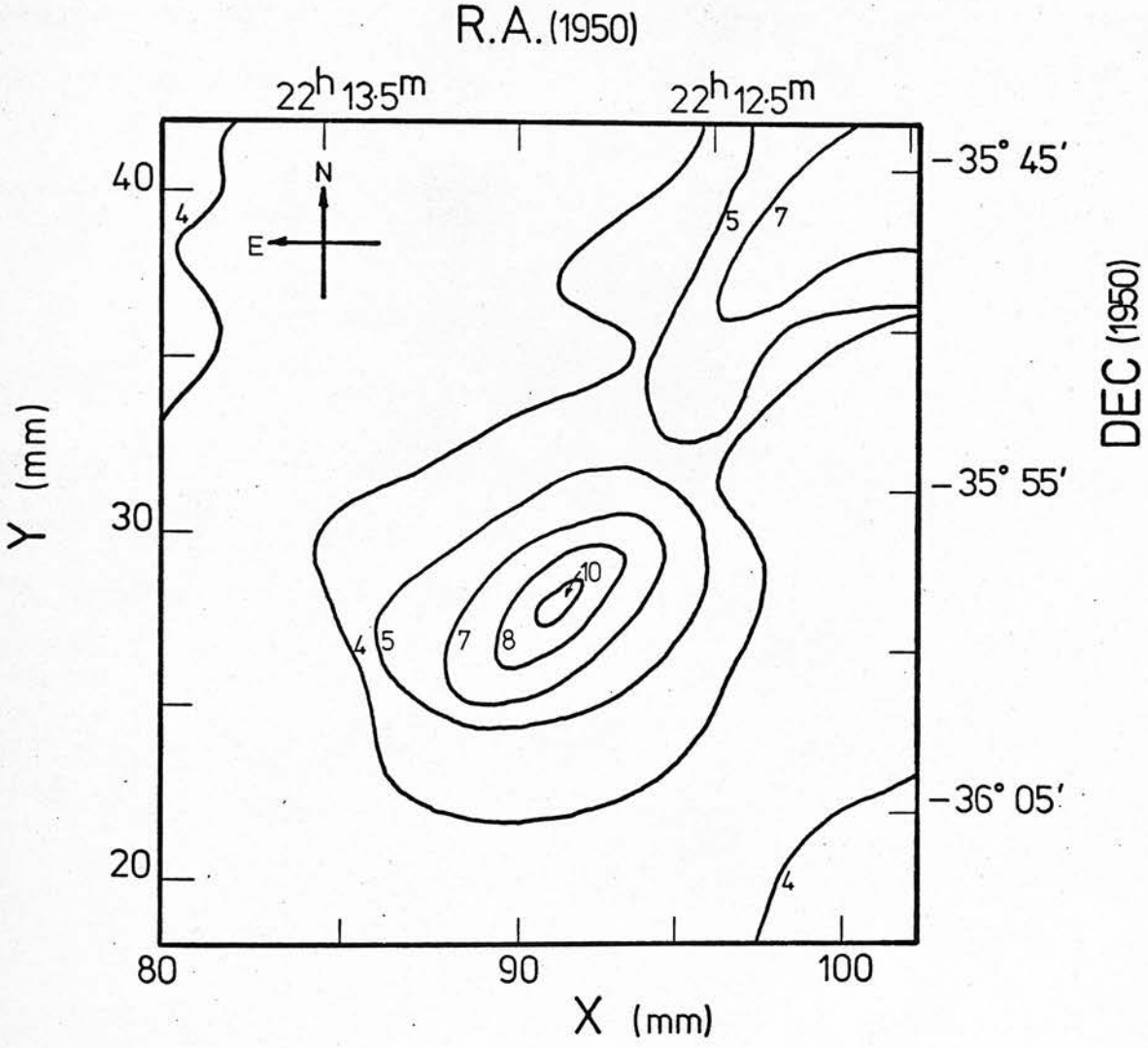

Figure 10. The distribution of galaxies in the cluster 22129 -3558. The contour levels represent the number of galaxies detected per square mm.

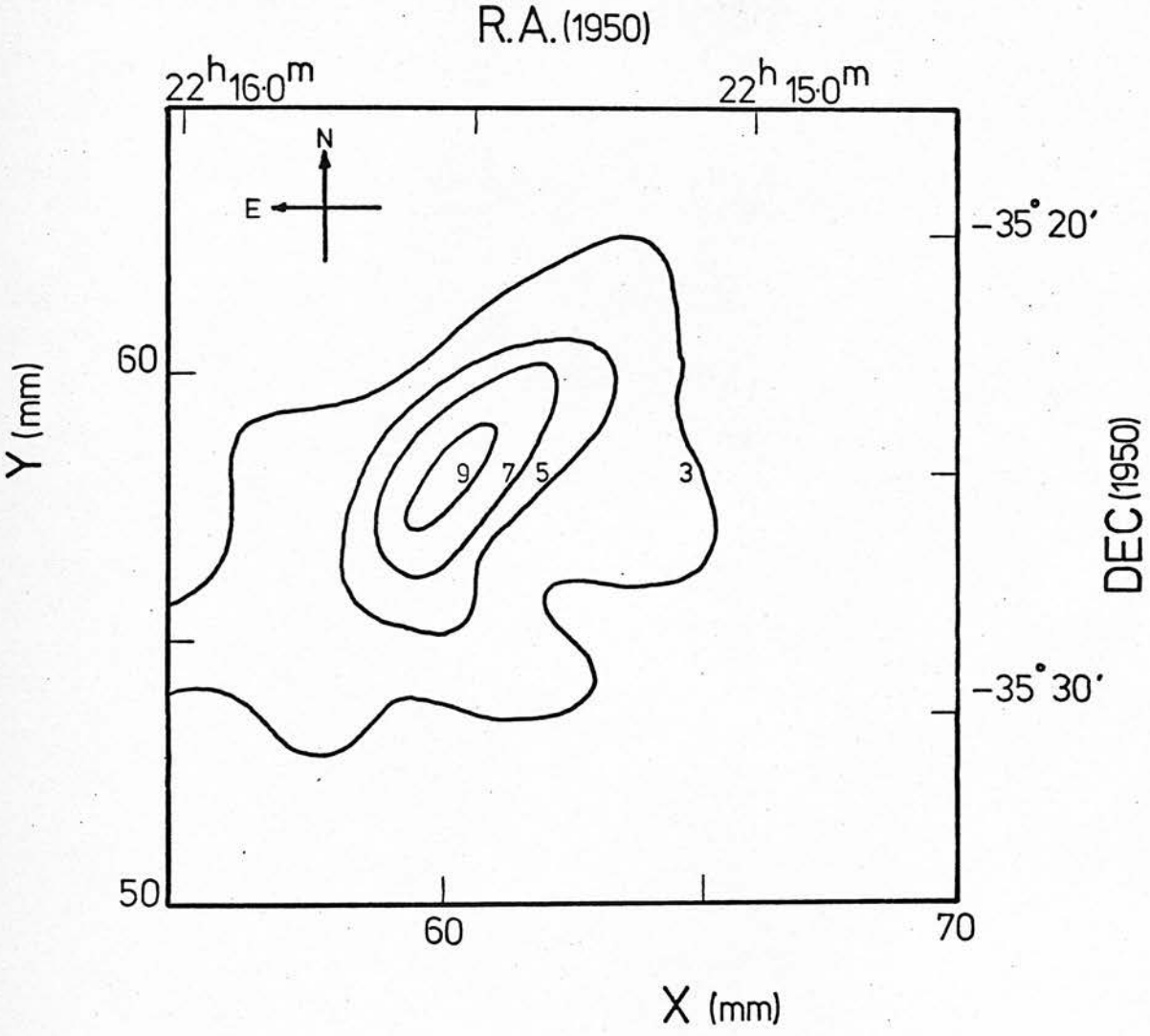

Figure 11. The distribution of galaxies in the cluster 22156 -3525. The contour levels represent the number of galaxies detected per square mm.

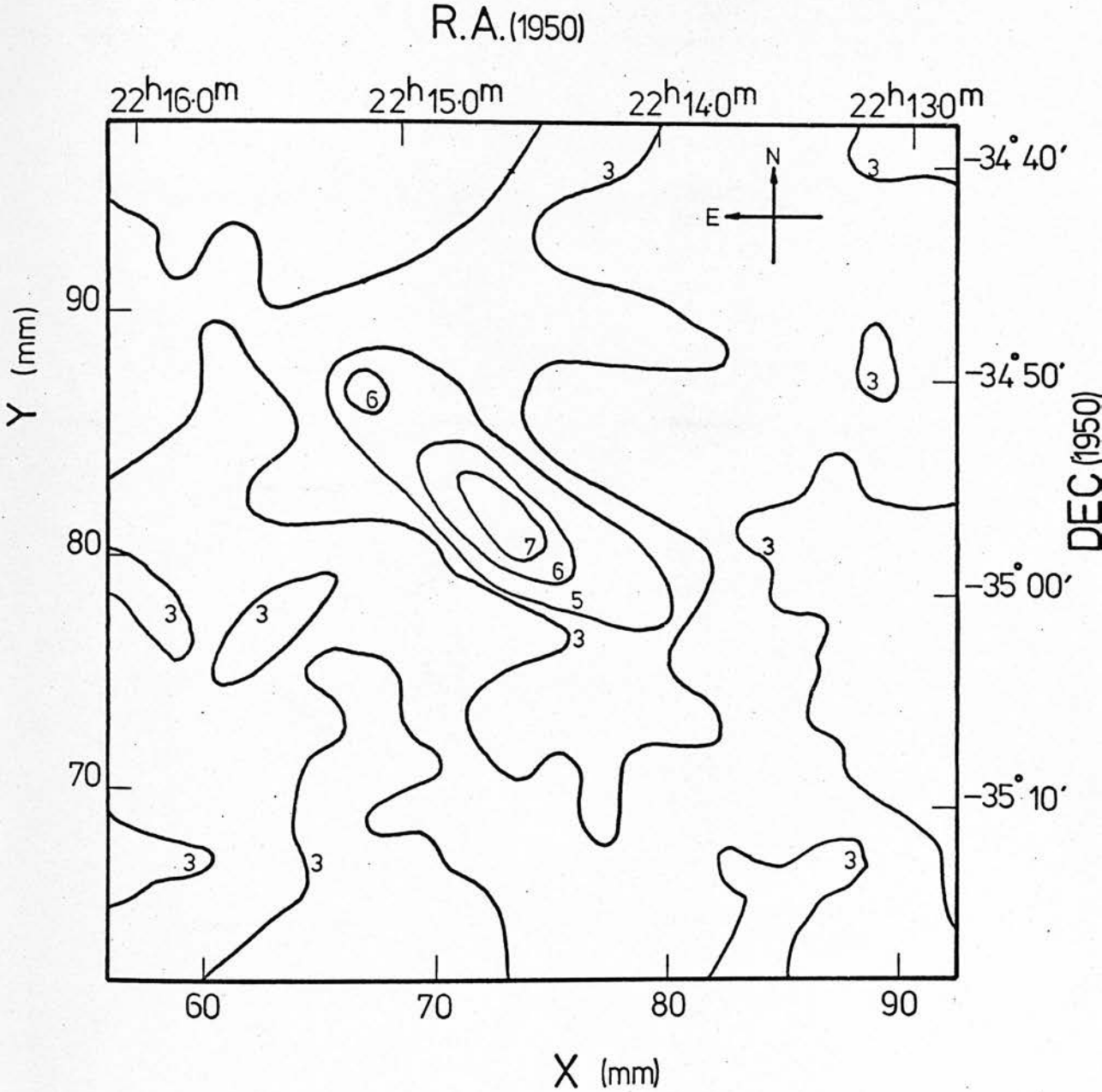

Figure 12. The distribution of galaxies in the cluster 22146 -3457. The contour levels represent the number of galaxies detected per square mm.

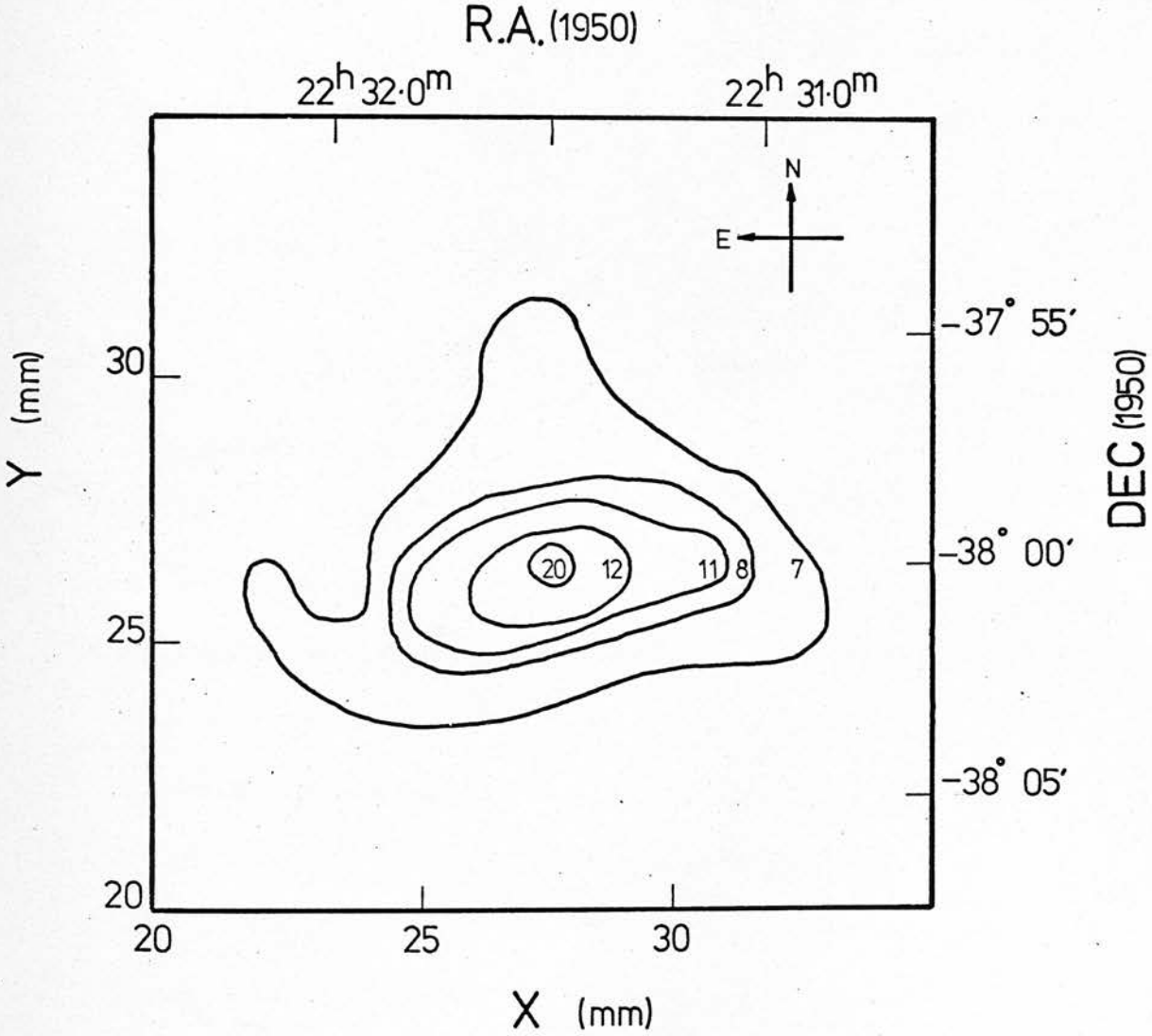

Figure 13. The distribution of galaxies in the cluster 22315 - -3800. The contour levels represent the number of galaxies detected per square mm.

ring counts of galaxies and the cumulative cluster galaxy counts. The method for obtaining the cumulative cluster count from the cumulative ring count and hence the mean cluster or halo radius has been explicitly described by Noonan (1972) and Austin & Peach (1974a). The corresponding quantities for the red plate are tabulated in Table 18.

The distributions are presented as plots of the radial densities, for the cluster as a whole and separately for the bright and faint members, in figures 14-19. The radial densities for the cluster 02392 -2852 on the blue and on the red plate are plotted for comparison in figure 20. Error bars in the figures represent the statistical ($\sqrt{N}$) errors in the observed counts. The insets are the plots for the cumulative cluster counts. Arrows indicate the outermost extent of the cluster, R, and the cluster population, $N_c(R)$.

A quantity of value in an investigation of luminosity segregation in clusters is the so-called "structural length", β, (Zwicky 1957) which is a measure of the radius of the core of the cluster and is formally the width at half-height of the projected Emden isothermal gas sphere distribution. The structural length is obtained on fitting this distribution (values of which are tabulated in Zwicky 1957 and Chandrasekhar 1942) to the observed density distribution. Analyses of this type have been performed by Bahcall (1972, 1973a, 1973b, 1973c, 1974, 1975) and Austin & Peach (1974a).

A computer program has been written which employs a minimising χ^2 procedure to fit the projected isothermal distribution to the observed radial density distribution. The quantities are formally

Table 12

The radial distribution of galaxies in the cluster 22129 -3585

Ring No.	r (mm)	N	ρ (galaxies/ sq. mm)	N_b	ρ_b (galaxies/ sq. mm)	N_f	ρ_f (galaxies/ sq. mm)	N_{cum}	$N_c(r)$
1	1.0	65	10.35	29	4.62	36	5.73	82	73
2	2.0	83	6.61	38	3.02	45	3.58	165	128
3	3.0	113	6.00	46	2.44	67	3.56	278	195
4	4.0	103	4.10	36	1.43	67	2.67	381	233
5	5.0	123	3.92	39	1.24	84	2.67	504	273
6	6.0	120	3.18	32	0.85	88	2.33	624	291
7	7.0	143	3.25	47	1.07	96	2.18	767	313
8	8.0	137	2.73	37	0.74	100	1.99	904	312
9	9.0	165	2.92	47	0.83	118	2.09	1069	319
10	10.0	166	2.64	54	0.86	112	1.78	1235	309
11	11.0	180	2.60	45	0.65	135	1.95	1415	295
12	12.0	239	3.17					1654	
13	13.0	254	3.11					1908	
14	14.0	315	3.58					2223	
15	15.0	271	2.88					2494	
16	16.0	318	3.16					2812	

Table 13

The radial distribution of galaxies in the cluster 22156 -3525

Ring No.	r (mm)	N	ρ (galaxies/ sq. mm)	N_b	ρ_b (galaxies/ sq. mm)	N_f	ρ_f (galaxies/ sq. mm)	N_{cum}	$N_c(r)$
1	1.0	33	5.25	13	2.07	20	3.18	38	31
2	2.0	49	3.90	10	0.80	39	3.10	87	58
3	3.0	70	3.71	24	1.27	46	2.44	157	92
4	4.0	72	2.87	20	0.80	52	2.07	229	113
5	5.0	86	2.74	20	0.64	66	2.10	315	134
6	6.0	86	2.28	25	0.66	61	1.62	401	140
7	7.0	92	2.09	25	0.57	67	1.52	493	138
8	8.0	109	2.17	29	0.58	80	1.59	602	139
9	9.0	115	2.03	25	0.44	90	1.59	717	131
10	10.0	142	2.26	35	0.56	107	1.70	859	135
11	11.0	167	2.42	49	0.71	118	1.71	1026	150
12	12.0	161	2.14	40	0.53	121	1.60	1187	144
13	13.0	176	2.16	41	0.50	135	1.65	1363	139
14	14.0	185	2.10	37	0.42	148	1.68	1548	
15	15.0	219	2.32	56	0.59	163	1.73	1767	
16	16.0	213	2.12	45	0.45	168	1.67	1980	

Table 14

The radial distribution of galaxies in the cluster 22146 -3457

Ring No.	r (mm)	N	ρ (galaxies/ sq. mm)	N_b	ρ_b (galaxies/ sq. mm)	N_f	ρ_f (galaxies/ sq. mm)	N_{cum}	$N_c(r)$
1	1.0	41	6.53	16	2.55	25	3.98	48	38
2	2.0	62	4.93	20	1.59	42	3.34	110	71
3	3.0	65	3.45	18	0.96	47	2.49	175	87
4	4.0	83	3.30	28	1.11	55	2.19	258	101
5	5.0	94	2.99	23	0.73	71	2.26	352	107
6	6.0	112	2.97	28	0.74	84	2.23	464	111
7	7.0	168	3.82	44	1.00	124	2.82	632	152
8	8.0	148	2.94	40	0.80	108	2.15	780	153
9	9.0	169	2.99	31	0.55	138	2.44	949	155
10	10.0	179	2.85	39	0.62	140	2.23	1128	148
11	11.0	195	2.82	49	0.71	146	2.11	1323	137
12	12.0	190	2.52	38	0.50	152	2.02	1513	102
13	13.0	195	2.39	45	0.55	150	1.84	1708	
14	14.0	210	2.39	54	0.61	156	1.77	1918	
15	15.0	214	2.27	57	0.61	157	1.67	2132	
16	16.0	227	2.26	43	0.43	184	1.83	2359	

Table 15

The radial distribution of galaxies in the cluster 22316 -3800

Ring No.	r (mm)	N	ρ (galaxies/ sq. mm)	N_b	ρ_b (galaxies/ sq. mm)	N_f	ρ_f (galaxies/ sq. mm)	N_{cum}	$N_c(r)$
1	1.0	68	10.82	37	5.89	31	4.93	92	80
2	2.0	96	7.63	51	4.06	45	3.58	188	140
3	3.0	108	5.73	49	2.60	59	3.13	296	189
4	4.0	132	5.25	56	2.23	76	3.02	428	238
5	5.0	135	4.30	51	1.62	84	2.67	563	266
6	6.0	178	4.72	57	1.51	121	3.21	741	313
7	7.0	182	4.14	71	1.61	111	2.52	923	340
8	8.0	179	3.56	69	1.37	110	2.19	1102	341
9	9.0	189	3.34	86	1.52	103	1.82	1291	327
10	10.0	235	3.74	88	1.40	147	2.34	1526	336
11	11.0	253	3.66	77	1.11	176	2.55	1779	340
12	12.0	276	3.66	104	1.38	172	2.28	2055	342
13	13.0	299	3.66	98	1.20	201	2.46	2354	344
14	14.0	309	3.51	86	0.98	223	2.54	2663	331

Table 16

The radial distribution of galaxies in the cluster 01454 -3216

Ring No.	r (mm)	N	ρ (galaxies/ sq. mm)	N_b	ρ_b (galaxies/ sq. mm)	N_f	ρ_f (galaxies/ sq. mm)	N_{cum}	$N_c(r)$
1	0.5	15	9.55	9	5.73	6	3.82	18	16
2	1.0	23	7.32	10	3.18	13	4.14	41	35
3	1.5	20	4.24	13	2.76	7	1.49	61	47
4	2.0	17	2.71	7	1.11	10	1.59	78	54
5	2.5	18	2.29	11	1.40	7	0.89	96	58
6	3.0	24	2.55	13	1.38	11	1.17	120	66
7	3.5	19	1.73	7	0.64	12	1.09	139	65
8	4.0	21	1.67	9	0.72	12	0.96	160	64
9	4.5	31	2.19	12	0.85	19	1.34	191	39
10	5.0	26	1.66	16	1.02	10	0.64	217	67
11	5.5	30	1.74	10	0.58	20	1.16	247	65
12	6.0	28	1.49	9	0.48	19	1.01	275	
13	6.5	30	1.47	11	0.54	19	0.93	305	

Table 17

The radial distribution of galaxies in the cluster 02392 -2852

Ring No.	r (mm)	N	ρ (galaxies/ sq. mm)	N_b	ρ_b (galaxies/ sq. mm)	N_f	ρ_f (galaxies/ sq. mm)	N_{cum}	$N_c(r)$
1	0.5	16	10.19	6	3.82	10	6.37	19	17
2	1.0	17	5.41	6	1.91	11	3.50	36	28
3	1.5	23	4.88	8	1.70	15	3.18	59	40
4	2.0	28	4.46	9	1.43	19	3.02	87	54
5	2.5	20	2.55	3	0.38	17	2.16	107	55
6	3.0	20	2.12	8	0.85	12	1.27	127	52
7	3.5	19	1.73	6	0.55	13	1.18	146	44
8	4.0	42	3.34	11	0.88	31	2.47	188	55
9	4.5	35	2.48	10	0.71	25	1.77	223	54
10	5.0	23	1.46	7	0.45	16	1.02	246	
11	5.5	33	1.91	13	0.75	20	1.16	279	
12	6.0	37	1.96	15	0.80	22	1.17	316	
13	6.5	46	2.25	20	0.98	26	1.27	362	
14	7.0	29	1.32	9	0.41	20	0.91	391	
15	7.5	28	1.19	8	0.34	20	0.85	419	
16	8.0	50	1.99	16	0.64	34	1.35	469	
17	8.5	51	1.91	18	0.67	33	1.24	520	

Table 18

The radial distribution of galaxies in the cluster 02392 -2852 on the red plate

Ring No.	r (mm)	N	ρ	N_{cum}	$N_c(r)$
1	0.5	12	7.64	13	10
2	1.0	22	7.00	35	23
3	1.5	28	5.94	63	36
4	2.0	38	6.05	101	53
5	2.5	31	3.95	132	56
6	3.0	39	4.14	171	62
7	3.5	51	4.64	222	74
8	4.0	38	3.02	260	66
9	4.5	50	3.54	310	65
10	5.0	52	3.31	362	59
11	5.5	66	3.82	428	62
12	6.0	72	3.82	500	64
13	6.5	52	2.55	552	
14	7.0	66	3.00	618	
15	7.5	68	2.89	686	
16	8.0	62	2.47	748	

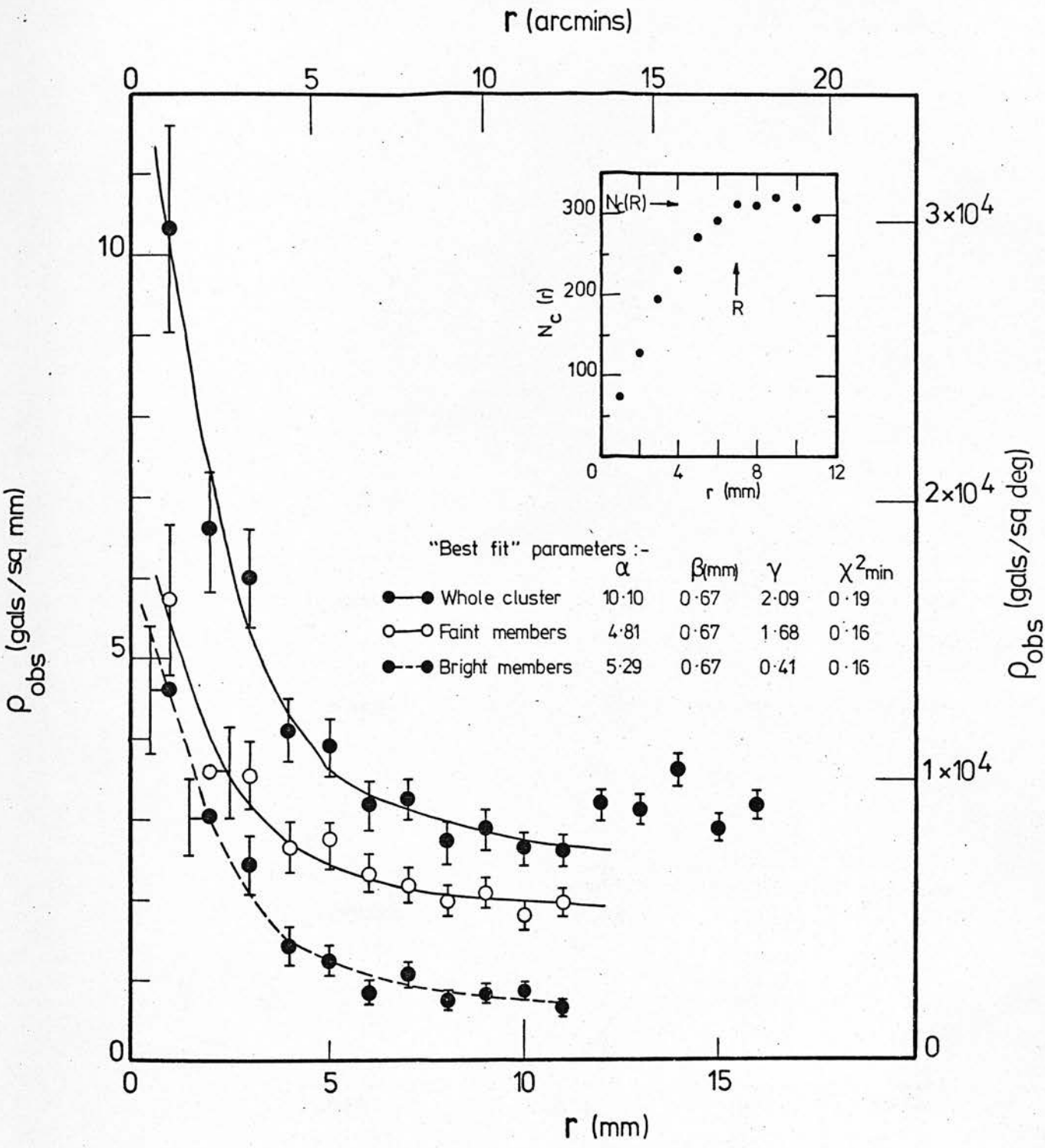

Figure 14. The radial densities of galaxies in the cluster 22129 -3558. The curves represent the "best fit" models of the projected isothermal gas sphere distribution.

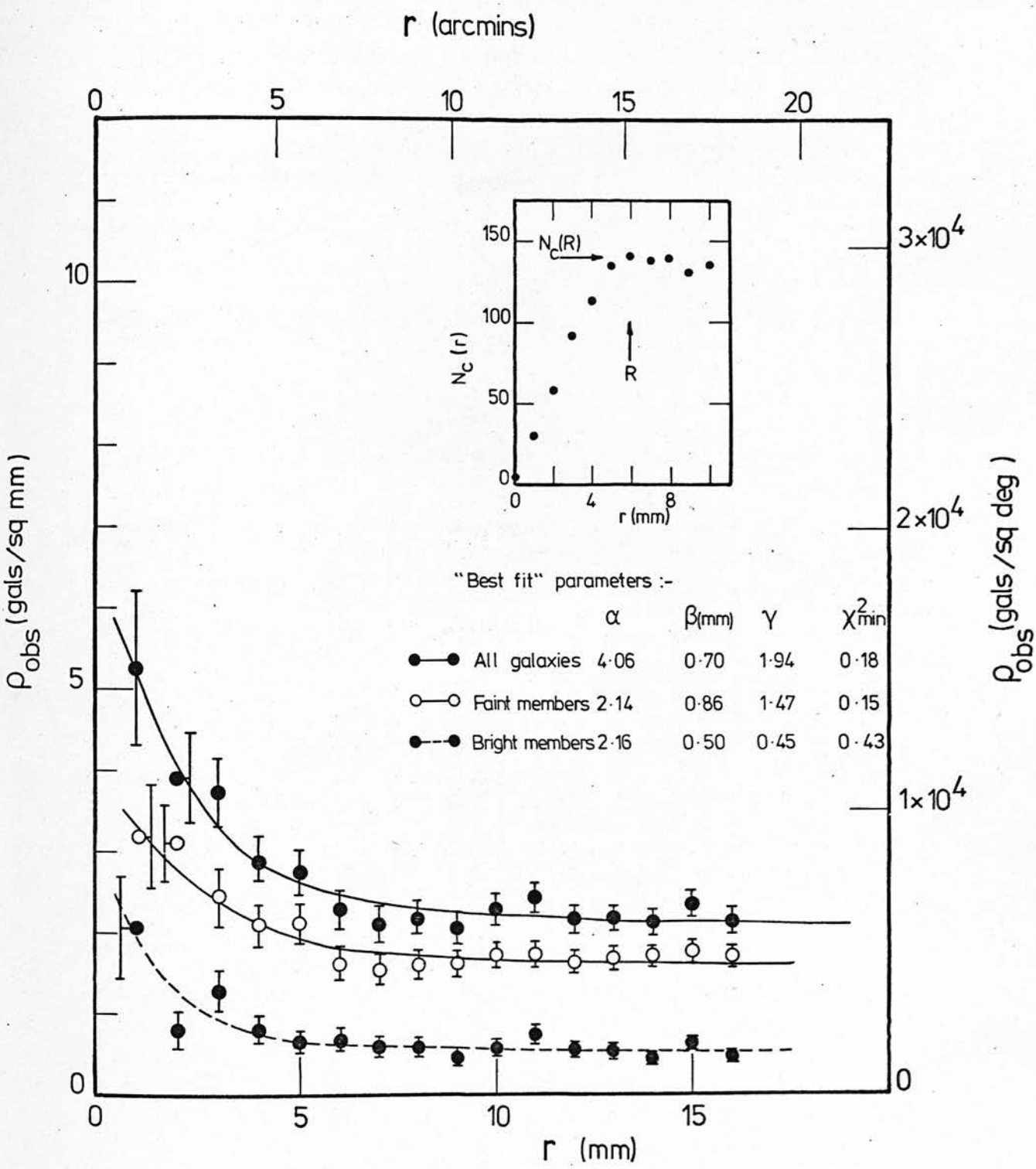

Figure 15. The radial densities of galaxies in the cluster 22156 -3525. The curves represent the "best fit" models of the projected isothermal gas sphere distribution.

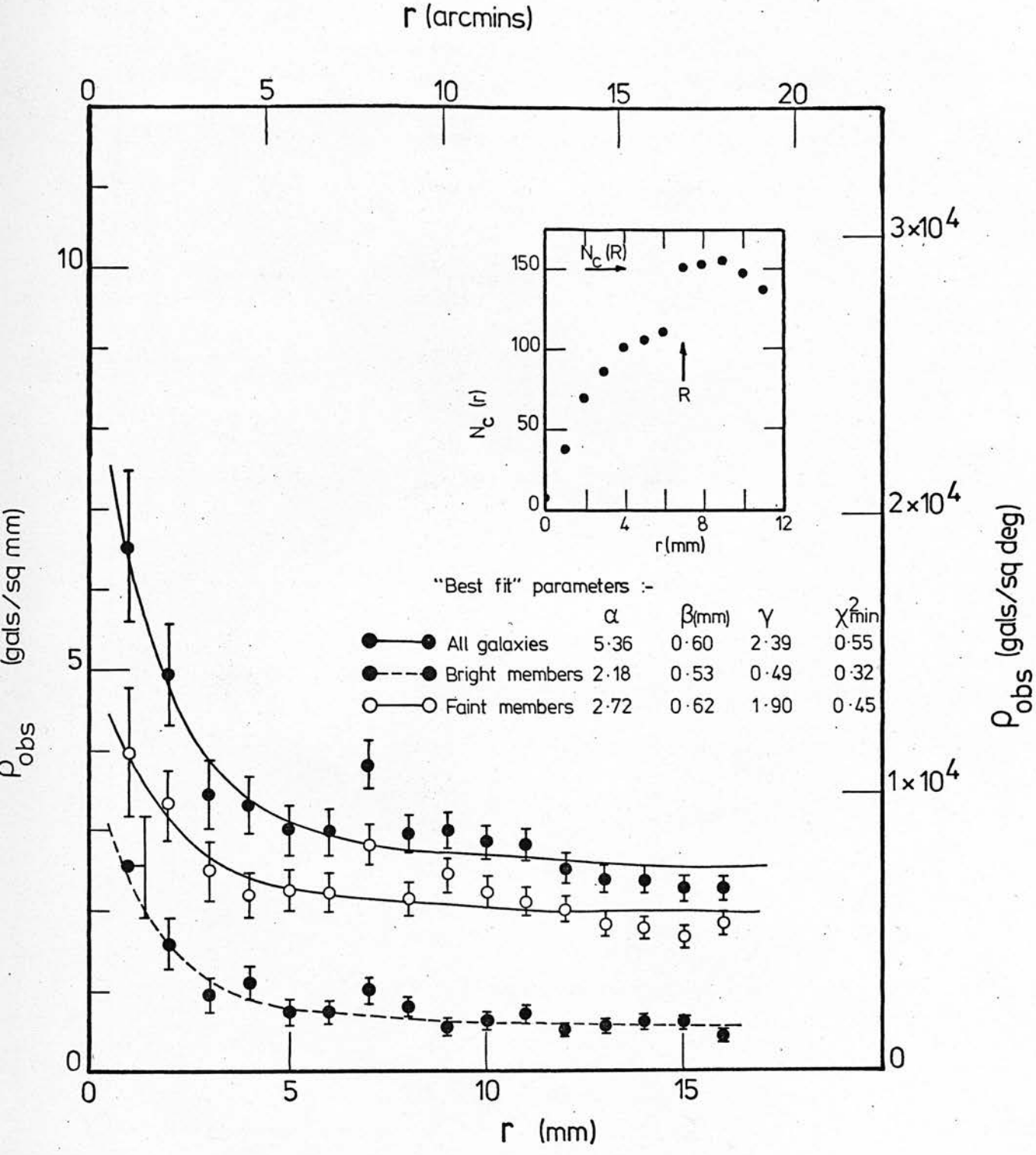

Figure 16. The radial densities of galaxies in the cluster 22146 -3457. The curves represent the "best fit" models of the projected isothermal gas sphere distribution.

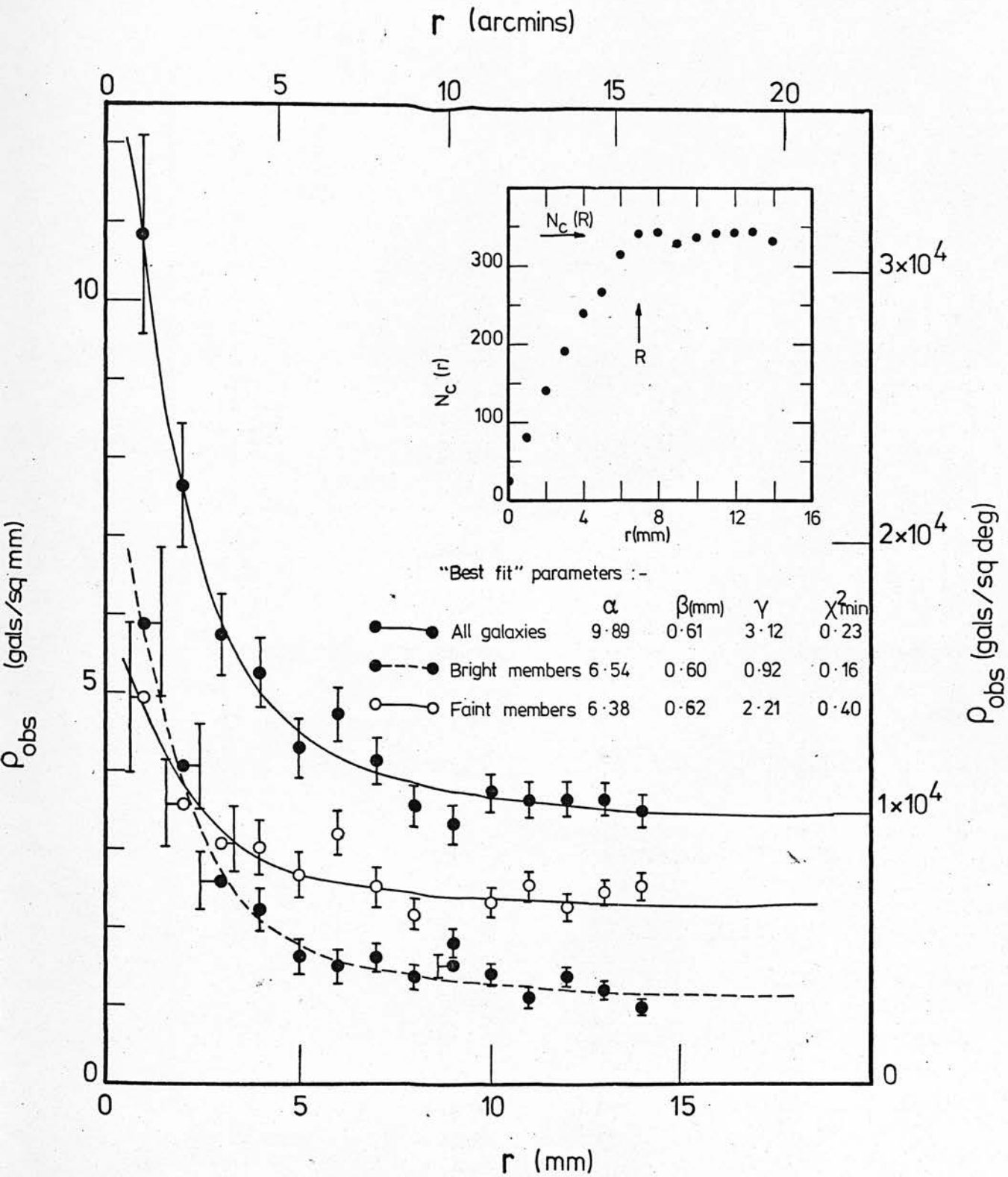

Figure 17. The radial densities of galaxies in the cluster 22315 -3800. The curves represent the "best fit" models of the projected isothermal gas sphere distribution.

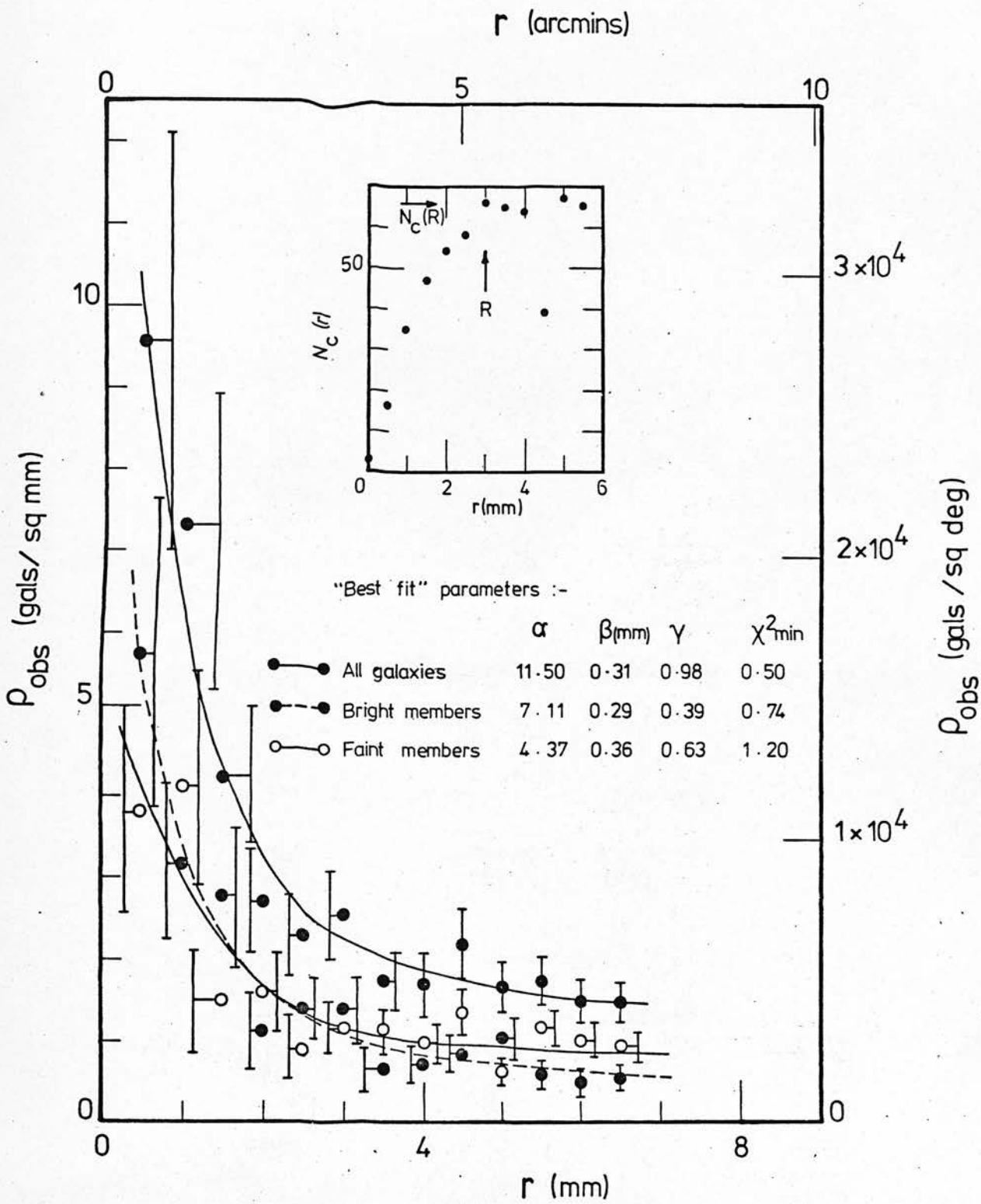

Figure 18. The radial densities of galaxies in the cluster 01454 -3216. The curves represent the "best fit" models of the projected isothermal gas sphere distribution.

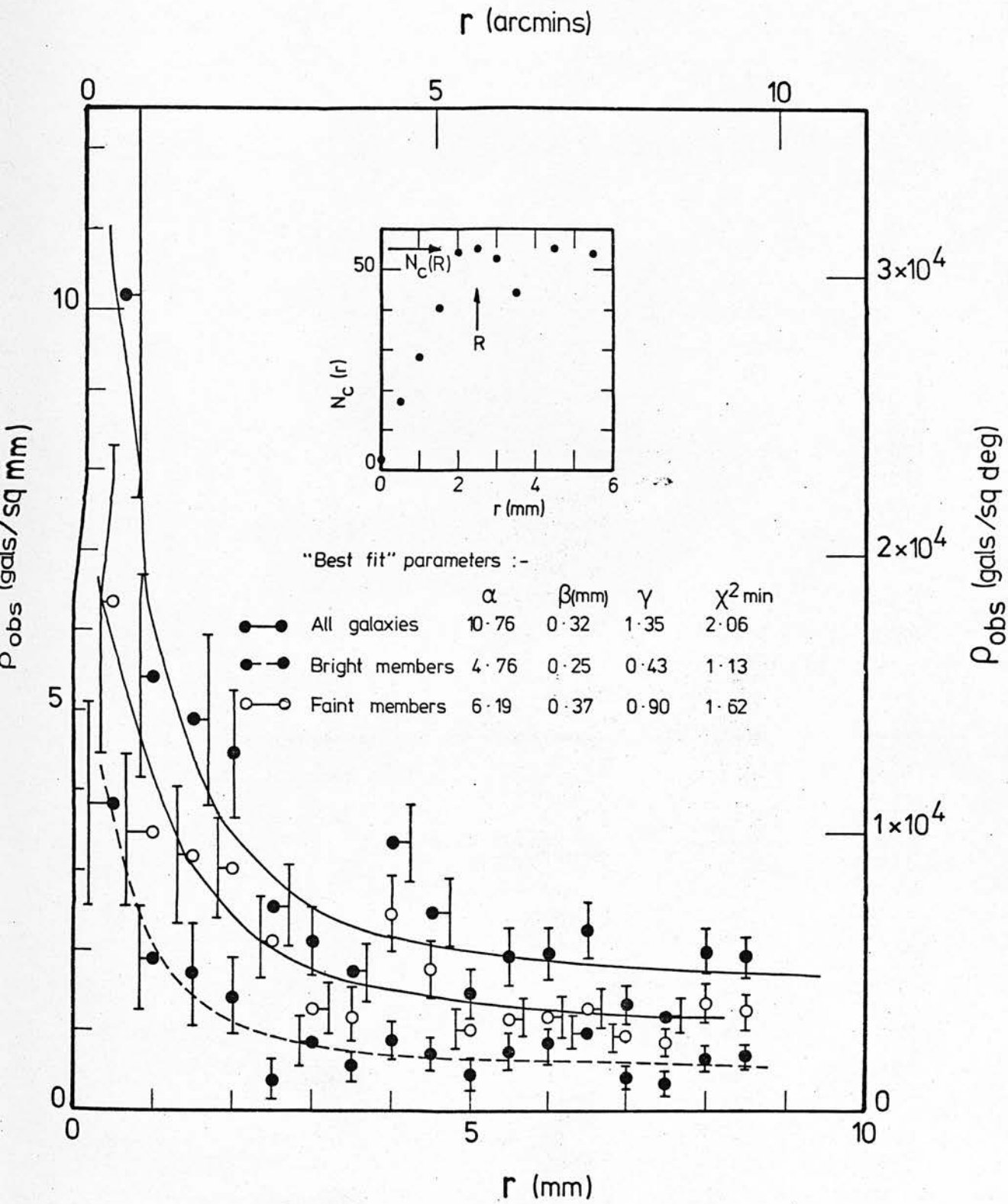

Figure 19. The radial densities of galaxies in the cluster 02392 -2852. The curves represent the "best fit" models of the projected isothermal gas sphere distribution.

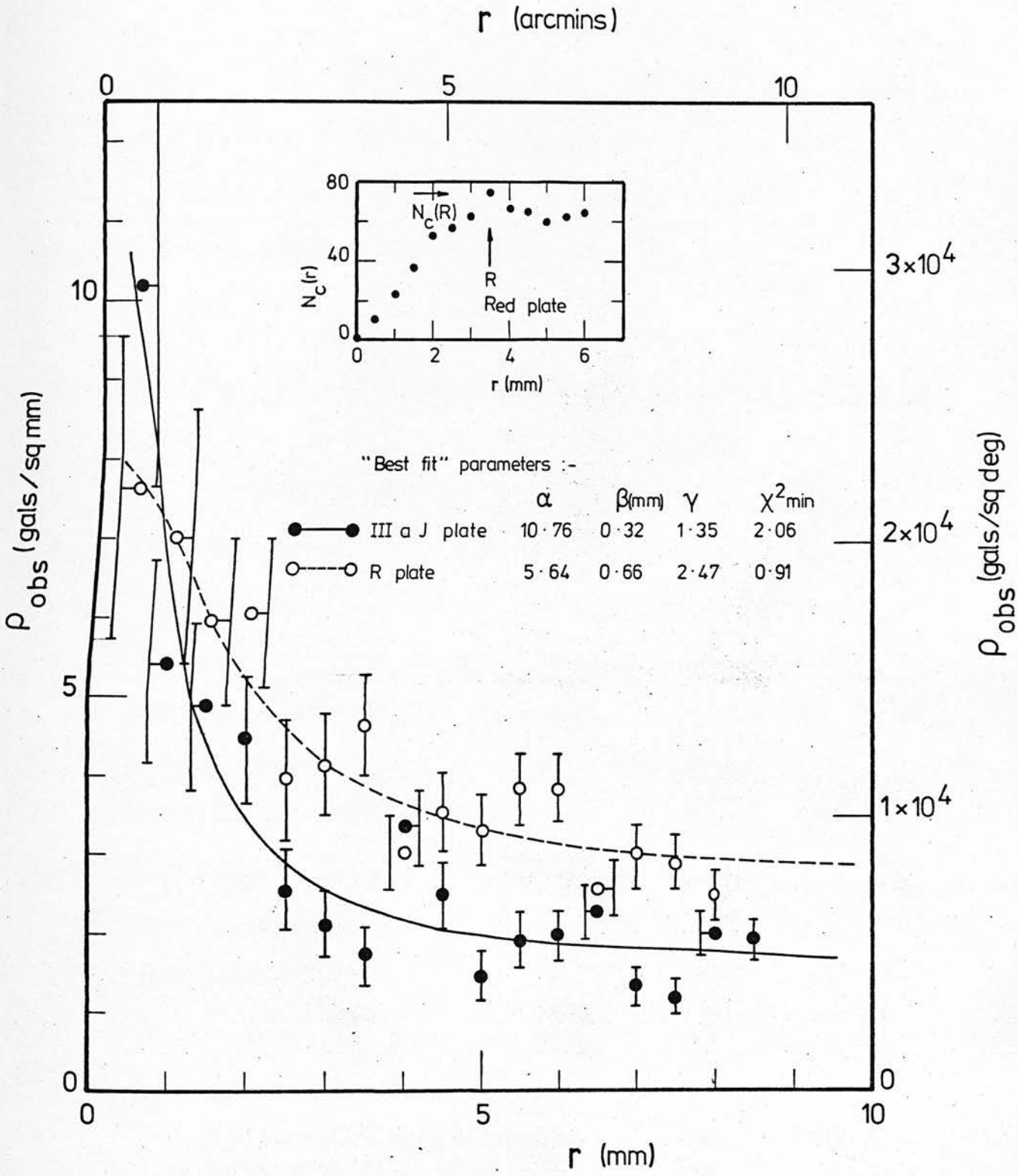

Figure 20. The radial densities of galaxies in the cluster 02392 -2852 on the blue and on the red plates. The curves represent the "best fit" models of the projected isothermal gas sphere distribution.

related through the equation:-

$$\rho_{obs}(r) = \alpha \rho_{isoth}(r/\beta) + \gamma \qquad (6)$$

where $\rho_{obs}(r)$ is the observed density distribution, ρ_{isoth} ($\xi = r/\beta$) is the projected isothermal gas sphere distribution, α is a scaling factor in density, β is the structural length (or core radius) and γ is a quantity related to the background density of galaxies. The equation is sometimes also written in the form:-

$$\frac{1}{\alpha}(\rho_{obs}(r) - \rho_{b.g.}) = \rho_{isoth}(r/\beta) - D. \qquad (7)$$

where $\rho_{b.g.}$ is the background field density of galaxies and D is some constant cut-off in the gas sphere distribution.

In this investigation, equation (6) is used; the quantities α, β and γ are all determined in the fitting.

The curves in figures 14-20 represent the "best fit" models of the isothermal gas sphere to the observed density distribution. In each case, the best fit parameters for α, β, γ and χ^2_{min} are included in the figure. The uncertainties in the values for β obtained in the fits are discussed in the next section. Fits to the values for the cluster 22129 - 3558 are performed only on the first 11 rings due to the effect on the counts of the presence of the nearby cloud of galaxies (figure 10).

IV. 5. Results

The results for the 6 clusters are summarised in Table 19. Column 2 contains the estimated Bautz-Morgan (1970) type, column 3 contains the Rood-Sastry (1971) type, and column 4 contains

visual estimates for the size of the cluster major and minor axes respectively obtained from plots of the machine output. The core radii (in arcmins) for the cluster taken as a whole and separately for the bright and faint members are given in columns 5, 6 and 7. The halo radius and concentration ($c = 3\beta/\bar{r}$, originally defined by Austin & Peach 1974a) are given in columns 8 and 9, and finally column 10 contains the cluster population, $N_c(R)$.

The quantities following the $\overset{+}{-}$ signs in the columns for the core radii represent the differences on taking the cluster centre 1mm (0.5mm for the clusters of smaller apparent angular size) away from the chosen centre. These values are taken to represent reasonable estimates for the uncertainties in the respective core radii and are in general $\lesssim$ 30% of the adopted values. The corresponding quantities for the halo radii are the standard errors in their determination as derived originally by Noonan (1972), and for the concentration they represent the resulting uncertainties from both.

No difference in core radius between the bright and faint members is detected in the cluster 22129 -3558. Small differences are present in 3 clusters (22146 -3457, 22315 -3800 and 01454 -3216) but the uncertainties are great. Similarly, in the cluster 02392 -2852 segregation may be present but the difference in core radii is within the limit on the uncertainty. The difference between the distribution of bright and faint members in the cluster 22156 -3525 is, however, significant ($>$50% difference in their core radii) and certainly well outside the limit on the uncertainty.

Table 19

Properties for the six clusters

(1) Cluster	(2) BM	(3) RS	(4) Size (arcmins x arcmins)	(5) β (arcmins)	(6) β_b (arcmins)	(7) β_f (arcmins)	(8) $\bar{r}$ (arcmins)	(9) C	(10) $N_c(R)$
22129 -3558	I	cD	14.3 x 11.5	0.75 ± 0.02	0.75 ± 0.16	0.75 ± 0.03	5.4 ± 0.3	0.417 ± 0.024	313
22156 -3525	I	B	18.3 x 4.8	0.78 ± 0.15	0.56 ± 0.14	0.96 ± 0.18	4.6 ± 0.5	0.509 ± 0.064	140
22146 -3457	III	F	20.4 x 5.4	0.67 ± 0.17	0.59 ± 0.15	0.69 ± 0.17	5.0 ± 0.4	0.402 ± 0.047	152
22315 -3800	I-II	C	10.9 x 6.2	0.68 ± 0.18	0.67 ± 0.21	0.69 ± 0.21	5.2 ± 0.3	0.392 ± 0.041	340
01454 -3216	II-III	C	7.4 x 3.5	0.35 ± 0.01	0.32 ± 0.09	0.40 ± 0.08	2.4 ± 0.3	0.438 ± 0.055	66
02392 -2852 (blue plate)	II	C	6.2 x 3.1	0.36 ± 0.07	0.28 ± 0.02	0.41 ± 0.15	2.0 ± 0.15	0.540 ± 0.088	55
(red plate)	II	C	6.2 x 4.0	0.74 ± 0.21			2.4 ± 0.3	0.925 ± 0.145	74

An increase in the degree of segregation with elongation of the cluster is suggested in the results. For the cluster 22129 -3558, which is the most spherical, no segregation is detected while the cluster showing the greatest degree of segregation is also the most highly flattened (22156 -3525). The cluster 02392 -2852, which is also highly flattened, also exhibits a possibly high degree of segregation.

There is also a suggestion in the results of an increase in segregation with concentration. The two clusters displaying the greatest degrees of segregation are also the only clusters with values exceeding 0.5 in their concentration. The remaining clusters all have lower values for c.

The core radius for the cluster 02392 -2852 from the measurements on the red plate is about double that on the blue and is, in any case, well outside the uncertainties. The halo radius is also slightly larger on the red plate but is such that the concentration ($c = 3\beta/\bar{r}$) approaches unity. Visual estimates for the size of the major and minor axes from plots of the machine output indicate that the cluster is more spherical on the red plate than on the blue. This observation is somewhat subjective. However, due to the small angular size of the distribution of cluster galaxies and the high degree of central concentration, the apparent outer boundaries of the cluster above the background galaxy distribution are well defined.

IV. 6. Azimuthal distribution of galaxies

No difference in azimuthal distribution for galaxies is detected between the bright and faint members for all clusters apart

from the cluster 22156 -3525. In Table 20, the azimuthal counts (measured clockwise from the north vector, i.e. west through north) for all the galaxies in this cluster and bright and faint members separately are tabulated. The distributions are plotted as histograms in figure 21. Two symmetrical peaks in the distribution are evident. The two curves represent visually determined fits to the histograms for the bright and faint members. The half widths for the distributions in the first peak are the same for the two curves but different for the second (roughly 40 degrees for the bright members, 80 degrees for faint ones). The bright galaxies are in a more highly flattened configuration than the faint.

Table 20

Azimuthal distribution of galaxies
in the cluster 22156 -3525.

ϕ (degrees)	N	N_b	N_f
0- 19	14	4	10
20- 39	22	10	12
40- 59	29	8	21
60- 79	26	10	16
80- 99	22	5	17
100-119	14	5	9
120-139	11	2	9
140-159	17	5	12
160-179	21	10	11
180-199	21	5	16
200-219	25	7	18
220-239	32	10	22
240-259	22	6	16
260-279	18	2	16
280-299	20	5	15
300-319	16	4	12
320-339	11	2	9
340-359	15	4	11

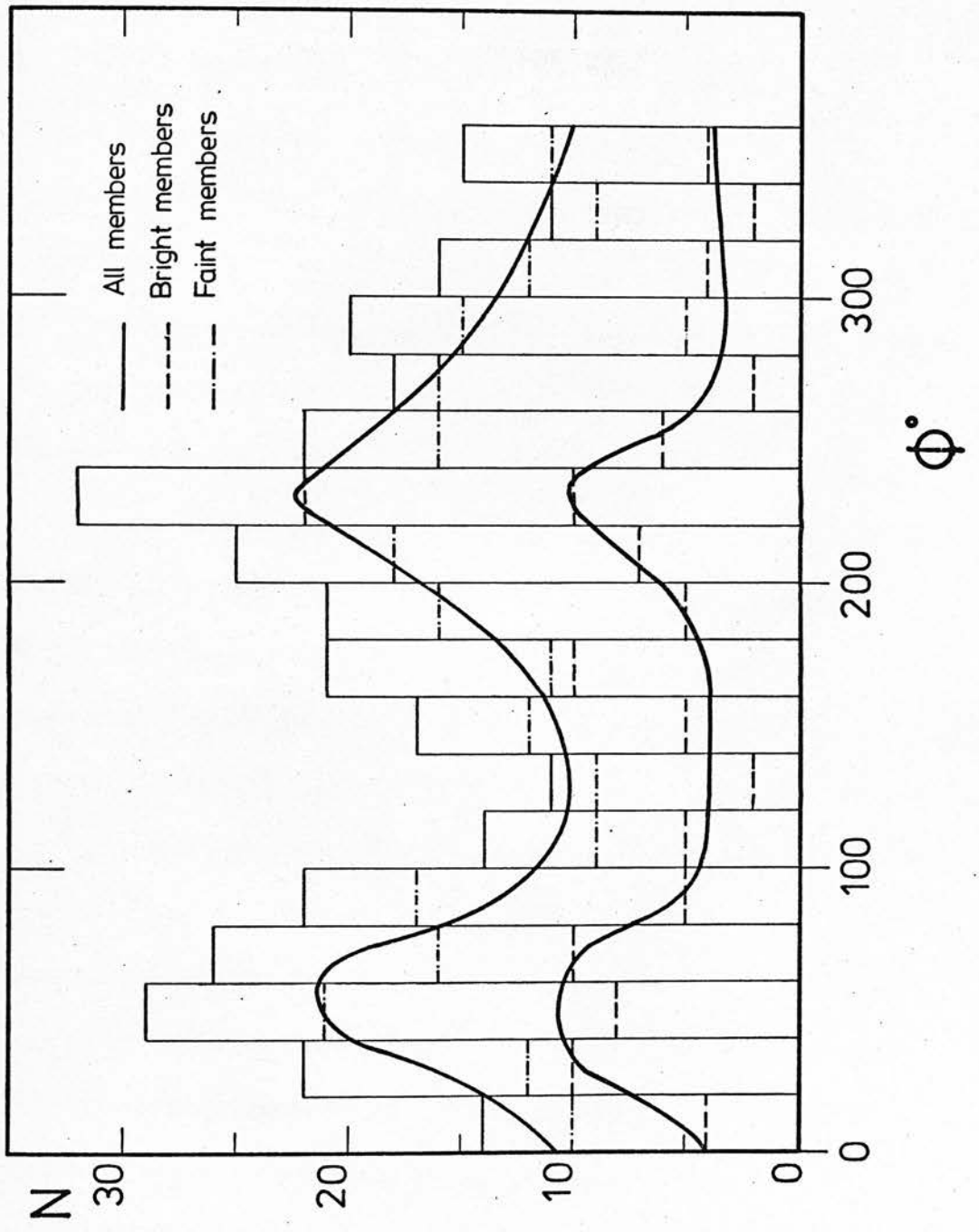

Figure 21. The azimuthal distribution of galaxies in the cluster 22156 -3525.

V. VISUAL MEASUREMENTS OF DISTANT CLUSTERS

V. 1. The clusters

The material presented in this chapter is the result of visual measurements of the properties (positions, sizes, orientations and shapes) of distant clusters of galaxies on a UK 48-inch Schmidt Telescope plate. In this context, the term 'cluster' is used here to represent compact groups of galaxies rather than rich clusters of the type catalogued by Abell (1958) and those studied in the previous chapter of this thesis.

It is recognized that, insofar as these measurements are concerned, severe subjective effects, in particular selection effects of the type discussed by Öpik (1969) and references therein, have most probably operated on the data. It is felt, however, that investigations of this type, although subjective, are merited, especially in view of the deeper penetration in space of plates taken with the UK 48-inch Schmidt Telescope and the corresponding insight gained by approaches of this nature.

The clusters in this investigation consist of distant associations on the plate of 5 or more galaxies with more or less the same apparent angular size. For a practical criterion, the mean galaxy separation had to be a few times the typical galaxy diameter. In order to be selected, a cluster had to have clearly definable outlines. Lines of galaxies were automatically dismissed since there was no satisfactory evidence that these were physically associated

entities.

For several of the clusters, the typical galaxy population were just distinguishable above the limiting plate magnitude. Considering that plates taken with the UK 48-inch Schmidt Telescope have been shown to reach magnitude B = 23 (Corben, Reddish & Sim 1974), then these clusters must be very distant indeed, possibly in fact extending out to as far as z = 0.5 (Dodd et al. 1975).

There is the possibility of contamination of the sample at this great distance by Abell-type clusters, the expected numbers of which may be computed. It is possible to eliminate these clusters by means of the typical colours of their galaxy population. Since groups of galaxies are comprised mainly of spirals, the colours of which are blue, they are distinguishable from richer clusters of galaxies, the brightest members of which are typically elliptical and therefore generally redder. Such distinctions are beyond the scope and capability of this thesis. However, since large-scale luminosity segregation in rich clusters is not a general phenomenon (from the previous chapter), the distribution of brightest members may be taken to be a reasonable representation of the distribution of the total galaxy population.

V. 2. The measurements

A 7.5cm (1.42 degree) square region near the centre of the UK 48-inch Schmidt Telescope plate number 149 was systematically scanned with a binocular microscope (magnification 25x) to detect distant groups and clusters of galaxies. The symmetrical outlines

of the clusters allowed the determination of cluster centres, shapes and orientations. Measurements of the cluster parameters were made using the 50x power of the microscope and a graticule, calibrated in tenths of a mm, at the focus of one of the eyepieces. Cluster centres were determined to the nearest tenth of a mm on the plate with respect to the lines of a superimposed film grid; semi-major and semi-minor axes were determined to the nearest hundredth of an arc minute, and position angles measured to within $\pm$2 degrees using a scale around one of the eyepieces calibrated in 5 degree intervals.

In all 178 clusters were detected on the plate in this region representing a mean smoothed-out density of 88 clusters per square degree. The parameters for these clusters, sorted into order of decreasing X coordinate on the plate are given in Table 21. Column 1 contains a running number, columns 2 and 3 contain the X and Y coordinates respectively of the cluster from the bottom left hand corner of the plate, columns 4 and 5 contain the semi-major (a) and semi-minor (b) axes in arc minutes, and column 6 contains the position angle (θ) (measured east from the north meridian, where the north meridian is represented by the vertical axis of the film grid) in degrees. Where the cluster appeared spherical on the plate, the last two columns in Table 21 are left blank.

V. 5. The contribution from rich clusters

It is possible to estimate the possible contribution to the sample by the presence of rich Abell-type clusters of galaxies, the

Table 21

Parameters for the distant groups and clusters

No.	X (mm)	Y (mm)	a (arcmins)	b (arcmins)	$\ominus$ (degrees)
1	219.1	205.0	0.22	0.09	45
2	218.8	191.2	0.62	0.22	169
3	218.7	153.0	0.52	0.22	118
4	218.4	187.6	1.25	0.29	17
5	218.1	182.3	0.54	0.18	172
6	217.8	200.5	0.43	0.13	57
7	217.8	160.5	0.63	0.39	136
8	217.5	201.5	0.32	0.30	162
9	217.2	175.5	0.37	0.10	109
10	216.8	156.6	0.30	0.12	152
11	216.4	145.6	0.48	0.24	120
12	216.4	181.3	0.47	0.09	170
13	215.6	180.6	0.32	0.22	39
14	215.3	150.7	0.36	0.15	109
15	215.1	169.8	0.40	0.17	172
16	214.2	194.6	0.49	0.21	72
17	214.0	218.4	0.53	0.11	12
18	213.9	160.1	0.50	0.18	35
19	213.8	217.7	0.36	0.21	134
20	212.8	183.5	0.63	0.30	67
21	212.7	157.9	0.90	0.25	154
22	211.7	171.9	0.50	0.19	133
23	210.3	210.2	0.32		
24	210.3	159.6	0.67	0.15	59
25	210.1	215.6	0.39	0.15	24
26	209.0	180.5	0.72	0.11	151
27	208.6	200.3	0.21		
28	208.5	162.8	0.96	0.28	41
29	207.5	180.9	0.69	0.11	99
30	207.4	160.1	0.54	0.13	2
31	207.3	185.9	0.41	0.14	171
32	206.7	145.7	0.34	0.17	55
33	206.1	192.4	0.56	0.12	76
34	205.8	154.1	0.37	0.19	162
35	205.7	217.6	0.76	0.24	82
36	204.9	161.8	1.24	0.41	25
37	204.5	216.5	0.52	0.08	83
38	203.7	161.0	1.41	0.34	21
39	203.0	156.7	0.43	0.07	65
40	202.1	188.5	0.18	0.14	16
41	201.3	168.1	0.47	0.19	20
42	201.0	198.2	0.24	0.10	103
43	200.9	171.7	0.34	0.17	50

Table 21 continued

No.	X (mm)	Y (mm)	a (arcmins)	b (arcmins)	Θ (degrees)
44	200.3	168.0	0.22	0.11	67
45	199.8	171.3	0.38	0.11	88
46	199.1	144.3	0.39	0.18	150
47	199.0	145.3	0.40	0.25	5
48	198.8	217.7	0.40	0.22	130
49	198.2	210.3	0.72	0.18	120
50	197.6	156.2	0.29	0.20	50
51	197.6	151.5	0.46	0.09	31
52	197.1	155.2	0.52	0.18	8
53	196.5	189.4	0.88	0.41	159
54	196.3	176.2	1.10	0.39	117
55	195.8	197.3	0.21		
56	195.4	166.4	0.68	0.24	64
57	195.3	211.6	0.78	0.30	21
58	195.2	154.3	0.57	0.17	176
59	195.1	192.2	0.38	0.08	58
60	195.0	186.6	0.45	0.12	16
61	194.9	164.8	0.38	0.15	106
62	194.9	149.0	0.33	0.07	169
63	193.9	147.9	0.45		
64	193.8	158.0	0.20	0.11	115
65	193.6	195.2	0.59	0.16	89
66	192.7	165.6	0.49	0.28	16
67	192.2	143.9	0.30	0.10	57
68	191.6	184.9	1.00	0.24	35
69	191.5	180.9	0.50	0.14	86
70	191.4	188.5	0.68	0.34	50
71	190.1	195.1	0.46	0.33	144
72	189.6	165.0	0.35	0.24	151
73	189.5	187.6	0.40	0.21	25
74	189.1	190.0	0.46	0.07	69
75	188.4	200.4	0.43	0.20	159
76	186.8	183.1	1.12	0.36	4
77	185.8	166.8	0.63	0.17	112
78	185.5	145.5	0.52	0.13	129
79	185.1	165.8	0.31	0.18	174
80	184.7	210.9	0.37	0.11	4
81	184.7	185.8	0.36	0.08	78
82	183.6	148.6	0.42	0.13	110
83	183.5	184.6	0.41	0.07	61
84	182.4	200.9	0.17	0.08	150
85	182.3	148.3	0.49	0.21	101
86	182.2	170.8	0.40	0.17	100
87	180.5	195.6	0.57	0.47	29
88	180.3	203.6	0.75	0.36	16

Table 21 continued

No.	X (mm)	Y (mm)	a (arcmins)	b (arcmins)	θ (degrees)
89	179.8	162.7	0.41	0.08	131
90	179.7	185.0	0.96	0.15	16
91	179.6	154.5	1.40	0.21	98
92	179.3	174.9	0.24	0.06	94
93	177.3	193.5	0.48	0.15	78
94	177.0	157.2	0.24	0.11	89
95	176.7	192.6	0.21	0.15	176
96	176.7	197.5	0.73	0.36	91
97	176.3	203.7	1.06	0.28	5
98	176.3	178.3	1.02	0.21	3
99	175.6	188.0	0.31	0.18	42
100	174.7	184.2	0.97	0.15	24
101	173.5	191.5	0.44	0.13	78
102	173.3	192.3	0.30	0.24	154
103	173.3	195.1	0.19	0.08	64
104	173.3	201.2	0.41	0.25	161
105	172.9	199.1	0.34	0.12	172
106	172.4	200.1	0.92	0.22	168
107	172.0	197.8	0.24	0.15	148
108	171.9	192.2	0.43	0.28	144
109	171.9	188.3	0.35	0.18	11
110	171.9	197.2	0.38	0.09	125
111	171.1	162.2	0.47	0.20	52
112	171.0	200.5	0.37	0.13	61
113	169.6	188.6	0.62		
114	169.3	168.1	0.69	0.29	161
115	168.3	207.8	0.39	0.18	81
116	168.2	193.9	1.03	0.30	89
117	168.1	201.4	0.32		
118	167.6	192.5	0.38	0.07	51
119	167.1	149.6	0.49	0.19	170
120	167.0	156.6	0.58	0.32	130
121	166.5	159.1	0.44	0.20	77
122	166.5	195.9	0.43	0.10	47
123	166.4	170.7	0.44	0.17	52
124	165.8	147.4	0.26	0.13	177
125	165.7	169.8	0.31	0.15	61
126	165.5	162.0	0.25	0.15	69
127	163.1	163.4	0.37	0.16	158
128	162.7	164.5	0.45	0.11	16
129	162.4	199.7	0.48	0.20	53
130	161.7	175.8	1.08	0.24	93
131	161.5	153.9	0.59	0.21	4
132	161.4	165.2	0.45	0.27	94
133	161.4	166.5	0.34	0.24	164

Table 21 continued

No.	X (mm)	Y (mm)	a (arcmins)	b (arcmins)	Θ (degrees)
134	161.4	159.0	1.20	0.45	24
135	160.9	208.8	0.22	0.14	88
136	159.4	147.1	0.74	0.17	96
137	158.4	156.8	0.81	0.27	18
138	157.7	160.3	0.36	0.15	76
139	157.6	217.9	0.27	0.10	10
140	157.2	196.0	1.06	0.27	168
141	156.8	195.0	0.25	0.15	160
142	156.7	163.3	0.40	0.24	43
143	156.6	213.7	0.31	0.13	138
144	156.4	217.4	0.80	0.13	49
145	155.2	215.0	0.27	0.11	88
146	155.0	168.5	0.77	0.25	84
147	154.3	187.6	0.26	0.09	52
148	154.1	193.5	0.24	0.08	94
149	154.1	190.0	0.40	0.16	13
150	153.1	176.0	0.52	0.25	79
151	153.1	164.4	0.71	0.18	170
152	152.9	216.4	0.31		
153	152.9	193.6	0.25	0.07	81
154	152.8	147.9	2.37	0.78	21
155	152.3	200.4	0.90	0.26	38
156	151.7	195.1	0.54	0.21	136
157	151.6	198.2	0.82	0.34	55
158	151.5	158.1	0.40	0.22	132
159	151.5	179.9	0.97	0.12	119
160	151.2	161.1	0.81	0.36	46
161	150.7	148.9	0.45	0.25	51
162	150.6	159.2	0.69	0.13	125
163	149.9	178.9	1.08	0.24	28
164	149.2	149.4	0.75	0.50	153
165	149.0	177.5	0.84	0.28	152
166	148.7	168.3	0.97	0.22	96
167	148.4	195.2	0.29	0.17	52
168	148.2	180.8	0.58	0.24	70
169	147.9	163.3	0.48	0.14	157
170	147.3	213.6	0.78	0.60	143
171	146.2	198.4	0.29		
172	145.8	178.3	0.34	0.13	69
173	145.7	182.0	0.91	0.32	155
174	145.2	169.4	0.72	0.15	89
175	145.1	171.0	0.71	0.19	55
176	144.8	177.1	1.00	0.37	15
177	144.5	147.7	1.21	0.26	177
178	143.7	143.8	0.28	0.13	53

expected numbers of which (assuming no effects of evolution with time) will simply be proportional to the volume of space included in this survey.

Abell (1958) detected 2712 rich clusters in some 1.5×10^4 square degrees of sky down to a redshift z ($= \Delta\lambda/\lambda$) ~ 0.2. This gives a mean smoothed-out density of 0.2 clusters per square degree of sky. In the field in this investigation there should thus be 0.4 clusters down to the limit of Abell's survey.

Now, the expected numbers of Abell-type clusters out to the limit of plate 149 will be:-

$$N_C = \left(\frac{D_{149}^2 \, R_{149}}{D_A^2 \, R_A} \right) N_A \qquad (8)$$

where R_{149} and R_A are the depths of space of this and Abell's survey respectively, D_{149} and D_A are the sides of space represented by 1.42 degrees at the depths of the surveys, and N_C and N_A are the expected numbers of rich clusters.

Using $v = HR$ (Hubble's Law) and $v = cz$, this equation simplifies to:-

$$N_C = \left(\frac{D_{149}^2 \, Z_{149}}{D_A^2 \, Z_A} \right) N_A \qquad (9)$$

where z_{149} and z_A are the redshifts corresponding to the depths of each survey. Furthermore, using:-

$$\theta_o = \frac{D H_o (1+Z)^2}{cZ} \quad \text{with} \quad q_o = +1$$

(Mattig 1958; Sandage 1961; and equation (33) of this thesis), this reduces to:-

$$N_C = \frac{Z_{149}^3 (1+Z_A)^4}{Z_A^3 (1+Z_{149})^4} \qquad (10)$$

which, with $z_{149} \sim 0.5$ (Dodd et al. 1975) finally gives $N_C = 6.4 N_A \sim 3$ Abell-type clusters. Assuming each rich cluster has a probability of unity of being detected, then their contribution to the sample is only a few percent and their effect on the results therefore negligible.

V. 4. Distribution of the clusters

Figure 22 is a plot showing the relative positions of the 178 clusters detected in this survey. The scales in the figure are in terms of mm from the lower left-hand corner of the plate. The cluster distribution from the plot appears somewhat clumpy, the physical significance of which may be tested.

To test the significance of the apparent clustering of these distant groups and clusters, a method originally devised by Wagoner (1967) and developed more fully in the subsequent analysis of Bogart & Wagoner (1973) is used. The method involves a search for departure from randomness in the distribution of projected nearest neighbour angular separations. For this purpose, use is made of the central limit theorem.

The central limit theorem gives the result that in the limit of large N, the mean nearest neighbour separations will have a Gaussian distribution centred on μ with standard deviation $N^{-\frac{1}{2}} \sigma$ where μ and σ are the mean and standard deviation respectively of the probability distribution of nearest neighbour distances. The estimated probability distribution, with computed values for μ and σ, is obtained from a set of random clusters.

A random-number generator program, written by Dr. Dodd at the Royal Observatory Edinburgh, was used to produce 178 clusters distributed at random in 3 dimensional space from 1000 Mpc to 4000 Mpc distant within an angle of 1.42 degrees. The clusters were projected onto the plane of the sky and their projected nearest neighbour separations gave the random probability function.

The results are tabulated in Table 22. The first column contains the nearest neighbour separations in arc minutes, the second, third and fourth columns contain the observed distribution, the Poisson distribution centred on the observed mean (2.86 arcmins) and the frequency distribution corresponding to the randomly generated clusters respectively. These distributions are shown as histograms in figure 23. The solid histogram represents the observed distribution, the dashed histogram is the Poisson distribution around the observed mean, and the histogram consisting of a series of dots and dashes in turn is the distribution obtained from the randomly generated clusters.

It is seen from the figure that the observed distribution peaks before the random one and falls off less rapidly. The random distribution has a mean and standard deviation of 2.53 and 1.74 respectively. With these values, the difference between the observed and expected means is $(\langle d \rangle - \mu).N^{\frac{1}{2}}.\sigma^{-1}$ = +2.6 standard deviations.

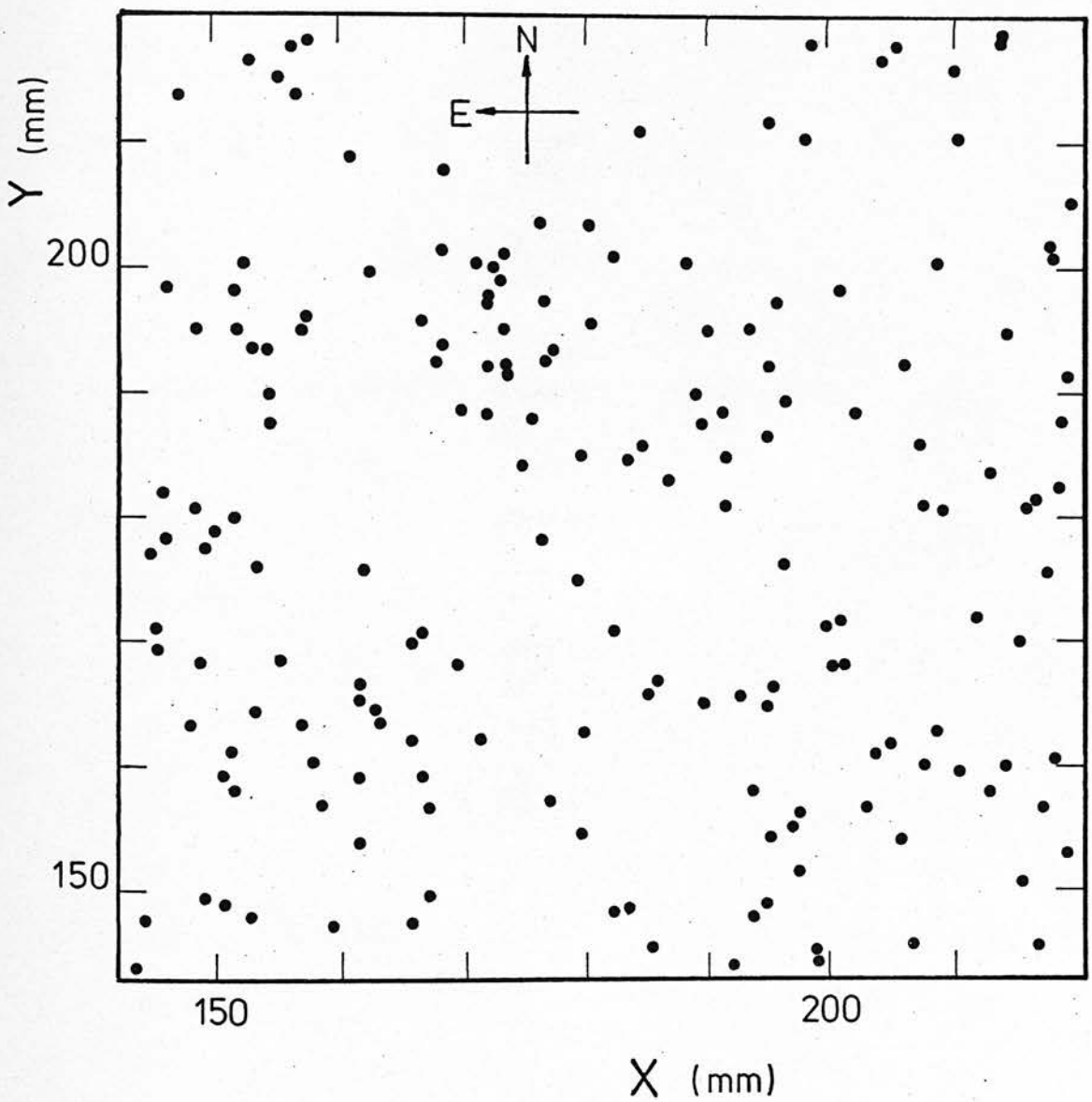

Figure 22. Plot showing the relative positions of the distant groups and clusters on plate 149. The origin for the X and Y axes is at the lower left hand corner of the plate.

Table 22

Frequency distributions for the nearest neighbour separations:-

Separation, d (arcmins)	N (observed)	Poisson (mean = 2.86 arcmins)	N (random case)
0-1	8	10.2	19
1-2	45	29.2	32
2-3	36	41.7	44
3-4	24	39.7	41
4-5	35	28.4	22
5-6	13	16.3	11
6-7	8	7.7	5
7-8	7	3.2	0
>8	2	1.6	4

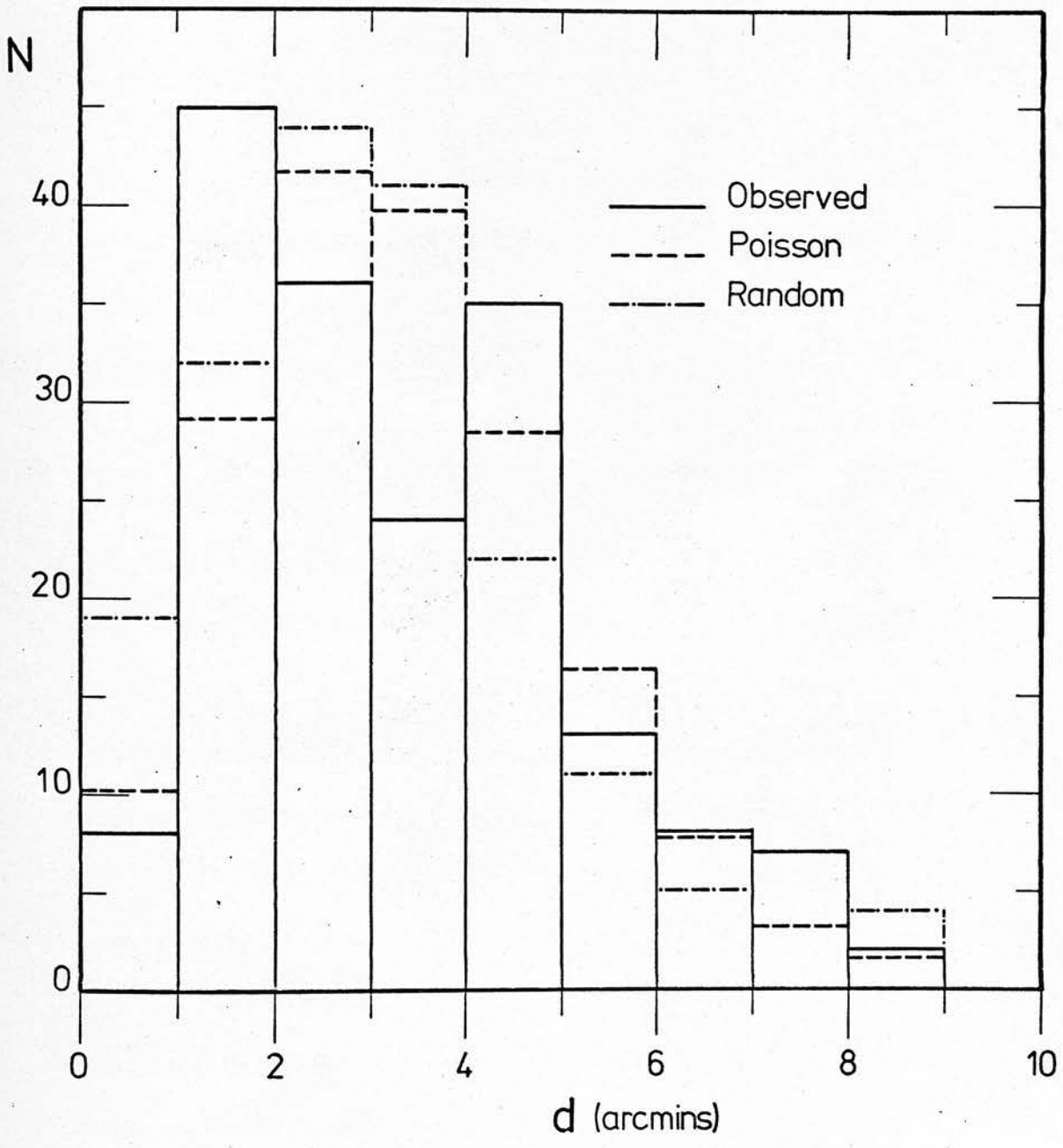

Figure 23. Histograms for the frequency distributions of nearest neighbour projected separations for the distant groups and clusters.

Thus the observed mean is more than 2.5 standard deviations from the expected mean. This is taken as evidence that these distant groups and clusters of galaxies are indeed significantly clustered.

V. 5. Shapes and orientations of the clusters

The frequency distribution for cluster ellipticities ($e = 1 - b/a$) is presented in Table 23. Also tabulated are the expected frequencies from two theoretical models of the distribution of apparent ellipticities. The first of these, model A, is the case in which all intrinsic ellipticities from $e = 0.0$ to $e = 0.7$ occur with the same probability and we observe as a result a system of random intrinsic ellipticities distributed with random inclinations to the line of sight. The second model, B, represents the case in which intrinsic ellipticities $e = 0.7$ have the highest probability of occurrence and we observe a distribution in which only intrinsic ellipticities of $e = 0.7$ occur, but with random inclinations to the line of sight.

The frequency distributions are shown plotted in figure 24 where the histogram represents the observed frequency distribution and the curves are for the two models. It is seen that high ellipticities are predominant among the clusters. In fact, the situation is more extreme than that predicted by model B. It is concluded that these groups and clusters have the appearance on the plate of highly flattened systems.

The frequency distribution for cluster orientations is tabulated in Table 24 and shown in figure 25. On application of

Table 23

Frequency distribution for cluster ellipticities (e = 1 - b/a)

e	Observed No.	Curve A	Curve B
0.00-0.05	8	40.2	9.8
0.05-0.15	1	41.1	19.8
0.15-0.25	4	30.1	20.3
0.25-0.35	8	23.1	20.6
0.35-0.45	16	17.8	21.5
0.45-0.55	25	13.0	23.5
0.55-0.65	41	8.7	29.2
0.65-0.75	35	4.1	33.3
0.75-0.85	38		
0.85-0.95	2		

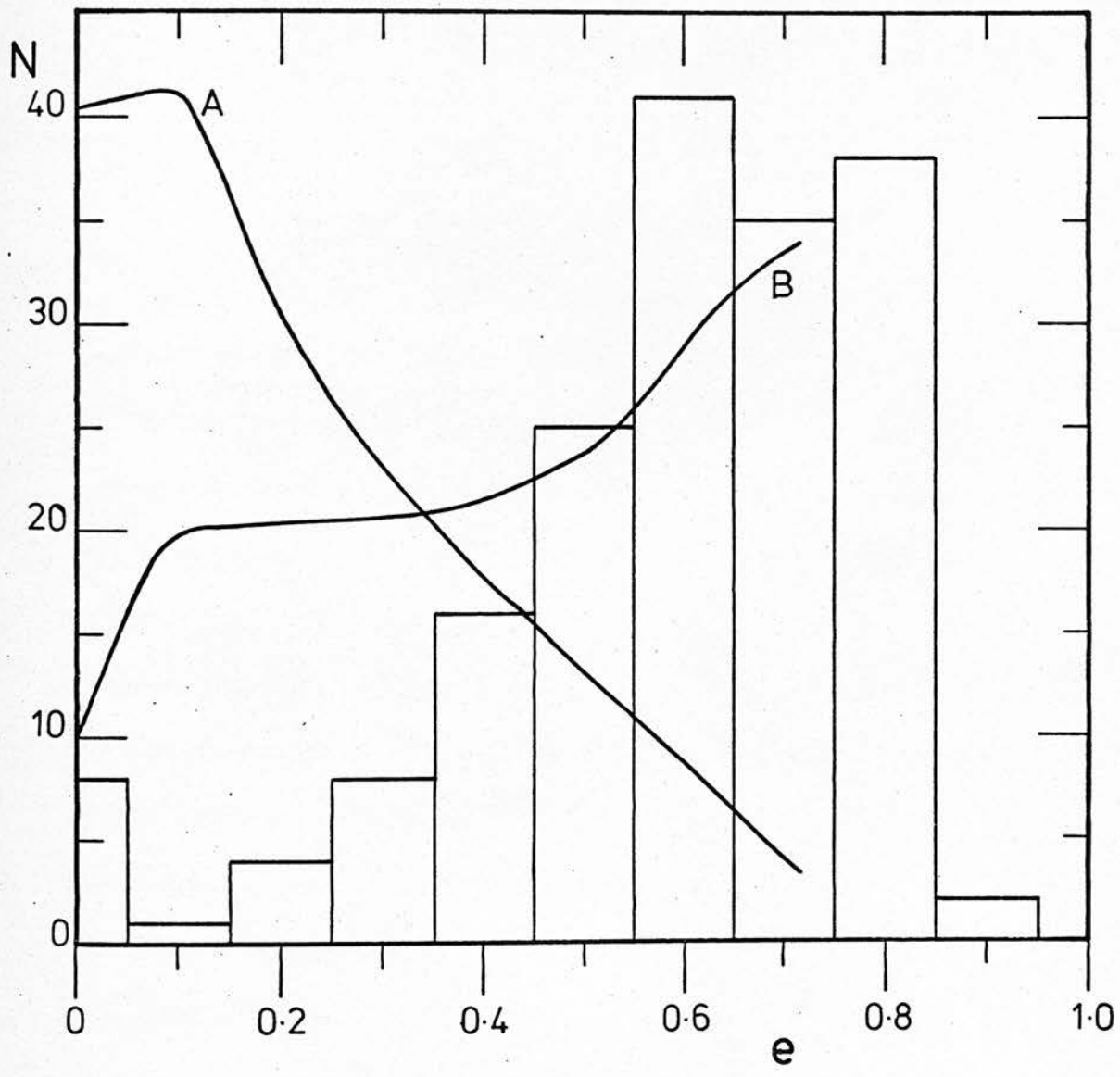

Figure 24. Histogram for the frequency distribution of observed ellipticities for the distant groups and clusters. The two curves represent theoretical models for the distribution.

a χ^2 test, the distribution has a 7.5% probability of having been produced in a random distribution. Due to the subjective nature of the measurements, however, this effect is unlikely to be real. The reason for presenting the distribution of orientations is to show that there is no general preferred direction for cluster orientation. The significance of this and the consequences are discussed in the final chapter.

V. 6. Relationships between the parameters

The distribution of cluster ellipticities for each of three different ranges of semi-major axis is tabulated in Table 25 and shown plotted as the solid histogram in figure 26. The top histogram represents the distribution for the largest clusters, the bottom that for the smallest. The diagram shows that the peak in the distribution systematically shifts towards smaller ellipticities as we go from large clusters to small. There is no major difference, however, such as the majority of small clusters being spherical while the majority of larger clusters are highly flattened. The dashed histograms represent the result of correcting the distribution for the smallest clusters by removing a seeing disk of 0.05 arcmins. The peak in this corrected distribution is seen to be displaced towards greater ellipticity. The shift in the position of the peak with different size may, therefore, be interpreted as due to the effect of seeing which blurs the images of the constituent galaxies and which has a more pronounced effect on smaller clusters. It is concluded that there is no detectable difference

Table 24

Frequency distribution for cluster orientations

$\ominus$ (degrees)	N
0- 9	8
10- 19	13
20- 29	11
30- 39	5
40- 49	7
50- 59	18
60- 69	11
70- 79	9
80- 89	13
90- 99	9
100-109	6
110-119	6
120-129	5
130-139	9
140-149	4
150-159	14
160-169	10
170-179	12

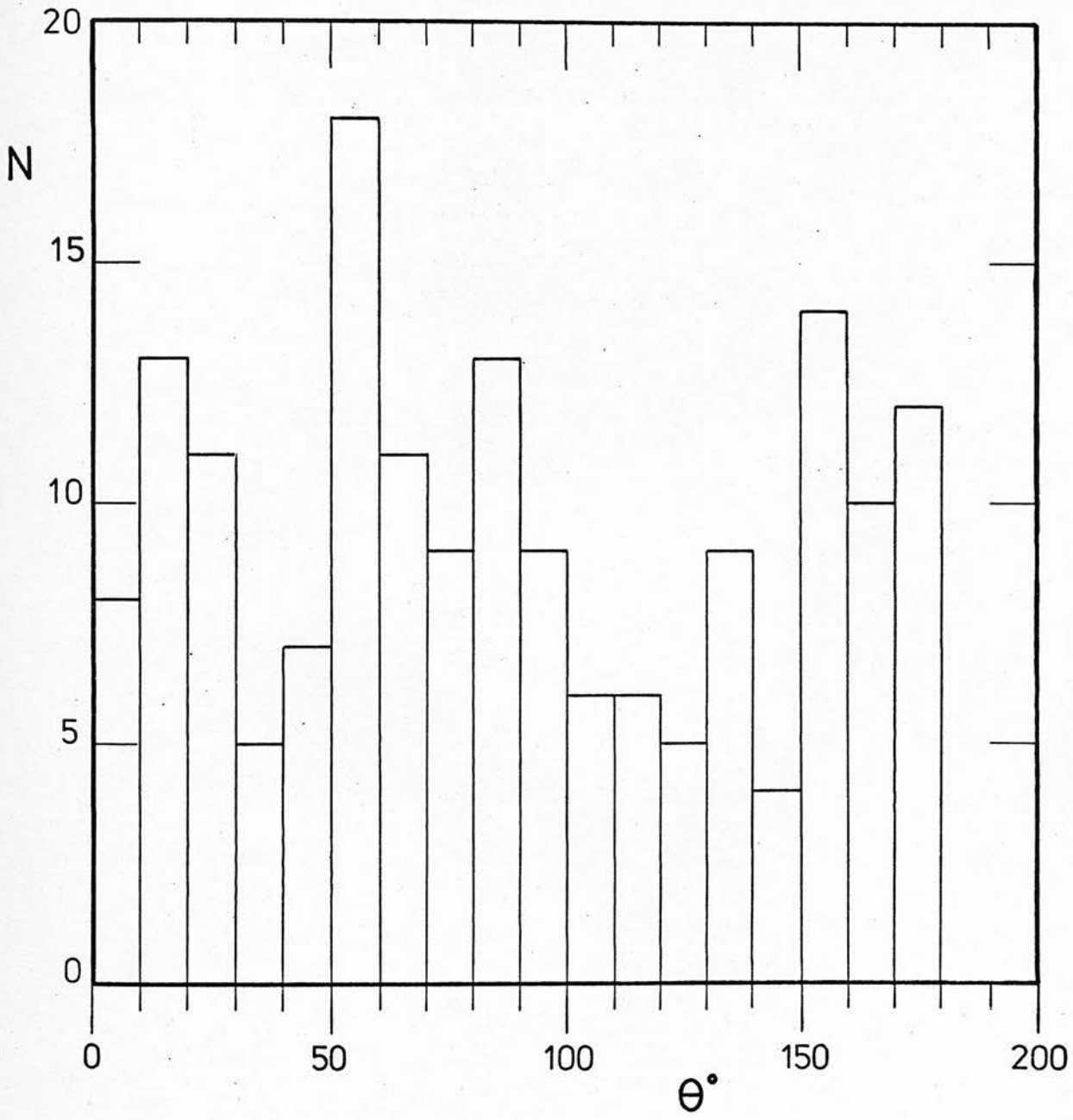

Figure 25. The distribution of orientations for the distant groups and clusters showing no generally preferred direction for orientation.

Table 25

Frequency distributions for cluster ellipticities in 3 size ranges

e	$N_{a > 0.57}$	$N_{0.58 > a > 0.38}$	$N_{a < 0.39}$	$N_{a < 0.39}$*
0 -0.05	1	1	6	6
0.05-0.15	0	0	1	1
0.15-0.25	1	1	2	1
0.25-0.35	1	2	5	2
0.35-0.45	2	6	8	4
0.45-0.55	5	9	11	8
0.55-0.65	12	15	14	8
0.65-0.75	17	11	7	12
0.75-0.85	19	13	6	11
0.85-0.95	2	0	0	7

* Distribution with 0.05 arcmin correction for seeing.

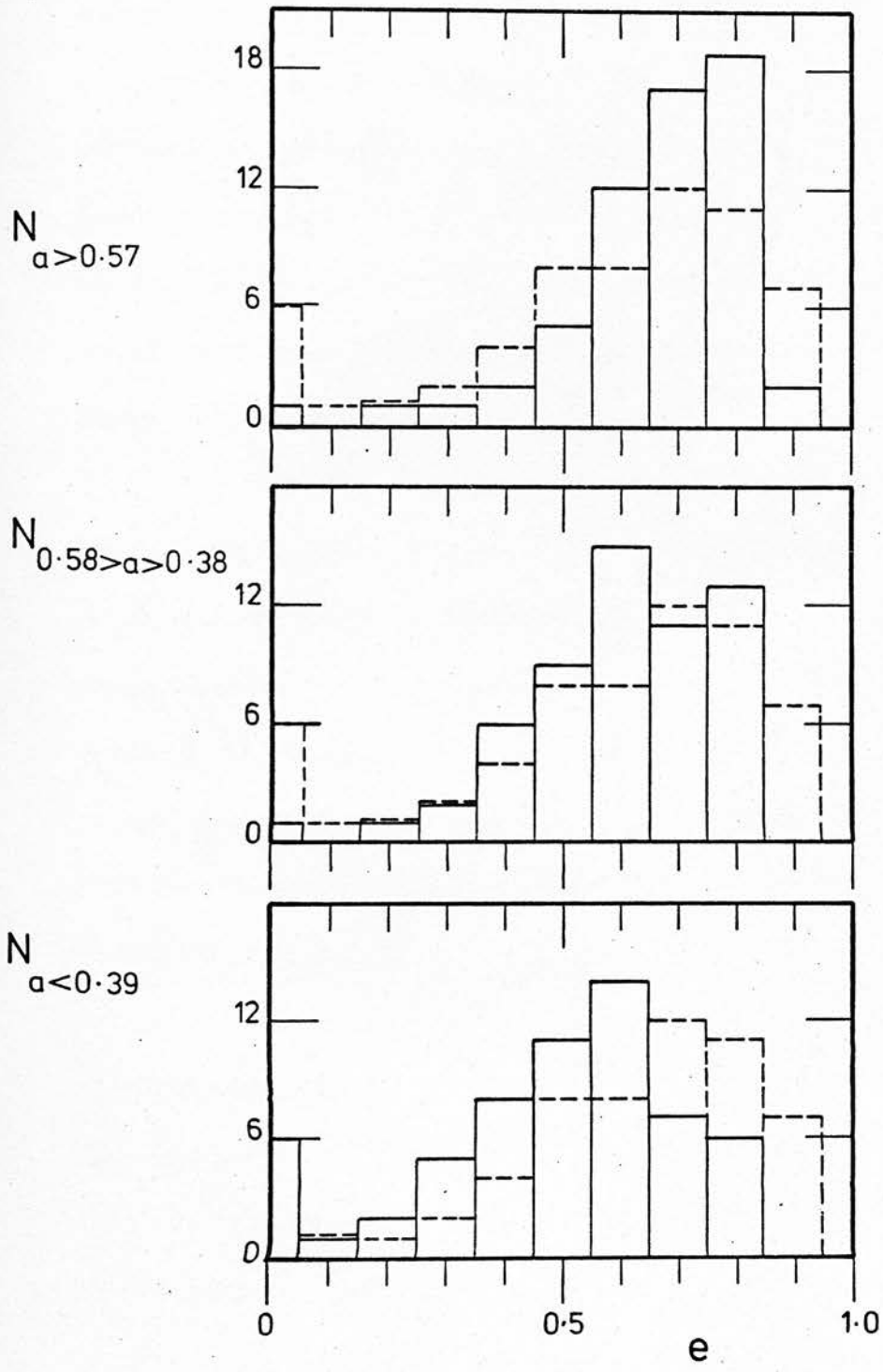

Figure 26. Frequency distributions for cluster ellipticities for each of 3 different ranges of sizes (solid histograms). The dashed histogram represents the distribution for the $N_{a<0.39}$ distribution with a correction of 0.05 arcmin for seeing.

in shape properties between the more distant and nearby clusters.

In Table 26, contingency tables representing the clusters binned into 3 ranges each of size, shape and orientation are presented. The first of these shows the relationship between cluster size and orientation. There is a slight tendency for large clusters to be preferentially aligned with position angles between 0 and 60 degrees. On application of a χ^2 test, there is a confidence of 26.5% of this result being produced by a non-random distribution. The result is probably not significant.

The second of the contingency tables shows the relationship between shape and orientation. More flattened clusters appear to be preferentially orientated with position angles from 0 to 120 degrees, while clusters which are less flattened are preferentially orientated from 120 to 180 degrees. The result has a confidence limit of 94.8% of having been produced by a non-random distribution. However, with the complicated relationship between cluster size and shape this relationship is doubted.

The relationships obtained from the contingency tables, although interesting, are thought highly unlikely to have a basis in physical reality. Due to the presence of effects such as observer bias, astigmatism, and other subjective effects the reality of these relationships is open to question.

Table 26

Contingency tables for orientation and size, and shape and orientation.

a (arcmins) \ Θ (degrees)	0-60	60-120	120-180
>0.57	25	18	16
$0.58 > a > 0.38$	21	18	18
<0.39	16	20	18

Θ (degrees) \ e	<0.54	$0.70 > e > 0.54$	>0.70
0- 60	17	23	22
60-120	11	22	23
120-180	24	14	14

VI. DISCUSSION

VI. 1. The rich clusters

The results obtained in chapter IV, although from a small sample of rich clusters, do permit some preliminary conclusions to be drawn. The findings are now discussed in more detail and combined with other observations to produce a framework basic for further research into the structure of rich clusters.

The elongation in the distribution of galaxies for all 6 rich clusters studied here is a striking property having fundamental consequences for our understanding of the structure of rich clusters. There is no reason to suspect the presence of untoward selection effects, e.g. the preferential selection of non-spherical clusters, in the cluster selection. The selected clusters are taken to be fairly representative of the body of rich clusters as a whole.

Elongation in the galaxy distribution is known in other well-studied rich clusters - in the Coma cluster (Abell 1965; RPKK 1972), in Abell 2199 (Rood & Sastry 1972), in the Perseus cluster (Bahcall 1974) and in the cluster Abell 1413 (Austin & Peach 1974a, 1974b). This being the case, elongation may be a fairly common feature in rich clusters. Where a cluster does appear to be spherical may be due to the fact that we are observing a disk-like structure face-on. An interesting investigation is to obtain shape properties for a number of rich clusters in order to analyse the distribution of apparent shapes

and to compare the distribution with that expected from theoretical models.

Flattening in a system is usually associated with a rotation, detectable as systematic properties in the radial velocities of member galaxies. So far, no investigation has revealed the presence of rotation in rich clusters - in the Perseus cluster, Chincarini & Rood (1971) nor in the Coma cluster, RPKK (1972) and Gregory (1975). Absence of a net orbital angular momentum in these two systems must not preclude such in other clusters. Satisfactory steps must be taken to survey the radial velocities in other rich clusters to establish whether the absence of rotation is a general phenomenon.

Although significant luminosity segregation (i.e. a $>$ 50% difference in core radii between the bright and faint members) has been detected in one cluster studied here, the results of this investigation have shown that the presence of large-scale segregation is not a general effect, in agreement with other results in the literature. Small scale segregation ($<$ 30%) may be present on the whole, but the differences are well within the uncertainties in the data.

Evidence is also present for azimuthal segregation in the distribution of galaxies for the cluster in which significant radial segregation was detected. The brighter galaxies form a more flattened system than do the fainter ones. The brighter galaxies are thus more centrally concentrated and in a more disk-like configuration than are the fainter ones.

A tendency is found for the degree of radial segregation to increase with increased flattening of the total galaxy distribution. This type of effect might be expected from systems with non-zero total orbital angular momenta undergoing relaxation by two-body close encounters.

Austin & Peach (1974a) have discussed a possible correlation between cluster concentration ($c = 3\beta/\bar{r}$) and crossing time (Rood, Rothman & Turnrose 1970) in that the higher the concentration the smaller is the crossing time. This is tentatively taken to suggest that clusters with high values for concentration are the more relaxed, their extensive halos being indistinguishable above the background distribution of galaxies. The evidence for this is, however, slender and Austin and Peach point out that it is possible the opposite may be the case. The original conclusion of Austin & Peach (1974a) is supported by an observation made in this investigation that clusters with high values for concentration tend to have higher degrees of luminosity segregation. It would therefore appear that clusters with high concentrations are indeed the more relaxed systems and we observe mainly their dense cores, their extensive halos being lost in the general background of galaxies.

Comparison of the distribution of galaxies in one cluster on a red and a blue plate has revealed that the core radius in the red is about double that in the blue, indicating the segregation of galaxies according to colour. Bluer galaxies are more centrally concentrated that the red. The bluer galaxies also form a more flattened system. The cluster concentration in red light is very nearly unity indicating

that the core of the cluster in red light almost fills the cluster halo, i.e. that there is no distinction between the core and halo in red light.

These observations of the distribution of galaxies in the cluster in different colours are consistent with the picture for the structure of the cluster in which the cluster consists of a flattened core of bluer galaxies surrounded by a more spherical halo of redder galaxies. It is interesting to compare the properties of this idealised model for the structure of the cluster with the properties of a spiral galaxy which when seen in red light appears almost spherical but when seen in blue light consists of a disk. If this analogy may be used then it may be concluded that the flattened core of the cluster consists generally of younger galaxies than in the halo. Perhaps galaxy formation is still in process in this flattened core.

There are several areas in which direct comparison may be made between the observations described here and the model developed by Icke (1973) for the formation of galaxies within clusters due to turbulence. The theory predicts that predominantly elongated clusters are formed due to turbulence within collapsing prolate spheroidal regions of space. The first galaxies to condense out reheat the surrounding gas, effectively increasing the Jean's mass and shifting the mass spectrum towards higher masses. Smaller galaxies are therefore expected to have a more spherical distribution than the larger ones and this spherical distribution is also reflected in the distribution of older galaxies, the younger galaxies having a more flattened distribution.

There is good concordance between the predictions of Icke's (1973) theory and the observations made in this thesis. All 6 rich clusters studied here are elongated. For one cluster, the brighter galaxies were found to form a more highly flattened system than the fainter ones, although for the other clusters no differences in azimuthal distribution were discernible. In another cluster (for which a red and a blue plate were available), the older (by analogy to the spiral galaxy) galaxies were found to form a more spherical structure while the younger galaxies formed a more disk-like core. Clearly further observations of the properties of clusters are required to confirm these results.

Icke's (1973) theory also predicts that the asymmetry due to the initial shape of the parent protocluster causes an asymmetry in the appearance of the perturbations resulting in a preferential alignment of the galaxies with the major axis of the cluster. Analyses of the distribution of shapes and orientations of member galaxies in rich clusters would be of great value. Shandarin (1974) has discussed the possibility of discriminating in this way between turbulence theories of this sort and vortex theories.

VI. 2. The distant clusters

The results from measurements on the distant groups and clusters, although subjective, are nevertheless important for the extension of quantitative investigations of these objects out to very great distances, $z \sim 0.5$.

The existence of second-order clustering on scales of 2 to 3 objects per supercluster has been established among rich

clusters (Bogart & Wagner 1973; Hauser & Peebles 1973). This investigation has shown that the distant groups and clusters studied here are themselves significantly clustered. This clustering is present in scales from pairs up to large cloud complexes.

The highly flattened nature of the distant groups is indeed interesting. The situation is more extreme than the theoretical distribution for the apparent ellipticities in which only intrinsic ellipticities of $e = 0.7$ occur and with random inclinations to the line of sight. One possible cause of the high degree of flattening may be due to the action of some distorting agent, e.g. cosmological distortion (Kristian & Sachs 1966; Kristian 1967; Refsdal 1970). This hypothesis is unlikely, however, in view of the fact that one preferred direction for apparent orientation of the groups would be required in the data and this has not been found. The physical nature of the flattening appears, therefore, to be real.

Whether these groups represent complete entities or whether they are only the brightest members of richer clusters or clouds of galaxies is immaterial. What is important is that elongation appears to be an integral part of all systems, whether rich clusters or small groups. It would therefore seem of use to seek mechanisms for such flattening, whether due to a rotation or some perturbation for example.

No appreciable evidence for evolutionary effects in the shapes of these groups and clusters is found. Only large differences, however, such as all the more distant clusters appearing spherical while the nearer ones appear more flattened, would have been detected.

VI. 3. Conclusion

In this thesis, a method has been developed allowing the computer to distinguish automatically between the images of galaxies and those of stars from measurements made with the COSMOS fast, automatic, plate-measuring machine at the Royal Observatory Edinburgh. The distribution of galaxies in 6 rich clusters has been examined, using this technique, from measurements made on plates taken with the U.K. 48-inch Schmidt Telescope in Australia in a study of the cluster properties and a search for systematic trends.

Analysis of the overall galaxy distribution has revealed that all 6 clusters are unambiguously elongated. Comparison of the core radii of bright and faint members has indicated that there is no general evidence for the presence of large-scale luminosity segregation, although significant segregation (i.e. > 50% difference in core radii between the bright and faint members, accompanied by a higher degree of flattening) has been detected in one cluster. Evidence is found to suggest that the degree of luminosity segregation increases with elongation and also with concentration indicating that clusters which are highly flattened or which have high concentrations are more relaxed.

Evidence for colour segregation has been obtained in one cluster for which a blue and a red plate were available. The galaxies on the blue plate are much more centrally concentrated and in a more flattened configuration than those on the red. This observation permits the formulation of a picture for the structure of the cluster in which the bluer galaxies are seen to form a flattened core while

the red galaxies form a more spherical halo.

Visual measurements have been made, with the aid of a binocular microscope, on the properties of distant groups and clusters on a plate out to a redshift of $z \sim 0.5$. These groups and clusters show evidence for significant clustering, existing in systems from pairs up to large cloud complexes. They are also predominantly highly flattened. The presence of the cosmological distortion effect is not detected in the appearance of the clusters, nor is there found any appreciable effect of evolution in the cluster properties.

VI. 4. Suggestions for future work

The results presented in this thesis represent a preliminary contribution to the quantitative examination of rich clusters of galaxies. With measurements from COSMOS and automatic techniques for the separation of the images of galaxies and stars, we are now in a powerful position to carry out detailed systematic and objective studies of the properties of the matter within the Universe. In particular, it is intended to continue investigations along the lines of this thesis into the properties of rich clusters.

For a study of this nature, measurements involving a number of clusters are required. Since the characteristics may vary from cluster to cluster, only with a fairly large sample will true systematic trends be revealed.

The results of the present investigation have revealed a number of interesting characteristics: elongation in the shapes of the overall galaxy distribution, dependences of luminosity segregation

on elongation and on concentration, and the presence of some segregation according to colour. Further investigations along these lines should prove worthwhile. It is also intended to carry out detailed investigations of the distribution of galaxy shapes and orientations within clusters using the Fine Measurement mode of the COSMOS machine in order to investigate the distribution of these parameters, the relationships between them and their relationships with the integral properties of the parent cluster.

Photometric studies of rich clusters are also planned. Short exposure U.K. Schmidt Telescope plates of selected clusters in different colours have been obtained and it is intended to carry out detailed studies of colour differences across clusters and the relationships with other cluster properties.

Paralleling these studies, a program is being planned to carry out spectrophotometric investigations. It is intended to examine the radial velocities of individual galaxies in some nearby rich clusters in a systematic search for evidence of rotation. Redshifts of more distant clusters are also to be obtained in order to extend the (m - z) and (θ - z) relationships to greater redshifts.

Further work on distant groups and clusters along the lines of investigation in this thesis will also be worthwhile. Repetition of the measurements by some independent observer will help to identify and eliminate subjective effects. It is also intended, however, to carry out a systematic survey of the properties of these objects in different directions in the southern sky to continue studies of the large-scale properties of matter. Comparison of the properties of these

groups and clusters with similar properties of nearer groups and clusters would be informative. The detection of rotation in these systems by means of systematic effects in the radial velocities of member galaxies would also be of importance.

APPENDIX I

Cosmology and the role of clusters of galaxies

1. General equations

With the assumption that the Universe is homogeneous and isotropic, the Robertson-Walker line element in co-moving coordinates (that is each galaxy has fixed spatial coordinates r, θ and ϕ) may be written as (Refsdall, Stabell & de Lange 1966):-

$$ds^2 = c^2dt^2 - R^2(t)\left[\frac{dr^2}{1-Kr^2} + r^2\left(d\theta^2 + \sin^2\theta d\phi^2\right)\right] \qquad (11)$$

where k = +1, 0, or -1 and R is a scale factor with dimension length. This line element fixes the proper time or distance interval between two points (events) in space-time in terms of the coordinate interval between the points. For example, suppose that two points are separated by the interval:-

$$dt = d\theta = d\phi = 0, \quad dr > 0$$

then the proper distance between the points is:-

$$dl = Rdr\left(1 - Kr^2\right)^{-\frac{1}{2}}$$

Fixing the origin of the coordinates on any chosen galaxy, such as our own, then the proper distance to another galaxy at coordinate distance r ($r^2 \ll 1$) is:-

$$l(t) = R(t).\, r \qquad (12)$$

Since the coordinates are co-moving, the radial coordinate r of

a chosen galaxy is fixed, and the velocity of recession of the galaxy relative to our own is:-

$$v = \frac{dl}{dt} = \dot{R}r = \frac{Rl}{R} = Hl \tag{13}$$

with $$H = \frac{\dot{R}}{R}$$

which is Hubble's Law. Thus there is a direct connection between the assumed homogeneity and isotropy of the Universe and Hubble's Law.

Stabell & Refsdal (1965) obtain from Einstein's field equations two non-trivial equations:-

$$8\pi G\rho = \frac{3}{R^2}(kc^2 + \dot{R}^2) - \lambda \tag{14}$$

$$\frac{8\pi G P}{c^2} = \frac{-2\ddot{R}}{R} - \frac{\dot{R}^2}{R^2} - \frac{kc^2}{R^2} + \lambda \tag{15}$$

where G is the gravitational constant, λ the cosmical constant, ρ the mean density in the Universe and p is the pressure. In the absence of any secure evidence to the contrary it may be most reasonable to adopt the simplest assumption that in equations (14) and (15) the constant λ and the pressure p are negligibly small and that k = 0. This then implies that the mean mass density is:-

$$\rho_c = \frac{3H^2}{8\pi G} \approx 10^{-28}\ g\ cm^{-3} \tag{16}$$

with $H_0 = 100\,\mathrm{Km\ sec^{-1}\ Mpc^{-1}}$. This equation has a simple interpretation in that in a sphere of density ρ_c the material just has escape velocity, the kinetic energy of expansion just amounting to the total gravitational potential. The sphere would stop expanding and collapse if the density were greater than ρ_c. Usually, Ω is

defined to be the ratio of gravitational to kinetic energy in the Universe. It follows that $\Omega = \rho / \rho_c$. In the usual models, thus, where $\lambda = 0$, if $\Omega < 1$ then k must equal -1, $\dot{R}^2$ is always greater than zero and the Universe will expand forever. If $\Omega > 1$, then k = +1, $\dot{R}^2$ falls to zero when R gets large enough, the expansion stops and the Universe collapses again. Thus when k = -1 the model is said to be open, if k = +1 the model is closed, while if k = 0 the model is cosmologically flat.

It is found to be more convenient today to classify relativistic world models by means of the deceleration parameter q_0 and the density parameter σ_0 defined by:-

$$q_0 = \frac{-R_0 \ddot{R}_0}{\dot{R}_0^2} \tag{17}$$

$$\sigma_0 = \frac{4\pi G \rho_0}{3H_0^2} \tag{18}$$

where the subscript 0 denotes present value of the parameters. Using these quantities, when the matter pressure p = 0, equations (14) and (15) reduce to (Stabell & Refsdal 1965):-

$$\lambda = 3H_0^2 (\sigma_0 - q_0) \tag{19}$$

and

$$Kc^2 = H_0^2 R_0^2 (3\sigma_0 - q_0 - 1) \tag{20}$$

where K/R_0^2 is the spatial curvature.

For the models where $\lambda = 0$ <u>i.e.</u> $(\sigma_0 - q_0) = 0$ in equation (19), equation (20) becomes:-

$$\frac{Kc^2}{R_0^2} = H_0^2 (2q_0 - 1) \tag{21}$$

For the three possible values of k the limits of q_0 are (Sandage 1961):-

$q_0 > \frac{1}{2}$ for $K = +1$ (closed, hyperbolic models)

$q_0 = \frac{1}{2}$ for $K = 0$ (flat space)

$0 \leq q_0 \leq \frac{1}{2}$ for $K = -1$ (open, elliptical models)

The lower limit for exploding models is $q_0 = 0$ for $k = -1$. This is obtained from subtracting equation (15) from equation (14) and putting $\rho (= \rho_0) = 0$. Here the Universe is empty.

It also follows that $\Omega = 2q_0$.

2. Tests for deciding between the various world models

Most of the present day observational research in extra-galactic astronomy is directed towards determining the deceleration parameter q_0. Once q_0 is known the world model follows from the above equations.

In a review paper, Sandage (1961) put forward several observational tests. They include:-

i) the deviation from linearity of the redshift-magnitude relation.

ii) the galaxy-count-magnitude relation.

iii) the angular diameter-redshift relation.

i) The magnitude-redshift relation is a powerful method for finding q_0. For all models with $q_0 > 0$, Mattig (1958) has shown that:-

$$M_{BOL} = 5 \log \frac{1}{q_0^2} \left\{ q_0 z + (q_0 - 1)\left[\sqrt{(1 + 2q_0 z)} - 1\right] \right\} + C \quad (22)$$

where the constant C may be found by fitting the equations to observations at bright magnitudes. For the special case of $q_0 = 0$ the

equation is:-

$$M_{BOL} = 5 \log z \left(1 + \tfrac{1}{2} z\right) + C \qquad (23)$$

Sandage (1961) points out that in the (m - z) diagram the magnitude difference between the steady state model ($q_0 = -1$) and the exploding Euclidean case ($q_0 = \frac{1}{2}$) at the redshift $z = 0.5$ is 0.7 mag. This difference should be observable.

Observations are usually made on members of clusters of galaxies for two reasons. Firstly, the luminosity function of galaxies can be sampled at a definite part thereby restricting the study to those galaxies of nearly the same intrinsic luminosity. The second reason is that the brightest members in clusters have brighter absolute magnitudes than the average field galaxy. At a given redshift cluster galaxies will appear brighter than field galaxies. Cluster galaxies can hence be studied out to higher redshifts.

In practice, the first-ranked cluster member has been used for this purpose (Humason, Mayall & Sandage 1956). Sandage (1972) points out that the small scatter in the (m - z) diagram for the first-ranked cluster members and the dispersion in their absolute magnitudes of only 0.3m about the mean constitute evidence for their usefulness as distance indicators. There are, however, two possible selection effects which must be considered (Bautz & Abell 1973). There is the possibility of a correlation between cluster richness (Abell 1958) and the luminosity of the brightest cluster member, causing a systematic tendency to select richer clusters among the more distant, and of a dependence of the absolute magnitude of the

first-ranked cluster member with Bautz-Morgan type (Bautz & Morgan 1970). The latter effect is important at large distances where clusters with cD galaxies, i.e. clusters which have one or two outstandingly bright members compared to the bright galaxy population (Mathews, Morgan & Schmidt 1964; Morgan & Lesh 1965), are most suitable for spectroscopic observation.

Abell (1962, 1965, 1970) has suggested the use of the break in the differential cluster luminosity function, or the discontinuity in the integrated luminosity function, as a suitable distance indicator. Bautz & Abell (1973) have calibrated the difference in the apparent magnitude between the brightest galaxy and the break in the luminosity function against cluster richness and form type. Using this calibration, a revised velocity-apparent magnitude relationship is obtained from matching the luminosity functions of 14 of the Humason, Mayall & Sandage (1956) clusters. The revised (m - z) diagram shows a much tighter relationship than that based on the magnitude of the first-ranked cluster galaxy.

More observations are required before the preliminary calibration of Bautz and Abell can be verified. Consistent results have been obtained, however, by Austin & Peach (1974b) for the cluster Abell 1413. Using the break in the differential luminosity function instead of the magnitude of the first-ranked cluster member, Bautz and Abell find that the observed values fit well the curve for $q_0 = 0$, corresponding to the open, empty Friedmann universe.

ii) The method of galaxy counts is based on the expectation that if galaxies are uniformly distributed in space, then counts out to

successive distances r would yield numbers proportional to the volume enclosed by r. Because volumes in Riemann space vary either slower or faster than r^3, according to whether k is +1 or -1 then a determination of the spatial curvature should in principle be possible.

Observationally we do not count galaxies out to successive distances r but rather to successive apparent magnitudes. Let N(m) be the number of galaxies per square degree brighter than apparent magnitude m. Sandage (1961) shows that there is only a very small difference in N(m) at faint magnitudes between the closed, oscillating model with $q_0 = +1$ and the open, empty model $q_0 = 0$. A small observational error is thus sufficient to alter the conclusion drastically.

It is extremely difficult, therefore, to find the correct world model from galaxy counts. Furthermore, the contention that galaxies are distributed homogeneously on the plane of the sky is invalid. Galaxies show a strong tendency to cluster. Even if on the large scale galaxies are homogeneously distributed the fluctuations in any sample area preclude the use of counts for deciding between the models. The situation is made worse by the spread in the absolute luminosity of galaxies and the evolutionary effect of a change in $L(\lambda)$ with time.

iii) The use of the metric diameters of a suitable category of cosmological test object (such as clusters of galaxies) may prove a valuable means of testing cosmological models. Peach & Beard (1969) have shown that the angular diameter-redshift relation for rich

clusters is comparable in precision with the redshift-magnitude relation applied to brightest cluster members.

In terms of the dimensionless parameter 'u' representing the co-moving space coordinates r, θ, ϕ (i.e. independent of time) the Robertson-Walker line element is given by:-

$$ds^2 = c^2dt^2 - R^2(t)\,du^2 \tag{24}$$

The metric distance of a galaxy which emits photons at time t_1 that arrive at the observer at time t_0 is:-

$$u = c\int_{t_1}^{t_0} \frac{dt}{R(t)} = \int_0^{r_1} \frac{dr}{\sqrt{(1-Kr^2)}} \tag{25}$$

where r is the dimensionless radial coordinate and the observer is taken to be at r = 0. This equation integrates to:-

$$u = \begin{cases} \sin^{-1} r_1 & K = +1 \\ r_1 & \text{for} \quad K = 0 \\ \sinh^{-1} r_1 & K = -1 \end{cases} \tag{26}$$

or:-

$$r_1 = \begin{cases} \sin u & K = +1 \\ u & \text{for} \quad K = 0 \\ \sinh u & K = -1 \end{cases} \tag{27}$$

The metric distance at the time of photon emission is $r_1R_1 = r_1S(u)$ where $S(u) = \sin(u)$, u, or $\sinh(u)$ for $k = +1, 0,$ or -1.

A source whose metric distance is $R_1S(u)$ at the time of photon emission and whose linear diameter is y has an observed

angular diameter at t_0 of (Sandage 1961):-

$$\theta_0 = \frac{y}{R_1 S(u)} \tag{28}$$

Now, the frequency shift of the radiation from a galaxy is given by:-

$$\frac{\lambda_0 - \lambda_e}{\lambda_e} = \frac{\lambda_0}{\lambda_e} - 1 = z \tag{29}$$

$$\therefore (1+z) = \frac{\lambda_0}{\lambda_e} = \frac{R_0}{R_1} \tag{30}$$

Substituting for R_1 in equation (28) gives:-

$$\theta_0 = \frac{y(1+z)}{R_0 S(u)} \tag{31}$$

Mattig (1958) has shown that:-

$$r_1 = S(u) = \frac{c}{R_0 H_0 q_0^2 (1+z)} \left\{ q_0 z + (q_0 - 1)\left(\sqrt{(1+2q_0 z)} - 1\right) \right\} \tag{32}$$

for all $q_0 > 0$. Therefore we get, from equations (31) and (32) that the apparent angular diameter of a test object at redshift z is:-

$$\theta_0 = \frac{y H_0}{c} q_0^2 (1+z)^2 \left\{ q_0 z + (q_0 - 1)\left(\sqrt{(1+2q_0 z)} - 1\right) \right\}^{-1} \tag{33}$$

Thus θ_0 is proportional to $(1 + z)^2$. For the steady state cosmology, $q_0 = -1$, and $\theta_0 \propto (1 + z)/z$.

Clusters of galaxies are suitable for the angular diameter-redshift test. The difficulty lies, however, in the choice of definition for cluster diameter. If clusters of galaxies are to be used as distance indicators then it must be ensured that their diameters are themselves distance-independent. From an analysis of the diameters of clusters in Zwicky's catalogue (Zwicky et al. 1961-68), where the

definition of cluster diameter was the mean diameter of the isopleth at which the surface density of galaxies with apparent magnitudes in the range between that for the brightest galaxy in the cluster and 3 magnitudes fainter is twice that in the surrounding field, Peach & Beard (1969) found systematic effects leading to an underestimation of the sizes of more distant clusters. Noonan (1972) has discussed the reasons for this effect. An important requirement, then, is that the cluster diameter must be independent of background galaxy field count.

Two definitions of cluster diameter have been used extensively in the literature. The first involves fitting the observed surface density of galaxies to the projected isothermal gas sphere distribution (Zwicky 1957; Bahcall 1972, 1973a, 1973b, 1973c, 1974). The observed distribution may be expressed as:-

$$\rho_{obs}(r) = \alpha \rho_{isoth}(r/\beta) + \gamma \qquad (34)$$

or equivalently:-

$$\alpha^{-1}[\rho_{obs}(r) - \rho_{b.g.}] = \rho_{isoth}(r/\beta) - c \qquad (35)$$

where $\rho_{obs}(r)$ is the observed surface densities, $\rho_{b.g.}$ is the constant background density and $\rho_{isoth}(\xi = r/\beta)$ is the projected Emden gas sphere distribution for the dimensionless radius ξ. The quantity α is the normalisation factor in density, β (the "structural length") characterises the width at half height and determines the "core radius" of the cluster, and γ is related to the constant background density through the relation $\gamma = \rho_{b.g.} - \alpha c$ where c is a constant cut-off in the background distribution. Values for

the Emden gas sphere distribution are tabulated by Chandrasekhar (1942) and Zwicky (1957).

The second definition was suggested by Noonan (1972) and used by him on several distant clusters (Noonan 1972, 1974a, 1974b). It involves the calculation of the mean distance of cluster members from the line of sight through the cluster centre.

Let $N_c(r)$ be the number of cluster members on the plane of the sky within a radius r of the cluster centre. The mean value of r is:-

$$\bar{r} = \int_0^R \frac{r\,dN_c(r)}{dr}\,dr \Big/ N_c(R) \qquad (36)$$

On integrating by parts we get:-

$$\bar{r} = R - \int_0^R F(r)\,dr \qquad (37)$$

where R is the outermost radius of the cluster and F(r) is the fractional cumulative ring count defined by $F(r) = N_c(r)/N_c(R)$.

The cluster count is obtained by subtraction of the field count from the total count. What is observed is the total number $N_T(r)$ of galaxies within radius r. Assuming a constant field density of 'n' galaxies per square degree, then we have:-

$$N_c(r) = N_T(r) - \pi n r^2 \qquad (38)$$

Thus the value of $\bar{r}$ is essentially determined by the outer parts of the density distribution as opposed to β which is fixed by the core. Large changes in the core density produce only minor changes in $\bar{r}$ due to the relatively slow fall off in the density outside the core and the greater weight attributed to the outer regions.

The failure of both these definitions in producing significant results in the angular diameter-redshift cosmological test is due to two reasons. Firstly, we know nothing about the intrinsic dispersion in the sizes of clusters of galaxies, and secondly there is the possibility of radial segregation effects in luminosity, colour and type for the cluster galaxies. The presence of such effects will cause artificial dependences of cluster size on limiting magnitude, passband, and galaxy surface brightness respectively. There is no general evidence regarding the presence of segregation effects in clusters. However, there are particular cases of various types of definite segregation (see chapters I and IV). For the present it is assumed that the sizes of clusters of galaxies are indeed distance-independent with the provision that when segregation is more fully understood then a correction can in principle be applied to allow for the effect on cluster sizes.

Austin & Peach (1974a), from an investigation of the sizes of several rich clusters, have found a correlation between the mean cluster radius (sometimes referred to as the "halo radius") and the core radius in the sense that the core radius varies inversely with the halo radius. Thus for a particular cluster, the larger the core radius the smaller is the halo radius. They also found, to a lesser extent, a correlation with the cluster population as defined to be the number of cluster galaxies with magnitude in the range between the magnitude of the third brightest cluster member and 2.5 magnitudes fainter. They obtained the numerical expression

relating the quantities:-

$$R_{\bar{r}} = (0.31 \pm 0.02) R_{3\beta}^{-1} + (4.36 \pm 0.49 \times 10^{-3}) N_{pop} - (0.14 \pm 0.09) \quad (39)$$

where the coefficients are shown with their standard errors, $R_{\bar{r}}$ and $R_{3\beta}$ are the mean cluster radius and core radius respectively calculated in the world model with $q_0 = +1$ and $H_0 = 50\,\mathrm{Km\ sec^{-1}\ Mpc^{-1}}$, and N_{pop} is the cluster population. For the core radius, 3β is conventionally used. This is almost exactly equivalent to the radius at half the central density for the projected gas sphere.

Using equation (39) Austin and Peach can infer from the observed values of β, z, and N_{pop} the intrinsic cluster radius $R_{\bar{r}}$ to the precision of the uncertainties in the observations and the coefficients of equation (39). The next step is straightforward. The observed value of $\bar{r}$ is adjusted to that angular radius which would be subtended by a particular standard cluster at the same redshift. Let R_{SC} be the radius of the standard cluster. Then Austin and Peach define a corrected mean cluster radius as:-

$$\bar{r}_c = \left(R_{SC} / R_{\bar{r}}\right) \cdot \bar{r} \quad (40)$$

Defining an arbitrary standard cluster as one with $R_{SC} = 1.35\,\mathrm{Mpc}$ and calculating the corrected mean cluster radius for their measured clusters, Austin and Peach find that in the plot for corrected angular radius against redshift the dispersion of the points about the mean line compares favourably with the scatter of points in the (m - z) diagram applied to the brightest members of the Sandage & Hardy (1973) clusters.

APPENDIX II

List of programs used in analysing the COSMOS measurements

A) Coarse Measurement programs:-

HMCMO1 This is the first program in the series dealing with the Coarse Measurement data. The program reads down the magnetic tape containing the Coarse Measurement data until it finds the specified region within the measured area and outputs to the line-printer the data for a number of images. This may be repeated for as many regions as required and for as many images as required within each region.

HMCMO2 Using the criteria for distinguishing galaxies from stars, from the data output by the first program, this program selects the galaxies and outputs their X and Y coordinates onto another magnetic tape.

HMCMO3 The coordinates of the galaxies are read from the magnetic tape and punched onto paper tape for feeding into COSMOS as a finding list for obtaining more accurate measures from Fine Measurement.

HMCMO4 The galaxy coordinates are read from the magnetic tape and points, at the respective positions of the galaxies, are plotted on a frame of the SD 4020 plotter. The galaxies are also counted in cells of any specified grid size and a texture map representing the cell mesh is drawn. In this way the presence of rich clusters should be made

fairly obvious. The cell mesh is output onto a magnetic tape for storing.

HMCMO4B This program draws the contour map representing the distribution of galaxies using the mesh output onto magnetic tape by the previous program. The procedure for drawing the contours is a standard procedure supplied by the ACL. Because of the limit on the amount of core store available, the largest mesh that can be handled by an ALGOL program is an array 60 x 60. There will most certainly be times when a mesh larger than this is being used. For this reason, this program splits the map into four quadrants and draws the contours in each quadrant in turn.

HMCMO4C This is a contour drawing program similar to HMCMO4B; in this program, however, the contour map is drawn in a single unit. It is normally the program used when the mesh is less than 60 x 60.

B) Fine Measurement programs:-

HMFINE1 This is the first in the series of programs dealing with Fine Measurement data. This program reads down the fine measurement magnetic tape and outputs the parameters for a number of images. The purpose of this is for a visual check of the data and for calibration (i.e. calibration of the machine M-values in terms of image diameter, in microns, on the plate).

HMFINE2 This is a linear least-squares fitting program to calibrate the machine M-values for the images into microns.

HMFINE3 This program selects the required type of image from the fine measurement data (i.e. good elliptical-fit or bad elliptical-fit), converts the M-values into microns, theta into degrees and outputs the parameters onto another magnetic tape.

HMFINE4 Outputs the parameters on this new tape onto paper tape for purposes of safe-keeping (e.g. in case of accidentally over-writing the data on this tape).

EXTRAGAL1 Similar to HMCMO4 but deals with the distribution from fine measurement data. Points are plotted at the positions of the images, the images are counted in cells, a texture map is drawn and the cell mesh is output to a magnetic tape.

EXTRAGAL1B Similar to HMCMO4B - contours are drawn from the cell counts (mesh greater than 60 x 60). The map is drawn in four sections in turn.

EXTRAGAL1C Similar to HMCMO4C - the contour map is drawn as a complete unit. Normally to be used when the mesh is less than 60 x 60.

EXTRAGAL1D - carries out a preliminary analysis of the geometrical properties of the images by calculating, drawing histograms for and outputting the frequency distributions for size, orientation and shape.

EXTRAGAL2 - incorporates the methods in EXTRAGAL1 and EXTRAGAL1B to redraw the contour mesh and also plots the positions of NGC/IC galaxies within the region and draws boxes around the rich clusters which appear interesting for further study. These boxes will delineate the actual boundaries within which all galaxies are selected.

EXTRAGAL3 - reads down the magnetic tape and picks out all galaxies which lie within the box surrounding the cluster. The parameters for these galaxies are put onto another magnetic tape in the same format. The purpose of this is to save reading all the data when only one cluster is to be investigated.

EXTRAGAL4 This program counts the cluster galaxies in cells and draws contours representing the distribution of galaxies within the cluster. The mesh is output to another magnetic tape. The mesh is also used for determining the strip counts of the galaxies in both X and Y directions across the cluster. The centre of the clusters is determined from the strip counts and the symmetry of the isophotes.

EXTRAGAL5 - calculates the radial distribution of galaxies within the region of the cluster from the cluster centre outwards. It also calculates the cumulative ring count of galaxies.

EXTRAGAL5B - least-squares straight line fit of the straight-line part of the cumulative ring count in order to obtain the background field density of galaxies. The cumulative ring count minus the field galaxies then gives the cumulative ring count of cluster galaxies. The cluster extent and "halo" radius may then be determined in the manner of Noonan (1972).

EXTRAGAL5C - minimising χ^2 procedure to fit the projected Emden isothermal gas sphere distribution to the observed radial galaxy distribution. This allows the determination of the "structural length" for the cluster (Zwicky 1957) and hence of the "core" radius.

EXTRAGAL5D - calculation of the gravitational radius of the cluster from strip counts of the cluster galaxies. The method is from Schwarzschild (1954).

EXTRAGAL6 - finds the twenty largest galaxies within the cluster, outputs their parameters to the line printer and also attempts a crude estimation of the cluster richness (Abell 1958).

EXTRAGAL7 - draws the contour map of the cluster (from mesh stored on magnetic tape) with superimposed vectors representing the size and orientation of the major axes of, first of all, the ten largest galaxies within the cluster and then the twenty largest. From this it is hoped that one can determine the Rood-Sastry (1971) form type and the Bautz-Morgan (1970) type.

CLUSTER1 - a compound program designed to do most of the analysis of the previous programs but only for the galaxies within the cluster. Its purpose is to detect any non-random effects in positions, orientations and shapes.

CLUSTER2 - a test for the spherical or non-spherical symmetry in the distribution of the cluster galaxies by calculating the radial distribution of the galaxies in each of the four quadrants.

CLUSTER3 - a search is made for any segregation of the galaxies according to size.

CLUSTER4 - a search is made for any segregation of the galaxies in orientation or shape.

CLUSTER5 - searches for any correlation between size and position (radial and azimuthal), shape and position and orientation and position.

CLUSTER6 - searches for any correlation between orientation and size, and between shape and size.

CLUSTER7 - searches for any correlation between size and orientation, and between shape and orientation.

CLUSTER8 - searches for any correlation between size and shape, and between orientation and shape.

CONTINGENCY1 - calculates contingency tables for a statistical search for correlations of size, orientation and shape with both radial and azimuthal positions.

CONTINGENCY2 - calculates the contingency tables for shape and orientation with size, and for shape with orientation.

HMCHI1 - chi-squared tests for frequency distributions. This program calculates χ^2 where:-

$$\sum_i (o_i - e_i)^2 / e_i = \chi^2 \qquad (41)$$

HMCHI2 - calculates χ^2 for the contingency tables where (Cramér 1963):-

$$\chi^2 = n \left(\sum_{i,j} \frac{v_{ij}^2}{v_{i\cdot} \cdot v_{\cdot j}} - 1 \right) \qquad (42)$$

APPENDIX III

HMCMØ2 - the program which carries out the galaxy/star separation

```
'LIST' (LP)
'PROGRAM' (CM2C)
'INPUT' Ø = CRØ
'OUTPUT' Ø = LPØ
'OUTPUT' 1 = LP1
'TRACE' Ø
'OPTIMIZE' 2,3
'BEGIN'
'COMMENT' THIS PROGRAM CARRIES OUT THE GALAXY/STAR SEPARATION.
          THE PROGRAM FIRST OF ALL DETERMINES THE SEPARATION
          CRITERIA AND THEN USES THESE CRITERIA TO SELECT THE
          GALAXIES.  THE X AND Y COORDINATES FOR THE GALAXIES
          ARE PUT ONTO AN OUTPUT MAGNETIC TAPE;
'INTEGER' I,J,K, COUNT, M,N,L,TMAX,TMIN,STOP,ORD,FAC,HH,TH;
'REAL' WDTH,XY,LSC;
'INTEGER' 'ARRAY' TMAR [Ø:5Ø,Ø:1ØØ,Ø:19];
'INTEGER' 'ARRAY' G,A [1:1Ø24];

'INTEGER' 'PROCEDURE' NXPOINT (A,J,X,Y,W,Z);
'VALUE' J,X,Y;
'INTEGER' J,X,Y,W,Z;
'INTEGER' 'ARRAY' A;
'BEGIN'
          'COMMENT' THIS PROCEDURE FINDS THE NEXT POINT IN
                    THE CURVE FOR TMIN V.LOG AREA;
          'INTEGER' R,S,T,U;
          R:=X;  S:=Y;
          U:=-1;
P1:                 R:=R+1;
          'IF' R = 5Ø 'THEN'
```

```
          'BEGIN'
                    U:=S;  'GOTO' OUT;
          'END';
P2:       'FOR' T:=S 'STEP' -1 'UNTIL' Ø 'DO'
          'BEGIN'
                    'IF'[A R,T,J] 'NE' Ø 'THEN'
                    'BEGIN'
                         'IF'[A R+1,T,J] = Ø 'AND'
                         A[R,T+1,J] = Ø
                         'AND'[A R,T-1,J] = Ø
                         'AND' A[R+1,T+1,J] = Ø
                         'AND' A[R+1,T-1,J] = Ø
                         'AND' A[R+1,T-1,J] = Ø
                         'AND' A[R+1,T-1,J] = Ø
                         'AND' A[R-1,T+1,J] = Ø
                         'AND' A[R-1,T,J] = Ø 'THEN' 'GOTO' S1;
                         U:=T;
                    'END';
S1:       'END';
     'IF' U 'LT' Ø 'THEN' 'GOTO' P1 'ELSE' 'GOTO' OUT;
OUT:  W:=R;  Z:=U;
'END' NXPOINT;

'PROCEDURE' SIMSOLV (A,B,X,NN,Z);
'VALUE' NN;
'INTEGER' NN;
'REAL' Z;
'ARRAY' A,B,X;
'BEGIN'
          'COMMENT' THIS PROCEDURE SOLVES THE SET OF
          SIMULTANEOUS EQUATIONS IN THE POLYFIT;
          'INTEGER' 'ARRAY' PIVROW, PIVCOL 1:NN ;
          'REAL' PIVOT, PIVPROD, MULT, COMP;
          'INTEGER' I,J,II,JJ,IC,JC,IO,JO,N;
          'PIVPROD:=1;
          'FOR' I:=1 'STEP' 1 'UNTIL' NN 'DO'
               PIVROW I := PIVCOL I := I;
          'FOR' N:=1 'STEP' 1 'UNTIL' NN 'DO'
```

```
'BEGIN'
     PIVOT:= A[PIVROW[N], PIVCOL[N]]; IO:=JO:=N;
     II:= PIVROW[N];  JJ:= PIVCOL[N];
     'FOR' I:=N 'STEP' 1 'UNTIL' NN'PO'
     'BEGIN'
          'FOR' J:=N 'STEP' 1 'UNTIL' NN 'DO'
          'BEGIN'
               IC:= PIVROW[I];  JC:= PIVCOL[J];
               COMP:= A[IC,JC];
          'IF' ABS(COMP) > ABS(PIVOT) 'THEN'
          'BEGIN'
               PIVOT:= COMP;
               II:= IC;  IO:= I;
               JJ:= JC;  JO:= J;
          'END';
          'END';
     'END';
     PIVROW[IO]:= PIVROW[N];  PIVCOL[JO]:= PIVCOL[N];
     PIVROW[N]:= II;  PIVCOL[N]:= JJ;
     B[II]:= B[II]/PIVOT;
     PIVPROD:= PIVPROD*PIVOT;
     'FOR' J:= N+1 'STEP' 1 'UNTIL' NN 'DO'
     'BEGIN'
          JC:= PIVCOL[J];  A[II,JC]:= A[II,JC]/PIVOT;
     'END';
     'FOR' I:= 1 'STEP' 1 'UNTIL' NN 'DO'
     'BEGIN'
          'IF' I 'NE' II 'THEN'
          'BEGIN'
               MULT:= A[I,JJ];
               B[I]:= B[I]-B[II]*MULT;
               'FOR' J:= N+1 'STEP' 1 'UNTIL' NN 'DO'
               'BEGIN'
                    JC:= PIVCOL[J];
                    A[I,JC]:= A[I,JC]-A[II,JC]*MULT;
               'END';
          'END';
     'END';
'END';
```

```
        'FOR' I:= 1 'STEP' 1 'UNTIL' NN 'DO'
            X[PIVCOL[I]]:= B[PIVROW[I]];
        Z:= PIVPROD;
'END' SIMSOLV;

'PROCEDURE' POLYFIT (X,Y,A,MM,NN,DET);
'VALUE' MM,NN;
'INTEGER' MM,NN;
'REAL' DET;
'ARRAY' X,Y,A;
'BEGIN'
    'COMMENT' THIS PROCEDURE CARRIES OUT THE POLYFIT;
    'REAL' P,Q;
    'INTEGER' I,J,K,R;
    'ARRAY' PP[Ø:2*MM], BB[1:MM+1], AA[1:MM+1, 1:MM+1];
    'FOR' R:=Ø 'STEP' 1 'UNTIL' 2*MM 'DO'
    'BEGIN'
        PP[R]:= Ø;
        'IF' R 'LE' MM 'THEN' BB[R+1]:=Ø ;
    'END';
    'FOR' I:=1 'STEP' 1 'UNTIL' NN 'DO'
    'BEGIN'
        P:=1;  Q:= Y[I];
        'FOR' R:=Ø 'STEP' 1 'UNTIL' 2*MM 'DO'
        'BEGIN'
            PP[R]:= PP[R]+P;
            'IF' R 'LE' MM 'THEN' BB[R+1]:= BB[R+1]+Q;
            P:=P*X[I];  Q:=Q*X[I];
        'END';
    'END';
    'FOR' K:=1 'STEP' 1 'UNTIL' MM+1 'DO'
        'FOR' J:=1 'STEP' 1 'UNTIL' MM+1 'DO'
            AA[K,J]:= PP[K+J-2];
        SIMSOLV (AA,BB,A,MM+1,DET);
'END' POLYFIT;

SELECT INPUT (0);
SELECT OUTPUT (0);
```

```
'COMMENT' READ THE CONTROL DATA;
WDTH:= READ;
WRITETEST ('('CONTROL%DATA%READ%.')');
NEWLINE (2);
WRITETEXT ('('WIDTH%OF%FITTED%ENVELOPE%%%%=')');
PRINT (WDTH,4,2);
'COMMENT' INITIALISE THE MAG TAPES;
INPUT (100, '('COSMOSCOARSE')');
CREATE (101, '('COSMOSHARVEY')');
NEWLINE (2);
WRITETEST ('('MAG%TAPES%INITIALISED%.')');
'COMMENT' READ THE SENTINEL AND TRANSFER ONTO SECOND TAPE;
READBINARY (100,G,'C'COSMOSCOARSE')');
'FOR' I:=1 'STEP' 1 'UNTIL' 1024 'DO' A[I]:= G[I];
WRITEBINARY (101,A,'('COSMOSHARVEY')');
NEWLINE (2);
WRITETEXT ('('SENTINEL%TRANSFERRED%ONTO%SECOND%TAPE%.')');
NEWLINE (2);
WRITETEXT ('('RUN%BEGINS%.')');

L1:
'COMMENT' FIRST DETERMINE MAX AND MIN THRESHOLD VALUES ON TAPE;
TMAX:=0; TMIN:=128;
L2:
READBINARY (100,G,'('COSMOSCOARSE')');
'COMMENT' CHECK FOR END OF TAPE;
'IF' G[1024]= -9999 'THEN' 'GOTO' L5;
'COMMENT' FIND THRESHOLD BLOCKS;
'IF' G[1024] 'NE' -6666 'THEN' 'GOTO' L2;
'COMMENT' THRESHOLD BLOCK FOUND;
COUNT:=511;
'FOR' I:=1 'STEP' 1 'UNTIL' 511 'DO'
'BEGIN'
     'IF' G[2*I+1] = G[2*I+2] 'AND' G[2*I+2] = 0 'THEN'
     'BEGIN'
          COUNT:=I-1;  'GOTO' L4;
     'END' 'ELSE' 'GOTO' L3;
L3:  'END';
```

```
L4:
'FOR' I:=1 'STEP' 1 'UNTIL' COUNT 'DO'
'BEGIN'
     'IF' G[2*I+2] < TMIN 'THEN' TMIN:= G[2*I+2];
     'IF' G[2*I+2] > TMAX 'THEN' TMAX:= G[2*I+2];
'END';
'GOTO' L2;
L5:
REWIND (100);
NEWLINE (2);
WRITETEXT ('('TMIN%%%%=')'); PRINT (TMIN,6,0);
WRITETEXT ('('%%%%%%%%TMAX%%%%')'); PRINT (TMAX,6,0);
J:= TMAX - TMIN;
FAC:=1;
L6:
'IF' J/FAC 'GE' 19 'THEN'
'BEGIN'
     FAC:= FAC + 1; 'GOTO' L6;
'END';
I:=J-FAC*(J/FAC);
JTOP:= 'IF' I 'NE' 0 'THEN' J/FAC + 1 'ELSE' J/FAC;
NEWLINE (2);
WRITETEXT ('('JTOP%%%%=')'); PRINT (JTOP,6,0);
NEWLINE (2);
WRITETEXT ('('FAC%%%%=')'); PRINT (FAC,6,0);
'COMMENT' ZERO THE ELEMENTS IN THE TMIN/LOGA ARRAY;
'FOR' J:=0 'STEP' 1 'UNTIL' JTOP 'DO'
'FOR' K:=0 'STEP' 1 'UNTIL' TMAX 'DO'
     'FOR' I:=0 'STEP' 1 'UNTIL' 50 'DO'
          TMAR[I,K,J]:=0;
L7:
'BEGIN'
'REAL' RES,DET,THETA,GRAD,P1,P2,T1;T2;
'INTEGER' I1,I2,NGALS,H;
'ARRAY' COEFFS[1:4], GALCURV, GALPOINT[0:50],
     THRESH[1:1024], CRITERIA[1:8,0:JTOP];
'INTEGER' 'ARRAY' NJ,MJ[0:JTOP];
'COMMENT' ZERO THE ELEMENTS IN THE COUNTS;
```

```
'FOR' J:=Ø 'STEP' 1 'UNTIL' JTOP 'DO'    NJ[J]:= MJ[J]:=Ø;
NGALS:=Ø;  ORD:=3;
'COMMENT' READ THE SENTINEL;
READBINARY (1ØØ,G,'('COSMOSCOARSE')');
'COMMENT' NOW CALCULATE THE ARRAYS FOR DETERMINING THE CRITERIA;
L8:
READBINARY (1ØØ,G,'('COSMOSCOARSE')');
'COMMENT' THIS SHOULD BE A THRESHOLD BLOCK;
'IF' G[1Ø24] 'NE' -6666 'THEN' 'GOTO' L8;
L9:
'FOR' I:=1 'STEP' 1 'UNTIL' 511 'DO'
'BEGIN'
     'IF' G[2*I+1] = Ø 'AND' G[2*I+2] = Ø 'THEN'
     'BEGIN'
          HH:= I-1;  'GOTO' Z2;
     'END' 'ELSE' 'GOTO' Z1;
Z1:  'END'
Z2:
'FOR' I:=Ø 'STEP' 1 'UNTIL' 511 'DO'
'BEGIN'
     THRESH[2*I+1]:= G[2*I+1]/125;  THRESH[2*I+2]:= G[2*I+2];
'END';
LSC:= THRESH[2*HH+1];  TH:= ENTIER(THRESH[2*HH+2]);
A1:
READBINARY (1ØØ,G,'('COSMOSCOARSE')');
'COMMENT' CHECK FOR END OF TAPE;
'IF' G[1Ø24]= -9999 'THEN' 'GOTO' L14;
'COMMENT' CHECK FOR NEXT THRESHOLD BLOCK;
'IF' G[1Ø24]= -6666 'THEN' 'GOTO' L9;
'IF' G[1Ø24] < Ø 'THEN' 'GOTO' A1;
COUNT:=1Ø1;
'FOR' L:=Ø 'STEP' 1 'UNTIL' 1Ø1 'DO'
'BEGIN'
     'COMMENT' CHECK FOR LAST BLOCK IN LANE;
     H:=Ø;
     'FOR' M:=1 'STEP' 1 'UNTIL' 1Ø 'DO'
          'IF' G[1Ø*L+M] =Ø 'THEN' H:= H+1;
     'IF' H=1Ø 'THEN'
     'BEGIN'
          COUNT:= L-1;  'GOTO' L11;
     'END' 'ELSE' 'GOTO' L1Ø;
```

```
L10:  'END'
L11:
'FOR' L:=Ø 'STEP' 1 'UNTIL' COUNT 'DO'
'BEGIN'
     I:= ENTIER(2Ø*LN(G[1Ø*L+7])/LN(1Ø));
     'IF' I > 5Ø 'THEN' 'GOTO' L13;
     XY:= G[1Ø*L+2]/1ØØØØ;
A2:
     'IF' XY 'GE' LSC 'THEN' 'GOTO' L12 'ELSE'
     'BEGIN'
          HH:= HH+1;  LSC:= THRESH[2*HH+1];
          TH:= ENTIER(THRESH[2*HH+2]);  'GOTO' A2;
     'END';
L12:
     J:= TH;
     J:= (J - TMIN)/FAC;
     'IF' NJ[J] 'GE' 3ØØ 'THEN' 'GOTO' L13;
     K:= G[1Ø*L+8];
     TMAR[I,K,J]:= TMAR[I,K,J] + 1;
     'IF' G[1Ø*L+7] = 1 'THEN' 'GOTO' L13;
     NJ[J]:= NJ[J] + 1;
L13:  'END';
'GOTO' A1;
L14:
'COMMENT' END OF DATA REACHED;
REWIND (1ØØ);
NEWLINE (2);
WRITETEXT ('('%%%%%J%%%%%%NJ J ')');
NEWLINE (1);
'FOR' J:=Ø 'STEP' 1 'UNTIL' JTOP 'DO'
'BEGIN'
     NEWLINE (1);  PRINT (J,4,Ø);  PRINT (NJ[J],8,Ø);
'END';
'COMMENT' CHECK THAT THERE ARE SUFFICIENT NUMBERS OF IMAGES
     WITHIN EACH SET.   IF NOT, COMPOUND;
     'FOR' J:= JTOP 'STEP' -1 'UNTIL' 1 'DO'
'BEGIN'
     'IF' NJ[J] < 5Ø 'THEN'
     'BEGIN'
```

```
            NEWLINE (2);
            WRITETEXT ('('SET%%')');  PRINT (J,4,Ø);
            WRITETEXT ('('%%COMPOUNDED%WITH%SET%%')');
            PRINT (J-1,4,Ø);
            'FOR' K:=Ø 'STEP' 1 'UNTIL' TMAX 'DO'
                 'FOR' I:=Ø 'STEP' 1 'UNTIL' 5Ø 'DO'
                      TMAR[I,K,J]:= TMAR[I,K,J] + TMAR[I,K,J-1];
       'END';
  'END';
  'IF' NJ[Ø] < 5Ø 'THEN'
  'BEGIN'
       NEWLINE (2);
       WRITETEXT ('('SET%Ø%COMPOUNDED%WITH%SET%1.')');
       'FOR' K:=Ø 'STEP' 1 'UNTIL' TMAX 'DO'
            'FOR' I:=Ø 'STEP' 1 'UNTIL' 5Ø 'DO'
                 TMAR[I,K,Ø]:= TMAR[I,K,Ø] + TMAR[I,K,1];
  'END';
  'COMMENT' NOW CALCULATE THE SELECTION CRITERIA;
  'FOR' J:=Ø 'STEP' 1 'UNTIL' JTOP 'DO'
  'BEGIN'
       'FOR L:= TMAX 'STEP' -1 'UNTIL' Ø 'DO'
       'BEGIN'
            'IF' TMAR[Ø,L,J] > Ø 'THEN'
            'BEGIN'
                 K:=L;  'GOTO' L15;
            'END';
       'END';
L15:
       'FOR' L:=K-1 'STEP' -1 'UNTIL' Ø 'DO'
       'BEGIN'
            'IF' TMAR[Ø,L-1,J] 'NE' Ø 'THEN' 'GOTO' L16;
            'IF' TMAR[Ø,L,J] = Ø 'THEN'
            'BEGIN'
                 M:=L+1;  'GOTO' L17;
            'END';
L16:   'END';
L17:
       I:=Ø;  L:=M;  T1:=M;  K:=1;
L18:
       NXPOINT (TMAR,J,I,L,M,N);
```

```
      GRAD:= N-L;
      GRAD:= GRAD/(M-I);
      'IF' GRAD = Ø 'AND' K = 1 'THEN''GOTO' L2Ø;
      'IF' K 'NE' 1 'THEN' 'GOTO' L19;
      I1:= I-1;
      GALCURV[1]:= GALCURV[2]:=T1;
      GALPOINT[1]:= I1/2Ø;  GALPOINT[2]:= I/2Ø;
      K:= K+1;
L19:
      K:= K+1;
      THETA:= ARCTAN(GRAD);
      GALCURV[K]:= N + WDTH * COS(THETA);
      'IF' GALCURV[K] > T1 'THEN' GALCURV[K]:= T1;
      GALPOINT[K]:= (M + WDTH * SIN(ABS(THETA)))/2Ø;
L20:
      I:=M;  L:=N;
      'IF' I > 5Ø 'THEN' 'GOTO' L21 'ELSE' 'GOTO' L18;
L21:
      T2:= ENTIER (GALCURV[K] + Ø.5);
      'FOR' L:= K-1 'STEP' -1 'UNTIL' 1 'DO'
      'BEGIN'
           'IF' ENTIER (GALCURV[L] + Ø.5) 'LE' T2 'THEN'
                'GOTO' L22 'ELSE'
           'BEGIN'
                M:=L;  'GOTO' L23;
           'END';
L22:  'END';
L23:
      I2:= ENTIER(2Ø * GALPOINT[M+1]);
      POLYFIT (GALPOINT,GALCURV,COEFFS,ORD,M,DET);
      XY:= (1.Ø * I1)/2Ø;
      P1:= COEFFS[1] + COEFFS[2] * XY + COEFFS[3] * XY↑2
           + COEFFS[4] * XY↑3;
      P1:= 'IF' T1 < P1 'THEN' T1 'ELSE' P1;
      XY:= (1.Ø * I2)/2Ø;
      P2:= COEFFS[1] + COEFFS[2] * XY + COEFFS[3] * XY↑2
           + COEFFS[4] * XY↑3;
      P2:= 'IF' P2 < T2 'THEN' T2 'ELSE' P2;
```

```
     CRITERIA[1,J]:= P1;  CRITERIA[2,J]:= I1;
     CRITERIA[3,J]:= P2;  CRITERIA[4,J]:= I2;
     'FOR' I:=1 'STEP' 1 'UNTIL' 4 'DO'
          CRITERIA [I+4,J]:= COEFFS[I];
'END';

'COMMENT' EVERYTHING IS READY FOR THE GALAXY/STAR SEPARATION
     TO COMMENCE.  FIRST READ THE SENTINEL;
READBINARY (100,G, '('COSMOSCOARSE')');
I:=0;
L24:
READBINARY (100,G, '('COSMOSCOARSE')');
'COMMENT' FIND FIRST THRESHOLD BLOCK;
'IF' G[1024] 'NE' -6666 'THEN' 'GOTO' L24;
L25:
'FOR' M:=1 'STEP' 1 'UNTIL' 511 'DO'
'BEGIN'
     'IF' G[2*M+1]=0 'AND' G[2*M+2]=0 'THEN'
     'BEGIN'
          HH:= M-1; 'GOTO' Z4;
     'END' 'ELSE' 'GOTO' Z3;
Z3:  'END';
Z4:
'FOR' M:=0 'STEP' 1 'UNTIL' 511 'DO'
'BEGIN'
     THRESH[2*M+1]:= G[2*M+1]/125;  THRESH[2*M+2]:= G[2*M+2];
'END';
LSC:= THRESH[2*HH+1];  TH:= ENTIER(THRESH[2*HH+2] + 0.5);
L26:
READBINARY (100,G, '('COSMOSCOARSE')');
'COMMENT' CHECK FOR END OF TAPE;
'IF' G[1024] = -9999 'THEN' 'GOTO' L33;
'COMMENT' CHECK FOR NEXT THRESHOLD BLOCK;
'IF' G[1024] = -6666 'THEN' 'GOTO' L25;
'IF' G[1024] < 0 'THEN' 'GOTO' L26;
COUNT:= 101;
'FOR' L:=0 'STEP' 1 'UNTIL' 101 'DO'
'BEGIN'
```

```
     'COMMENT' CHECK FOR LAST BLOCK IN LANE;
     H:=Ø;
     'FOR' M:=1 'STEP' 1 'UNTIL' 1Ø 'DO'
          'IF' G[1Ø*L+M] = Ø 'THEN' H:=H+1;
     'IF' H = 1Ø 'THEN'
     'BEGIN'
          COUNT:= L-1;  'GOTO' L28;
     'END' 'ELSE' 'GOTO' L27;
L27: 'END';
L28:
'FOR' L:=Ø 'STEP' 1 'UNTIL' COUNT 'DO'
'BEGIN'
     DET:= 2Ø * LN (G[1Ø*L+7])/LN(1Ø);
     XY:= (1.0 * G[1Ø*L+2])/1ØØØØ;
A3:
     'IF' XY 'GE' LSC 'THEN' 'GOTO' L29 'ELSE'
     'BEGIN'
          HH:= HH-1;  LSC:= THRESH[2*HH+1];
          TH:= ENTIER(THRESH[2*HH+2] + Ø.5); 'GOTO' A3;
     'END';
L29:
     J:= TH;
     J:= (J;TMIN)/FAC;
     K:= G 1Ø*L+8 ;
     'IF' DET > CRITERIA[4,J] 'THEN'
     'BEGIN'
          'IF' K 'GE' CRITERIA[3,J] 'THEN' 'GOTO' L3Ø 'ELSE'
               'GOTO' L32;
     'END';
     'IF' DET < CRITERIA[2,J] 'THEN'
     'BEGIN'
          'IF' K 'GE' CRITERIA[1,J] 'THEN' 'GOTO' L3Ø 'ELSE'
               'GOTO' L32;
     'END';
     DET:= DET/2Ø;
     RES:= CRITERIA[5,J] + CRITERIA[6,J] * DET + CRITERIA[7,J]
          * DET↑2 + CRITERIA[8,J] * DET↑3;
     RES:= 'IF' RES > P1 'THEN' P1 'ELSE' RES;
     RES:= 'IF' RES < P2 'THEN' P2 'ELSE' RES;
```

```
     'IF' K 'GE' RES 'THEN' 'GOTO' L30 'ELSE' 'GOTO' L32;
L30: 'COMMENT' IMAGE SELECTED AS GALAXY;
     MJ[J]:= MJ[J] + 1;
     A[2*I+1]:= G[10*L+1];  A[2*I+2]:= G[10*L+2];
     I:= I+1;  NGALS:= NGALS + 1;
     'IF' I = 512 'THEN' 'GOTO' L31 'ELSE' 'GOTO' L32;
L31: 'COMMENT' GALAXY ARRAY FULL.  TRANSFER ONTO TAPE;
     WRITEBINARY (101,A, '('COARSEHARVEY')');
     I:=0; 'GOTO' L32;
L32: 'END';
'GOTO' L26;
L33: 'COMMENT' END OF DATA REACHED.  PUT TERMINATING BLOCKS
     ONTO SECOND TAPE;
'FOR' J:= 2*I+1 'STEP' 1 'UNTIL' 1024 'DO'  A[J]:=0;
WRITEBINARY (101,A, '('COSMOSHARVEY')');
'FOR' J:=1 'STEP' 1 'UNTIL' 1023 'DO'  A[J]:=0;
A[1024]:= -9999;
WRITEBINARY (101,A, '('COSMOSHARVEY')');
NEWLINE (2);
WRITETEXT ('('GALAXY/STAR%SEPARATION%COMPLETED%.')');
NEWLINE (2);
WRITETEXT ('('NO.%OF%GALAXIES%ON%TAPE%%%%=')');
PRINT (NGALS,12,0);
REWIND (100);
REWIND (101);
NEWLINE (2);
WRITETEXT ('('RUN%SUCCESSFUL%.')');
'COMMENT' OUTPUT THE CRITERION TABLE;
SELECT OUTPUT (1);
'FOR' J:=0 'STEP' 1 'UNTIL' JTOP 'DO'
'BEGIN'
     NEWLINE (1);  PRINT (FAC*J+TMIN,4,0);
     'FOR' I:=1 'STEP' 1 'UNTIL' 8 'DO'
          PRINT (CRITERIA[I,J],4,2);
'END';
SELECT OUTPUT (0);
NEWLINE (2);
WRITETEXT ('('%%%%%J%%%%%%%MJ[J]')');
NEWLINE (1);
```

```
'FOR' J:=Ø 'STEP' 1 'UNTIL' JTOP 'DO'
'BEGIN'
     NEWLINE (1);  PRINT (FAC*J+TMIN,4,Ø);
          PRINT (MJ[J],8,Ø);
'END';
'END';
FREEMT (1ØØ);
FREEMT (1Ø1);
NEWLINE (2);
WRITETEXT ('('MAG%TAPES%REWOUND%AND%FREED%.')');
NEWLINE (2);
WRITETEXT ('('RUN%COMPLETED%.')');
FREE INPUT;
FREE OUTPUT;
'END'
```

ACKNOWLEDGEMENTS

I owe the credit for this thesis to Dr. V. C. Reddish, whose inspiration and encouragement have guided me over the past three years. I wish to thank also Dr. M. T. Brück, Dr. A. C. Edwards and Dr. N. M. Pratt with whom I have had useful discussions concerning the subject matter presented here, and Professor H. A. Brück whose encouragement has influenced my progress. The COSMOS measurements were carried out under the supervision of Dr. N. M. Pratt, assisted by Mr. C. K. Barclay, and the raw machine data were processed expediently and efficiently by Mr. R. Martin, to whom I am indebted. I am grateful to Dr. R. J. Dodd for allowing me to use the random-number generator computer program, to Mr. A. McLachlan for providing SAO charts and grid overlays for the southern sky survey fields, to Mr. C. K. Barclay for making blow-up prints of the measured regions, to Mr. H. Seddon for giving editorial advice on the manuscript, to the Atlas Computing Laboratory for the use of computing facilities, and to the U.K. Schmidt Telescope Unit for allowing me ready access to the plate material and for the loan of the plates. Last, but by no means least, I wish to thank my wife, whose love, patience and understanding have played a major part in the completion of this thesis.

I was supported while working on this project by a maintenance grant from the Science Research Council.

REFERENCES

Aarseth, S.J., 1963. Mon. Not. R. astr. Soc., 126, 223.

Aarseth, S.J., 1966. Mon. Not. R. astr. Soc., 132, 35.

Aarseth, S.J., 1971. Astrophys. Space Sci., 14, 20.

Aarseth, S.J. & Saslaw, W.C., 1972. Astrophys. J., 172, 17.

Abell, G.O., 1958. Astrophys. J. Suppl., 3, 211.

Abell, G.O., 1961. Astr. J., 66, 607.

Abell, G.O., 1962. Problems of Extra-Galactic Research, IAU Symposium No. 15, ed. G. C. McVittie, MacMillan, New York.

Abell, G.O., 1965. A. Rev. Astr. Astrophys., 3, 1.

Abell, G.O., 1970. External Galaxies and Quasi-Stellar Objects, IAU Symposium No. 44, ed. A. R. Sandage, D. Reidel, Holland.

Albada, G.B. van, 1960. Bull. astr. Inst. Netherl., 15, 165.

Albada, G.B. van, 1961. Astr. J., 66, 590.

Ambartsumian, V.A., 1961. Astr. J., 66, 536.

Austin, T.B. & Peach, J.V., 1974a. Mon. Not. R. astr. Soc., 167, 437.

Austin, T.B. & Peach, J.V., 1974b. Mon. Not. R. astr. Soc., 168, 591.

Austin, T.B., Godwin, J.G. & Peach, J.V., 1975. Mon. Not. R. astr. Soc., 171, 135.

Bahcall, N.A., 1971. Astr. J., 76, 995.

Bahcall, N.A., 1972. Astr. J., 77, 550.

Bahcall, N.A., 1973a. Astrophys. J., 180, 699.

Bahcall, N.A., 1973b. Astrophys. J., 183, 783.

Bahcall, N.A., 1973c. Astrophys. J., 186, 1179.

Bahcall, N.A., 1974. Astrophys. J., 187, 439.

Bahcall, N.A., 1975. Astrophys. J., 198, 249.

Bautz, L.P., 1972. Astr. J., 77, 1.

Bautz, L.P. & Abell, G.O., 1973. Astrophys. J., 184, 709.

Bautz, L.P. & Morgan, W.W., 1970. Astrophys. J. Lett., 162, L149.

Bogart, R.S. & Wagoner, R.V., 1973. Astrophys. J., 181, 609.

Burbidge, G.R. & O'Dell, S.L., 1973. Astrophys. J. Lett., 182, L47.

Burbidge, E.M. & Sargent, W.L.W., 1971. Nuclei of Galaxies, ed. D. J. K. O'Connell, American Elsevier, New York.

Chincarini, G. & Rood, H.J., 1971. Astrophys. J., 168, 321.

Chandrasekhar, S., 1942. Principles of Stellar Dynamics, Cambridge University Press.

Clark, E.E., 1968. Astr. J., 73, 1011.

Corben, P.M., Reddish, V.C. & Sim, M.E., 1974. Nature, 249, 22.

Cramér, H., 1963. Mathematical Methods of Statistics, Princeton University Press.

Dearborn, D.S., 1973. Astrophys. J., 179, 45.

Dodd, R.J., Morgan, D., Nandy, K., Reddish, V.C. & Seddon, H., 1975. Mon. Not. R. astr. Soc., 171, 329.

Dyer, C.C. & Roeder, R.C., 1974. Astrophys. J., 189, 167.

Einasto, J., Kaasik, A. & Saar, E., 1974. Nature, 250, 309.

Einasto, J., Kaasik, A., Saar, E. & Chernin, A.D., 1974. Nature, 252, 111.

Field, G. B. & Saslaw, W. C., 1971. Astrophys. J., 170, 199.

Fullerton, W. & Hoover, P., 1972. Astrophys. J., 172, 9.

Geller, M. J. & Peebles, P. J. E., 1973. Astrophys. J., 184, 329.

Giovanelli, R. G., 1964. Mon. Not. R. astr. Soc., 127, 33.

Gott, J. R., III, Wrixon, G. T. & Wannier, P., 1973. Astrophys. J., 186, 777.

Gregory, S. A., 1975. Astrophys, J., 199, 1.

Haggerty, M. J., 1971. Astrophys. J., 166, 257.

Harrison, E. R., 1968. Mon. Not. R. astr. Soc., 141, 397.

Hauser, M. G. & Peebles, P. J. E., 1973. Astrophys. J., 185, 757.

Holmberg, E., 1946. Medd. Lunds. Observ., Series II, No. 117.

Humason, M. L., Mayall, N. U. & Sandage, A., 1956. Astr. J., 61, 97.

Icke, V., 1973. Astr. Astrophys., 27, 1.

Karachentsev, I. D., 1966. Astrofisika, 2, 81 (Engl. trans. 1967. Astrophysics, 2, 39).

Kiang, T., 1967. Mon. Not. R. astr. Soc., 135, 1.

Kiang, T. & Saslaw, W. C., 1969. Mon. Not. R. astr. Soc., 143, 129.

Kristian, J. & Sachs, R. K., 1966. Astrophys. J., 143, 379.

Kristian, J., 1967. Astrophys. J., 147, 864.

Kwast, T., 1966. Acta Astr., 16, 45.

Lemaître, G., 1958. Inst. Int. de Phys. Solvay, Onzième conseil de physique, ed. R. Stoops, Brussels.

Lifschitz, E. M. & Khalatnikov, I. M., 1963. Advances in Physics, 12, no. 46.

Limber, D. N., 1953. Astrophys. J., 117, 134.

Limber, D. N., 1954. Astrophys. J., 119, 655.

Limber, D. N., 1962. Problems of Extra-Galactic Research, IAU Symposium No. 15, ed. G. C. McVittie, MacMillan, New York.

Mathews, T. A., Morgan, W. W. & Schmidt, M., 1964. Astrophys. J., 140, 35.

Mattig, W., 1958. Astr. Nach., 284, 109.

Morgan, W. W. & Lesh, J. R., 1965. Astrophys. J., 142, 1364.

Napier, W. M. & Guthrie, B. N. G., 1975. Mon. Not. R. astr. Soc., 170, 7.

Neyman, J., Page, T. & Scott, E. L., 1961. Astr. J., 66, 533.

Neyman, J. & Scott, E. L., 1952. Astrophys. J., 116, 144.

Neyman, J., Scott, E. L. & Shane, C. D., 1953. Astrophys. J., 117, 92.

Noerdlinger, P. D., 1970. Astrophys. J. Lett., 159, L179.

Noonan, T., 1961. Publ. astr. Soc. Pacific, 73, 212.

Noonan, T., 1971. Astr. J., 76, 182.

Noonan, T., 1972. Astr. J., 77, 134.

Noonan, T., 1974a. Astr. J., 79, 358.

Noonan, T., 1974b. Astr. J., 79, 775.

Oemler, A., 1974. Astrophys. J., 194, 1.

Omer, G. C., Page, T. L. & Wilson, A. G., 1965. Astr. J., 70, 440.

Oort, J. H., 1958. La Structure et l'evolution de l'univers, Solvay Conference, ed. R. Stoops, Brussels.

Öpik, E., 1969. Irish astr. J., 9, 211.

Ostriker, J. P., Peebles, P. J. E. & Yahil, A., 1974. Astrophys. J. Lett., 193, L1.

Ozirnoi, L. M., 1971. Astron. Zhu., 48, 1160 (Engl. trans., 1972. Sov. Astron., 15, 923).

Ozirnoi, L. M. & Chibisov, G. V., 1970. Astron. Zhu., 47, 769 (Engl. trans., 1971. Sov. Astron., 14, 615).

Peach, J. V. & Beard, J. M. C., 1969. Astrophys. Lett., 4, 205.

Peebles, P. J. E., 1970. Astr. J., 75, 13.

Peebles, P. J. E., 1974a. Astr. Astrophys., 32, 197.

Peebles, P. J. E., 1974b. Astrophys. Space Sci., 31, 403.

Philip, A. G. D., 1970. Publ. astr. Soc. Pacific, 82, 69.

Philip, A. G. D. & Sanduleak, N., 1970. Publ. astr. Soc. Pacific, 82, 53.

Philip, A. G. D. & Sulentic, J. W., 1973. Publ. astr. Soc. Pacific, 85, 104.

Refsdal, S., 1970. Astrophys. J., 159, 357.

Refsdal, S., Stabell, R., & de Lange, F. G., 1966. Mem. R. astr. Soc., 71, 143.

Rood, H. J., 1969. Astrophys. J., 158, 657.

Rood, H. J., 1974a. Astrophys. J., 188, 451.

Rood, H. J., 1974b. Astrophys. J., 194, 27.

Rood, H. J., 1974c. Publ. astr. Soc. Pacific, 86, 99.

Rood, H. J., & Baum, W. A., 1967. Astr. J., 72, 398.

Rood, H. J., Page, T. L., Kintner, E. C. & King, I. R., 1972. Astrophys. J., 175, 627.

Rood, H. J., Rothman, V. C. A. & Turnrose, B. E., 1970. Astrophys. J., 162, 411.

Rood, H. J. & Sastry, G. N., 1971. Publ. astr. Soc. Pacific, 83, 313.

Rood, H. J. & Sastry, G. N., 1972. Astr. J., 77, 451.

Rood, H. J. & Turnrose, B. E., 1968. Astrophys. J., 152, 1057.

Rudnicki, K., 1967. Soviet Astronomy A.J., 11, 59.

Rudnicki, K. & Baranowska, M., 1966. Acta Astr., 16, 55.

Sandage, A., 1961. Astrophys. J., 133, 355.

Sandage, A., 1972. Astrophys. J., 178, 1.

Sandage, A., & Hardy, E., 1973. Astrophys. J., 183, 743.

Sandage, A., Tammann, G.A. & Hardy, E., 1972. Astrophys. J., 172, 253.

Saslaw, W.C., 1972. Astrophys. J., 177, 17.

Sastry, G.N., 1968. Publ. astr. Soc. Pacific, 80, 252.

Schücking, E. & Heckmann, O., 1958. Inst. Int. de Phys. Solvay, Onzième conseil de physique, ed. R. Stoops, Brussels.

Schwarzschild, M., 1954. Astr. J., 59, 273.

Scott, E.L., Shane, C.D. & Swanson, M.D., 1954. Astrophys. J., 119, 91.

Shandarin, S.F., 1974. Astron. Zhu., 51, 667 (Engl. trans., 1974. Sov. Astron., 18, 392).

Shapiro, S.L., 1971. Astr. J., 76, 291.

Shapley, H., 1933. Proc. Natl. Acad. Sci., 19, 591.

Silk, J. & Ames, S., 1972. Astrophys. J., 178, 77.

Stabell, R. & Refsdal, S., 1965. Mon. Not. R. astr. Soc., 132, 379.

Stein, R., 1974. Astr. Astrophys., 35, 17.

Tarter, J. & Silk, J., 1974. Q. Jl. R. astr. Soc., 15, 122.

Vaucouleurs, G. de, 1971. Publ. astr. Soc. Pacific, 83, 113.

Vorontsov-Vel'yaminov, B.A., 1970. Astrofizika, 6, 101 (Engl. trans., 1973. Astrophysics, 6, 47).

Wagoner, R.V., 1967. Nature, 214, 766.

Weizsäcker, C. F. von, 1951. Astrophys. J., 114, 165.

Wertz, J. R., 1971. Astrophys. J., 164, 227.

Wolf, R. A. & Bahcall, J. N., 1972. Astrophys. J., 176, 559.

Yu, J. T. & Peebles, P. J. E., 1969. Astrophys. J., 158, 103.

Zwicky, F., 1957. Morphological Astronomy, Springer-Verlag, Berlin.

Zwicky, F. & Berger, J., 1965. Astrophys. J., 141, 34.

Zwicky, F., Herzog, E., Karpowicz, M., Kowal, C. T. and Wild, P., 1961-1968. Catalogue of Galaxies and of Clusters of Galaxies, vols I-VI, California Institute of Technology, Pasadena.

Zwicky, F. & Karpowicz, M., 1965. Astrophys. J., 142, 625.

Zwicky, F. & Karpowicz, M., 1966. Astrophys. J., 146, 43.

Zwicky, F. & Rudnicki, K., 1963. Astrophys. J., 137, 707.